Liquid Metal Based Test Structures and Reconfigurable Microfluidic Microwave Devices and Antennas

by

Mersedeh Zandvakili

A thesis submitted in partial fulfillment of the requirements for the degree of

Master of Science

Department of Mechanical Engineering
University of Alberta

Abstract

Electrically reconfiguring communicational devices suffer from a number of drawbacks: incorporating electrical elements such as varactors in unit cell level to manipulate the inductance/capacitance of the circuits and maintaining RF/DC interference isolation in power supply is very challenging. In this thesis, a mechanical tuning approach for communicational devices is proposed with stretching or curving these devices. Devices are fabricated based on the gecko-fluidic reversible bonding technique with EGaIn liquid metal (LM) as their conductor and a new thermoplastic substrate (SEBS) with a versatile and cost effective manufacturing method. Selective filling of complex micro-fluidic features is realized with the use of hydrophobic valves which are optimized based on the measured critical pressure of oxidized EGaIn for filling SEBS channels. Laplace barriers are used to achieve “auto-filling” of extremely low aspect ratio channels of LM in SEBS substrate. Furthermore, a technique for making multiple discrete units of LM features from a monolithic injected LM pattern. As a proof of concept, mechanically reconfigurable antennas such as a half-wavelength folded dipole, a multilayer dipole with a soft via, and a micro-strip patch are fabricated and measured for tuning in their center frequency. A super stretchable beam reconfigurable FSS is also manufactured which shifts its beam direction by stretching or curving.

Preface

This thesis is an original work by Mersedeh Zandvakili under the supervision of Dr. Pedram Mousavi and Dr. Dan Sameoto. All the fabrication and measurement processes were conducted in Polymer Microfabrication Lab, University of Alberta Nanofab, and Intelligent Wireless Technology Lab. A section of Chapter 4 is published as a conference article: M. Zandvakili, M.M. Honari, D. Sameoto, and P. Mousavi, "Microfluidic Liquid Metal Based Mechanically Reconfigurable Antenna Using Reversible Gecko Adhesive Based Bonding," Microwave Symposium (IMS), 2016 IEEE MTT-S International, 22-27 May 2016, and some sections of Chapter 3 and Chapter 4 are prepared for submission to Advanced Materials as M. Zandvakili, M.M. Honari, P. Mousavi, and D. Sameoto, "Liquid Metal Based Reconfigurable Microfluidic Microwave Devices and Antennas". I was responsible for design, fabrication, measurements, and manuscript composition and M.M. Honari assisted in measurements and analyzing the results.

Chapter 5 of this thesis has accepted for publication as H. Moghadas, M. Zandvakili, D. Sameoto, and P. Mousavi, "Beam Reconfigurable Aperture Antenna by Stretching or Reshaping of a Flexible Substrate," IEEE Antennas and Wireless Propagation Letters, issue 99. I was responsible for structure design and fabrication, and some parts of manuscript composition. H. Moghadas has assisted in electrical measurement, analysis, and manuscript composition. A section of Chapter 5 is published as the conference article: M. Zandvakili, H. Moghadas, D. Sameoto, P. Mousavi, "Mechanically Tunable Periodic Electromagnetic Surface Using Stretchable Polymer,"

Antenna Technology and Applied Electromagnetics (ANTEM), 2016 17th International Symposium, 10-13 July 2016.

Throughout this work, Dr. Dan Sameoto and Dr. Pedram Mousavi have helped me in concept ideation, development, and manuscript edits.

Table of Contents

List of Tables

List of Figures

CHAPTER 1: INTRODUCTION

Microfluidics is the science of manipulation of fluids in micro-channels. Due to its interesting features such as miniaturized sizes, laminar flow regime, lower costs, and higher sensitivities, microfluidics has turned into an inseparable research tool in various fields: molecular analysis, biology, optics, and microelectronics to name a few [1-3]. The hope of applying silicon microelectronics techniques (such as photolithography) to microfluidic electronics in order to drop fabrication costs and complexity has been one of the driving forces in advancement of microfluidic electronics [4].

Flexible/soft electronics includes circuits and elements which can conform to a desired configuration, different from their original shape. This technology often utilizes soft and/or thin substrates instead of traditional rigid platforms to gain some degrees of flexibility for purposes such as enhanced user experience in wearable electronics [5-6]. Stretchable electronics is a division of flexible electronics in which the system can be elongated along one of the axes with a significant strain. Flexible/stretchable electronics started mainly with applications in flexible displays [9-11], medical devices [13], body worn electronics [14-16] [21], energy harvesting [17-18], and wireless power transfer [23]. In stretchable microfluidic wireless communication devices, by reconfiguring the physical shape of the elements (stretching, bending, twisting), their electromagnetic radiation characteristics can be tuned to meet network variations. For this purpose, the antenna structures are based on an elastic substrate with liquid conductor to provide

mechanical freedom that complies with surfaces such as human skin. In microfluidic electronics, elastomers which are polymers with viscoelastic behavior are good substitutes to traditional rigid substrates [5]. For the conductor, Eutectic Gallium Indium (EGaIn) is commonly used in stretchable microfluidic electronics due to its attractive properties such as decent conductivity and non-toxicity [7]. However, EGaIn is a non-Newtonian fluid with complex behavior arising from a constantly forming oxide layer on its surface when it is in contact with low levels of oxygen [8]. This gel-like liquid has both the elastic (due to its skin) and viscous characteristics which makes it behave unpredictably in micro-channels. For instance, although EGaIn has non-wetting characteristics on most of the polymers due to its high surface tension, its skin sticks to most of the surfaces and makes it stable. EGaIn can start to fill the microfluidic channels when its pressure exceeds a minimum value where the oxide skin is broken. This pressure depends on the dimensions and materials used for micro-channels.

Considering aforementioned discussions, the first objective of this thesis is to characterize the unique properties of oxidized EGaIn LM and use them to enhance the filling process of microfluidic channels. The goal is to achieve accurate control over the pressure and sequence of filling in complicated structures such as branched, low aspect ratio, multi-layered or discontinuous features. As a proof of concept, the second objective is to design functioning stretchable antennas from simple one layer dipole to antennas with multiple layers or complex geometrical configurations.

In Chapter 3, a cost effective and potentially mass manufactural fabrication method based on SEBS thermoplastic elastomer is introduced for manufacturing

microfluidic platforms for stretchable communicational devices. This fabrication method involves manufacturing of the gecko-adhesive pillars which provides a strong reversible bonding around the micro-channels. In Chapter 4, functioning stretchable antennas are designed, analyzed with FEM, fabricated, and tested. Chapter 5 describes the manufacturing of a LM based shape reconfigurable frequency selective surface with conventional microfluidics methods.

Overall, this thesis aims to provide a reliable, repeatable, and cost effective solution for fabrication of complex mechanically reconfigurable microfluidic electronic systems for soft-matter communicational devices.

CHAPTER 2: LITERATURE REVIEW

2.1 Flexible Electronics

Integrated circuits (IC) and packaging industry is constantly looking for methods to shrink component sizes and investigate highly flexible and stretchable circuits that can easily comply to complex surfaces [5]. In traditional rigid silicon-based electronics, there is no opportunity for ergonomic design of biomedical electronic systems with excellent user experience. Elastic substrates and flexible conductors revolutionized electronics in the last decade. It is being predicted that electronics with flexible substrates will take 33% of the electronics industry market by 2022 [9].

There are three main elements for a flexible electronic device (also known as a flex circuit [10]). They include the base material, the conductor, and the bonding adhesive. The base filling material usually dictates the most primary mechanical and electrical properties. The conductor may be thin films of metal, melted or LM, or conductive non-metallic solutions. Bonding adhesive is required to assemble layers of substrate matrix and it is possible to provide adhesion from the modified substrate itself instead of a separate adhesive [11].

There are a number of unsolved challenges for commercializing flexible electronics. These include finding a cost-effective and large scale manufacturing method, exploring new design concepts for fabrication of large and multi-layered structures, reliable sealing method and bonding improvement, standard and repetitive sub-processes

to name a few. In this section, we discuss methods and materials for flexible electronics devices and applications of soft electronics.

2.2 Selection of Conductor for Flexible Electronics

2.2.1 Rigid Metals

Since the bending strains are a function of thickness, any material which is sufficiently thin can be used in flexible electronics [12]. Such thin layers of metals can mostly be bent non-destructively in order to reshape the device but they are not significantly stretchable [13]. Embedding gold in silicone elastomers was one of the first efforts to fabricate electronics with resolutions as low as 15 micrometers [14]. However if the conductor needs to be thicker than a few microns, the high stresses would cause fractures and ultimately electrical disconnection [15]. Utilizing spring/helical shape wires in the elastomeric matrix instead of linear structures causes the metallic network to deflect out of the plane while deformed [16]. This will make the principal stresses smaller for a constant longitudinal strain. Pre-stretching the substrate prior to metal deposition has been another technique for fabricating wavy conductors that can handle larger amounts of strain before failure [17-18]. To achieve out-of-plane stresses for brittle conductors there are three “wavy” material structures as shown in Fig. 1: out of the plane wavy ribbon fully bonded to the elastomeric support, buckled wavy ribbon bonded to elastomeric support only in specific locations, and in plane meshed ribbon [19].

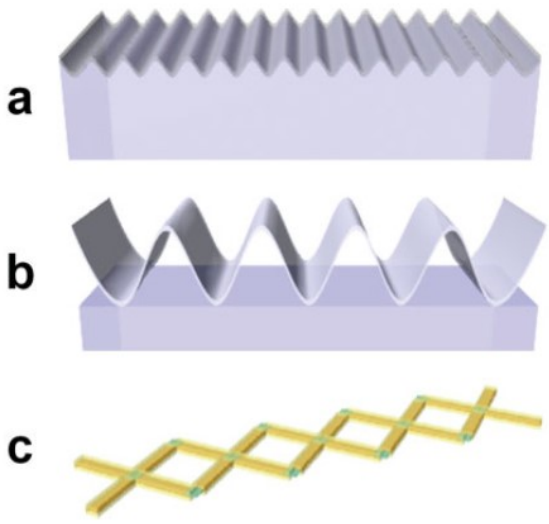

Fig. 1. Three wavy material structures to enhance stretching of brittle conductors: a: out of the plane wavy ribbon fully bonded to the elastomeric support, b: Buckled wavy ribbon bonded to elastomeric support only in specific locations, and c: in plane meshed ribbon [19]. [Reprinted by permission of John Wiley & Sons, Inc.]

Apart from gold, reconfigurable wavy nanomembranes can be made from silicon, which is inherently a brittle material, in a PDMS substrate [20]. Silicon and thin films of transparent oxides such as ZnO are being used as semi-conductor in flexible electronic devices such as transistors as well [21-26]. A stretchable patch antenna with capability of sustaining 15% strain realized by screen printing silver nanowires in PDMS is another example of flexible electronics with solid conductors [27]. The maximum strain reached before failure for solid conductors is only up to 100% in the case of using multiple parallel narrow traces instead of one single trace as shown in Fig. 2 [13][28]. Such tortuous traces limit the design of electrical elements to simple transmission lines with unnecessarily high inductances. Besides, fatigue failure is another disadvantage of these

types of conductors for long-term applications under repeated loading and unloading cycles [29].

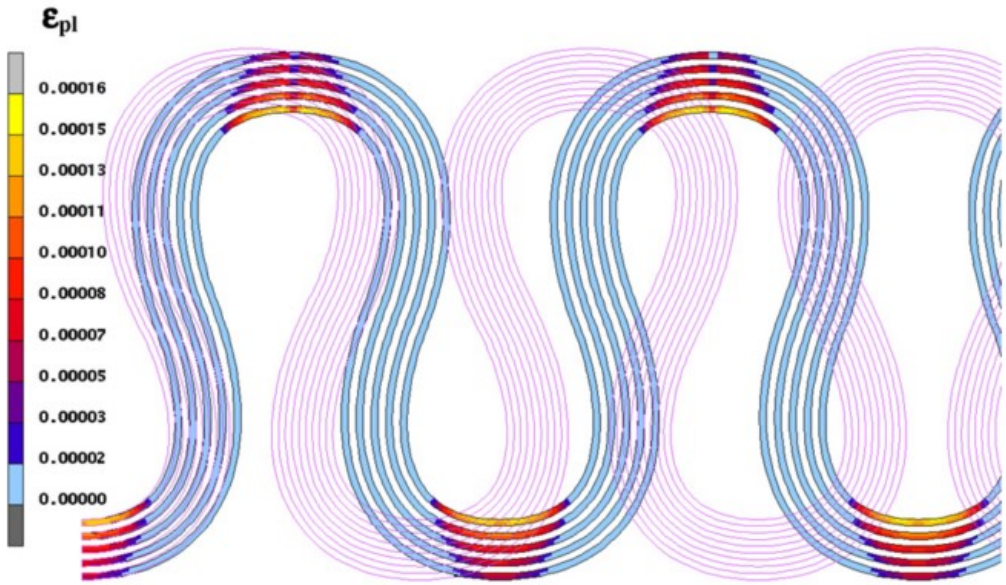

Fig. 2. Strain distribution in a multi-track conductor design. [Reprinted from [28] with permission from Elsevier]

2.2.2 Conductive Polymers

Conductive particles such as metals or carbon embedded in an elastomer as the filling material can form conductive polymers [30-31]. Several conducting particles such as carbon black, silver, and nickel nanoparticles have been used in elastomeric matrix among which single walled carbon nanotubes in a rubber matrix provides better stretchability and conductivity [10][32-34]. Overall, these conductors have been used mostly for fabrication of soft connectors, however, their electrical conductivity is very low compared to their counterparts and their electrical characteristics change considerably with strain [12][31]. Besides, they are not able to fully conform to the

surrounding environment due to the stretchability constraint of conductive polymers and rigid metals [35-36]. For these reasons, tortuous wires are usually preferred over conductive polymers for flexible electronics with considerable levels of deformation [13].

2.2.3 Liquid Conductor

Due to the aforementioned drawbacks of solid and particle conductors, fluidic conductors have become very popular over the last decade. Fluids have nearly zero shear modulus [37], therefore they can freely deform following the shape of substrate they are encapsulated in. This along with their generally higher conductivities and the fact that they have little hysteresis behavior, make them ideal substitutes for solid conductors. The most common liquid conductor in traditional microfluidics has been electrolyte solutions [5]. But their insufficient conductivity makes them inappropriate for radio frequency (RF) systems. Other fluidic conductors such as water have been used for simple monopole antennas, but they suffer from low conductivity [38] as well as the high evaporation rate issue [39]. LMs have higher conductivities and are more stable in standard conditions. Fabricating micro-scale structures with low temperature melting solders have been practiced to achieve flexible electronic systems. The first attempt for stretchable electronics originated from a strain sensor made of mercury in rubber tube [40]. Because of its toxicity, mercury has been replaced in electronic industry by indium, tin and gallium LM alloys [41-44]. In the following section, some of the most popular LMs and their unique properties are discussed:

2.2.3.1 Common Liquid Metals

Mercury (Hg) is perhaps the most well-known room temperature LM. It was widely used in the conventional thermometers, barometers, switches, and gauges. Despite its availability and ease of use, its health threatening toxicity and large surface tension has lead scientists to look for an alternative liquid conductor [45]. Gallium (Ga) and its alloys are considered to be a promising replacement for mercury in electronic applications. Ga is an non-toxic metal with a melting temperature of about 30º and a low vapor pressure which makes it safe to work with by reducing the risk of inhalation [46]. Also, this low vapor pressure increases the durability in long-term applications due to the small evaporation rate. This is especially important in micro/nano-scale manufacturing since the evaporation rate per volume is relatively high in these scales. To further bring down the melting point, eutectic gallium indium (EGaIn) is realized based on freezing point depression principle. EGaIn consists of 75% Ga and 25% In by weight and has a melting point of 15.5 [47]. Its interesting properties such as good electrical conductivity, low melting temperature, biocompatibility, and mobility makes it a compelling material for fabrication of flexible electronics. Galinstan is another alloy of gallium and is composed of gallium, indium and tin. Its melting temperature depends on the mixing ratio of its components. A typical composition is 68.5% Ga, 21.5% In, 10% Sn and has a melting temperature of -19° C [10]. By changing the composition to 62.5% Ga, 25% In, and 12.5% Sn, the melting temperature to shifts to 10° C [48]. Although conductors such as galinstan and EGaIn have a conductivity of 10 times lower than copper, since the

depth of microfluidic channels is higher than the typical thickness of copper sheet, the overall sheet resistance will be sufficient according to equation 1 [49].

$$R_s = \frac{1}{\sigma \times t} \quad \text{Eq.1}$$

In which R_s is the sheet resistance, σ is the conductivity, and t is the thickness. The properties of common LMs have been compared in Table 1.

Table 1: Comparison of LM Conductors

Liquid Metal	Gallium	EGaIn	Galinstan	Mercury
Surface Tension (N/m) in Ambient Conditions	0.680 [45]	0.624 [50]	0.718 [51]	0.428 [52]
Viscosity (cSt)	0.34 [53]	0.32 [8]	0.37 [54]	0.11 [54]
Melting Temperature (ºC)	29.77 [55]	16 [47]	-19 [54]	-39 [54]
Electrical Conductivity (10^7 S/m)	0.37 [55]	0.34 [56]	0.38 [54]	0.10 [54]
Boiling Temperature (ºC)	2205 [55]	>1000 [49]	>1300 [57]	357 [54]
Vapor pressure (Torr)	8×10^{-39} @ 30 ºC [45]	$<10^{-12}$ @ 300 ºC [58]	$<10^{-8}$ @500 ºC [57]	0.27 @100 ºC [45]
Density (g/cm^{-3})	6.1 [53]	6.3 [49]	6.4 [54]	13.5 [54]

2.3 Ga-based Liquid Metal Characteristics

2.3.1 Oxidization

When gallium and its alloys are exposed to oxygen levels above 1 ppm [41], a very thin oxide layer forms on their surfaces. X-ray photoelectron spectroscopy shows that Ga_2O_3 is the most stable form of Ga on the skin, however the existence of other forms such as Ga_2O is also demonstrated [59-60]. The atomic ratio of In:Ga:O at the surface is 1:15:17 [8]. This dull looking oxide skin is composed of only a few monolayers (with a thickness of 1-5 Aº [60-61]) and its thickness does not change over time [62] since the previously formed oxide layer acts as a barrier to stop oxidization of the underneath layers [60][63]. However, when the humidity level rises, an increase in the metal's viscosity has been observed. This increase in viscosity is correlated with the oxide skin growth and accumulative amount of oxygen in the metal [63]. Also in humid conditions unlike dry conditions, the oxide film thickness is dependent on the exposure time to oxygen[63].

When LM fills into channels made of permeable PDMS, the oxide skin is formed on the walls of channels as well as the front meniscus and the LM has a laminar flow within this thin oxide layer [64]. The presence of the oxide shell on the walls is justified by the fact that LM retracts at a slow pace after removing its meniscus's oxide skin (with acid/base/electrical current) rather than an immediate retraction [65].

This oxide layer determines the behavior of Ga alloys and alter some of its characteristics. Although the LM has a very large surface energy and low viscosity, this

passivating skin [66] decreases the surface tension of LM [67] and stabilizes the LM microstructures [8]. Measurements show that the surface tension of EGaIn changes from 624 (dynes/cm) in ambient environment to 435 (dynes/cm) when the oxide layer is removed with dilute hydrochloric acid (HCl) [8][56]. Since moldable structures in LM can be made only in micrometer to millimeter scale, the moldability of LM depends on the surface area to volume ratio, and is attributed to the oxide layer which has a much higher surface energy than the bulk LM [8]. This moldability makes the fabrication of mechanically stable structures using methods such as 3D printing or freeze casting possible [42][68].

The oxide layer is electrically insulating [69] but due to its small thickness, it does not influence the conductivity significantly [61]. However, when electrical current goes through LM, the oxide thickness changes and this results in modification of the electrical resistance [70]. This phenomenon is used in fabrication of soft matter memristors and diodes [69].

The visco-elastic behavior of the oxide layer of EGaIn measured with parallel plates rheometer determines that it has both the viscous and elastic natures (but mainly elastic) for a wide range of strains. Since both the elastic and viscous moduli dramatically drop after applying about 0.5 N/m stress, this value is assumed to be the critical surface stress for yielding the oxide skin of EGaIn [53] and negligible resistance to flow [8].

Sometimes it is essential to get rid of the oxide layer, for instance to switch back to non-wetting nature of Ga based LMs. The amphoteric oxide layer of gallium can be

eliminated in acidic (pH<3) or basic (pH>10) environments [71]. The reaction of gallium and gallium oxide with NaOH has been shown in equation 2 and 3, respectively [9]:

$$2\ Ga + 2\ NaOH + 2\ H_2O = 2\ NaGaO_2 + 3\ H_2 \quad \text{Eq.2}$$

$$Ga_2O_3 + 2\ NaOH = 2\ NaGaO_2 + H_2O \quad \text{Eq.3}$$

When galinstan comes close to HCl vapor, Ga_2O_3 and Ga_2O change to $GaCl_3$ and $lnCl_3$ and in this reaction water is released [72]. Another way to get rid of the oxide layer is by working in a sub-ppm oxygen conditions. However, achieving and maintaining this low oxygen environment is a complicated and costly process [73].

2.3.2 Contact Angle and Wetting

Contact angle is defined as the angle between solid-liquid, solid-gas, and liquid-gas at the contact line when these immiscible phases meet and is a function of interfacial energies among these phases [74]. This thermodynamic property explains the wetting properties of a liquid on a solid surface. The static contact angle can be expressed with Young's equation:

$$\gamma_{LV} \cos\theta + \gamma_{SL} = \gamma_{SV} \quad \text{Eq.4}$$

Where γ_{LV}, γ_{SL}, and γ_{SV} are the surface tension of liquid-vapor, solid-liquid, and solid-vapor interfaces respectively, and θ is the static contact angle. For the intended LMs, the surface tension is very high and this results in a contact angle of higher than 90 degrees.

This means that mercury and Ga alloys without the oxide skin, have little wetting characteristics which makes their actuation easier.

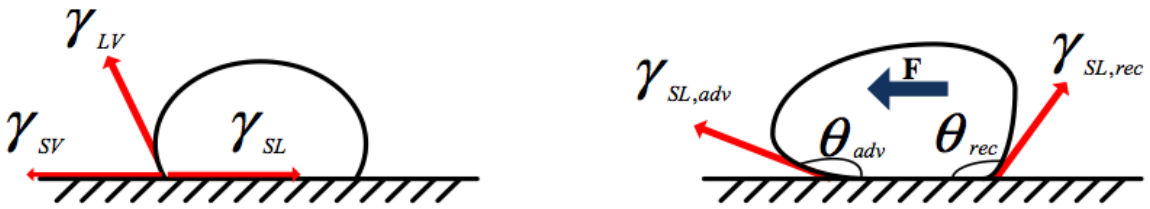

(a) (b)

Fig. 3. Contact angle of a liquid droplet on solid surface (a) without and (b) with the external forces.

In the presence of external forces such as electro-static force or gravity, droplet will move along a surface and dynamic contact angles are used instead. The dynamic contact angle includes advancing/receding contact angles and sliding contact angle [75].

The Young's equation describes the contact angle only on flat surfaces. For a textured surface, the Wenzel model is used to describe the contact angle [76-77].

$$\cos\theta_w = r\cos\theta \qquad \text{Eq.5}$$

In which θ_W is the apparent contact angle, r is a roughness factor (the ratio of actual area of the surface to equivalent area of a flat surface). However, for a dual-scale surface (micro/nano) it is maybe possible for the liquid droplet not to penetrate the nanoscale structures and make the surface fully wet, therefore Wenzel model is not suitable anymore and it is stated by Cassie state [78]. Cassie-Baxter equation extends the Wenzel model for a composite surface [79].

$$\cos\theta_c = \mathcal{F}_1\cos\theta_1 + \mathcal{F}_2\cos\theta_2 \qquad \text{Eq.6}$$

Where F_1 and θ_1 are the area fraction and contact angle of liquid on the component 1 of the surface, and F_2 and θ_2 are for the component 2 of the surface, and θ_c is the Cassie-Baxter contact angle. Since for a LM droplet on a dual-scale surface, it may not penetrate the nanocavities as shown in Fig. 4, the second component of the surface in which the LM is in contact with is air therefore and the equation 6 changes to [76].

$$\cos\theta_c = \mathcal{F}_s\,(1+\cos\theta) - 1 \qquad \text{Eq.7}$$

In this equation, F_s is the solid fraction which is in contact with the liquid, and θ_c is the Cassie-Baxter contact angle. This equation implies by making surfaces with small F_s, it is practical to have super-lyophobic surfaces that LM does not wet them. This concept has been used in the following sections for designing anti-wetting surfaces [80-81].

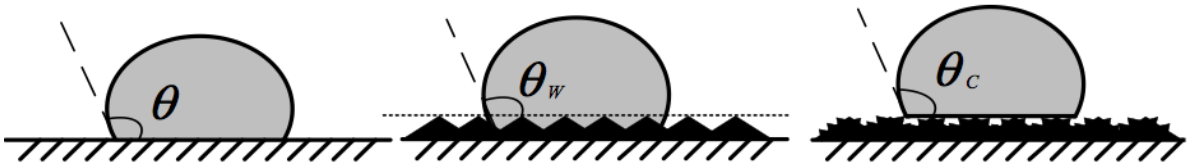

Fig. 4. LM droplet on (a) smooth surface (Young's state), (b) on micro-textured surface where wets the surface completely (Wenzel state), and (c) Dual micro/nano-textured surface where it cannot penetrate into nanostructures (Cassie-Baxter state)

Gallium, EGaIn and galinstan which have high non-wetting characteristics (high contact angles) before oxidation, stick and wet most of the surfaces once oxidized [67][82]. The very high adherence of Ga based alloys to most of the surfaces is attributed to the oxide layer on their surfaces [45]. There are two modes of adhesion between the

oxide layer and the substrate [83]: 1. if the oxide skin is not ruptured before contacting the surface a solid to solid contact happens which has a relatively low adhesion, and 2. if the oxide layer is ruptured and a composite interface of old oxide skin (rough), newly formed oxide skin (smooth) and bare LM is formed. This smooth new oxide layer contributes to the increase in the contact adhesion. This high adherence to most of the materials makes the actuation of LM within channels challenging and leaves residue on the substrates after retracting the metal [83]. On the other hand, LMs without this sticky skin such as mercury retract form channels immediately after removing the pressure and tend to bead up [10].

2.3.3 Laplace Pressure

The pressure difference across the boundary of two immiscible matters or across the interface of a curved surface is determined with Young-Laplace equation:

$$P_{inside} - P_{Outside} = \Delta P = -\gamma \nabla . n = 2\gamma H = \gamma \left(\frac{1}{R_1} + \frac{1}{R_2}\right) \text{(Nm^-2)} \quad \text{Eq.8}$$

where n is the unit normal vector pointing out of the surface of interface, H is the mean curvature, R_1 and R_2 are the principal radii of curvature, and γ is the surface tension. For a rectangular channel we have:

$$P_{inside} - P_{Outside} = 2\gamma \cos\theta \left(\frac{1}{W} + \frac{1}{H}\right) \quad \text{Eq.9}$$

In which W is the width and H is the height of channel, and θ is the contact angle of liquid on the channel walls. Since the selected LMs have great surface tension values, the Laplace pressure is high for them. The LM wets a microfluidic channel as soon as the applied pressure in the upstream surpasses the Laplace pressure imparted by the channel geometry on the liquid.

2.4 Handling of Liquid Metal

Handling of LM is very challenging due to the presence of its oxide layer which makes it tricky to manipulate within micro-channels without leaving residue. However, without a reliable method of manipulation, fabrication of electronic devices with embedded LM is not feasible [78]. To overcome this problem, there have been a number of attempts to lower the wetting characteristics of LM by modifying either the LM/substrate or by preventing their direct contact. In this section, we discuss about different methods for handing Ga based LMs.

2.4.1 Using a Carrying/Lubricating Solution

To reduce the super-lyophilic nature of oxidized LM on substrates, it is sometimes manipulated within a lubricating solution. Teflon solution, deoxygenated silicon oil, polyethylene glycol (PEG), and polyvinyl alcohol (PVA) have been used to prevent the surface of channels from getting stained with LM residue [7][82-85]. Furthermore, channels prefilled with some liquids like glycerol or water lubricate the flow of LM by creating a slip layer between the oxide and the channel's walls. Water

brings down the critical yield stress by weakening the oxide layer as well [86-87]. However, manipulating the LM within another solution can interfere with the movement of LM for some applications and it is not practical all the time. Such issues are discussed in detail in the following sections.

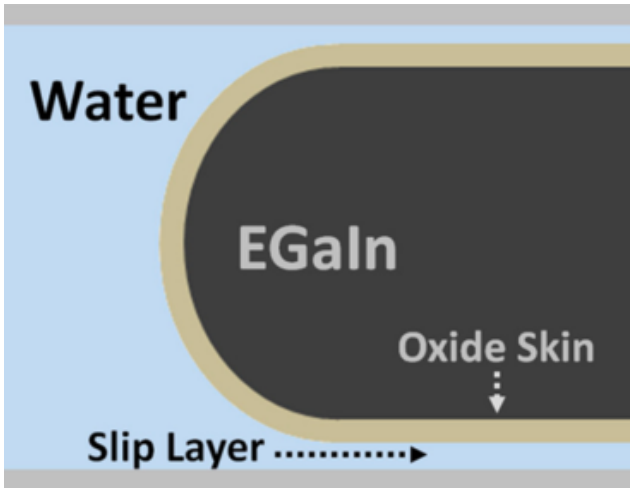

Fig. 5. Water slip layer. [Reprinted from [86], Copyright 2016 American Chemical Society]

2.4.2 Liquid Metal Oxide Layer Removal

If the oxide layer of Ga alloys is removed, it behaves like a Newtonian liquid and therefore its accurate manipulation is feasible in micro-scale. Acids with pH lower than 3 such as diluted hydrochloric acid have been widely used for enhancing LM manipulation in various applications [56][72][88]. This concept has been used in preparation of microfluidic channels made of papers that are previously impregnated with HCl for easy manipulation of oxidized galinstan [89]. PDMS is also extremely permeable to HCl vapor. This thickness dependent permeability is used for surface reduction of galinstan as shown in Fig. 6. Two parallel channels, one filled with LM and the other one filled with

37% wt HCl, are separated with a 200 μm thick PDMS wall. The HCl vapor diffuses through the PDMS to react with the oxide layer on the galinstan surface [90]. The high volatility of HCl, however, can damage the electronic components [78] especially in highly permeable substrates such as PDMS [78]. Therefore, it may be beneficial to use less permeable substrates such as styrene-ethylene-butylene-styrene (SEBS) in applications where microfluidic channels need to be filled with HCl to reduct Ga oxide layer [91].

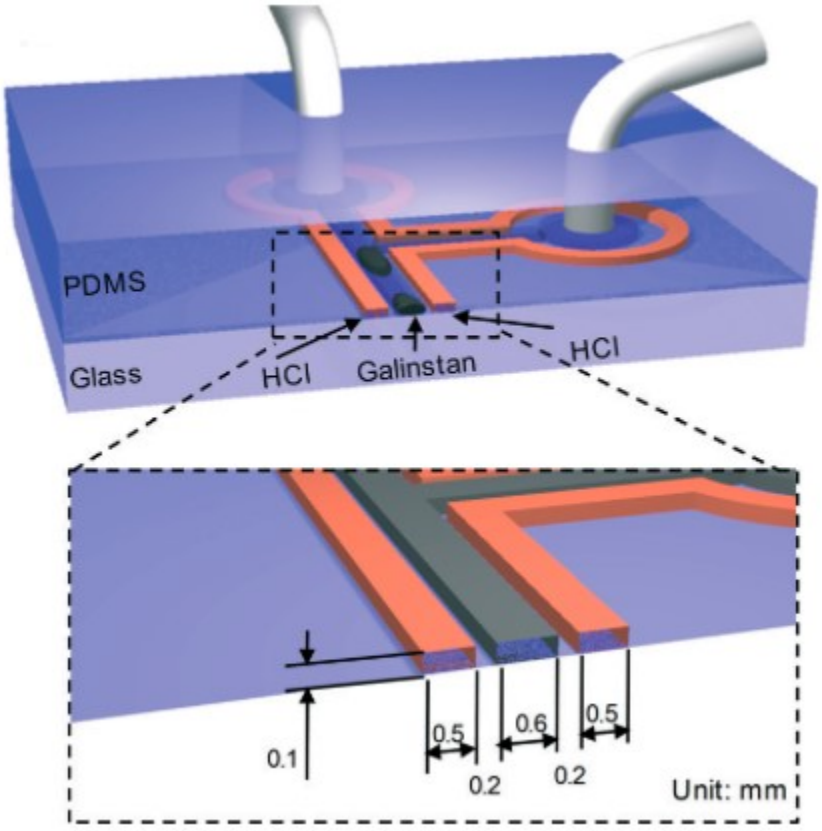

Fig. 6. On chip HCl treatment of galinstan droplets. [Adapted from [90] with Permission from Royal Society of Chemistry]

2.4.3 Lyophobic Coating of LM Droplets

Coating LM droplets with nanoparticles such as WO_3, TiO_2, MoO_3, In_2O_3, teflon powder, silica, and carbon nanotubes enhances the non-wetting characteristics of LMs [92]. These LM marbles have very high contact angles on various substrates, however this method is limited only to LM droplets.

2.4.4 Substrate Surface Modification

Another method to overcome the high adherence of LMs, is to modify the substrate's wetting properties. This can be done by physically texturing the substrate with the use of deposited particles or by using chemicals to micro-machine the surface.

2.4.4.1 Physical Method

Inspired by super-hydrophobic lotus leaves due to their dual scale texture, a PDMS surface can be modified to improve the non-wetting characteristics of oxidized LM as well. This is possible by transferring the micro-nano dual scale textures of another substrate (such as paper) to PDMS walls. By coating these textured channels with titanium oxide TiO_2 nano-particles, the advancing and receding contact angles of galinstan on PDMS increases from 130° and 9° to 167° and 151°, respectively [78]. The reason for this high contact angle growth is the transfer of nanoparticles to LM droplets from the PDMS channel walls which produces LM marbles. Imprinting carbon nanotubes grown initially on Si on PDMS also generates an anti-wetting surface for oxidized gallium oxide due to the its mixed micro-nano scale morphology [93].

In another study PDMS patterned with an array of micro-pillars is used for fabricating microfluidic channels as shown in Fig. 7. By changing the pillars pitch distance, from very large values to small values, the wetting changes from Wenzel state (completely wetting the surface) to Cassie state (complex air, liquid and solid interface) [94-95].

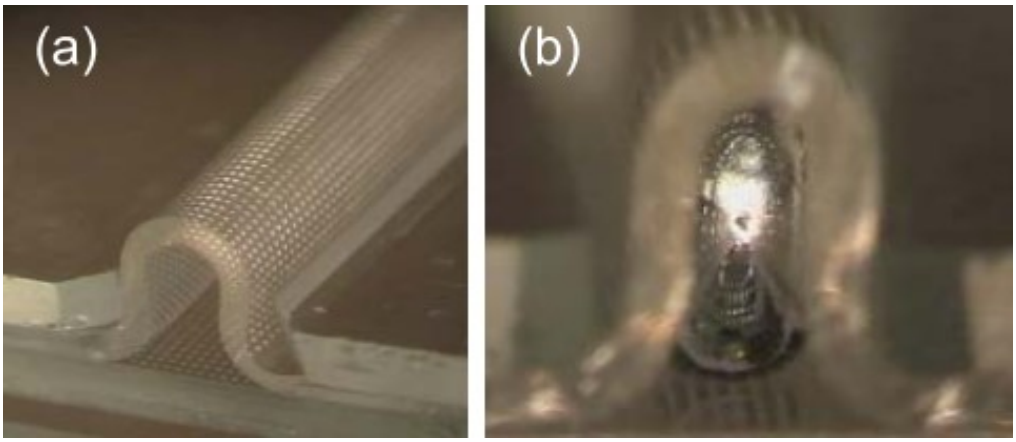

Fig. 7. (a) Cross section of super lyophobic micro-channel, (b) Galinstan flowing through the channel. [Reprinted from [94] © 2012 IEEE]

2.4.4.2 Chemical Method

Strong inorganic acids such as sulfuric acid H_2SO_4 are used for making dual-scale structures in PDMS channels by attacking the surface of channels. HF and HNO_3 have also be used to texturize PDMS, H_2SO_4 however, seems more effective by increasing the advancing contact angle to 167° and a minimum contact angle hysteresis of 14° [78]. Chemically machining of surfaces is a superior solution for increasing contact angle both in terms of reliability and contact angle hysteresis [78].

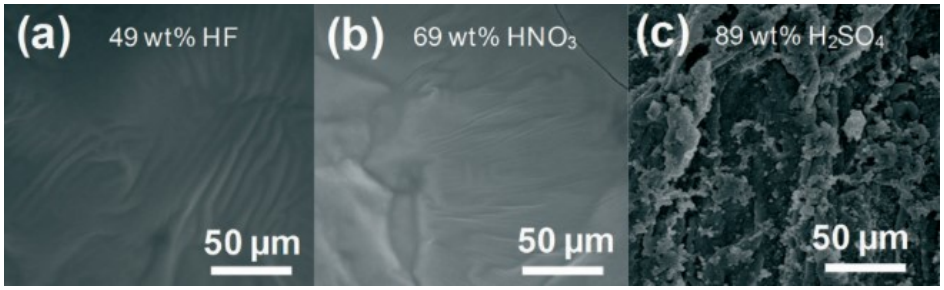

Fig. 8. PDMS surface after being in contact for 1 min with (a) HF, (b) HNO_3 and (c) H_2SO_4. [Adapted from [78] with permission from Royal Society of Chemistry]

2.5 Methods for Patterning LM

In order to make functional devices made of LM, it needs to be patterned in a fast, reliable, and accurate process. This step is equivalent to chemical etching process of copper in PCB manufacturing. In this section, different methods for patterning Ga based LMs, including additive and subtractive techniques, are discussed.

2.5.1 Additive Manufacturing

2.5.1.1 Masked Deposition or Stencil Printing

In this process the LM is deposited on the substrate through a contact mask. Once the deposition is complete, the mask is removed either by etching or simply peeling off and the patterned LM is left on the substrate. Afterwards LM needs to be frozen prior to casting the next elastomer layer so the patterns do not distort in the casting and curing process. The final substrate is usually semi-cured prior to LM deposition so that it can bond to the sealing layer later on. The resolution of this method mostly depends on the stencil's resolution and has been as low as 50 microns for a copper stencil patterned with

ultra violet (UV) lithography, however the surface roughness is still significant as shown in Fig. 9 [96]

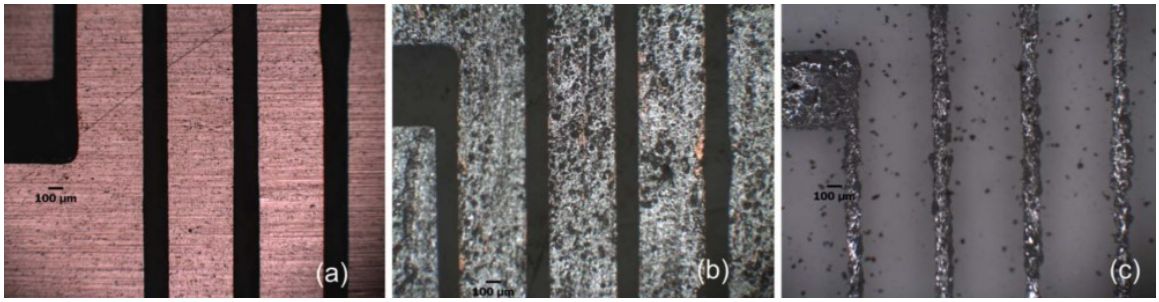

Fig. 9. (a) Front and (b) back side of copper stencil, and (c) patterned galinstan on PDMS. [Reprinted from [96] with permission of Royal Society of Chemistry]

The stencil can be made with laser machining or 3D printing if there is no need for accuracy [97]. To have higher resolution and smaller features the stencil is fabricated with photolithography process [98]. However even in these cases, the actual widths sometimes differ by 50% due to the aggressive etching of the stencil [99]. Moreover, there is no means of accurate height control in the existing literature.

2.5.1.2 Micro-contact Printing or Stamp Lithography

Micro-contact printing has been practiced for years as a parallel soft lithography method [100] but it was not until recently [101] that it was used for printing of LMs. In this method, a relief pattern on the stamp (made of different materials such as PDMS) is inked with LM (either by dipping into ink pool or brushing the stamp) and places the LM on the final substrate. When the pattern is printed entirely, another layer of elastomer is

cast and cured on the conductor surface which is in a fairly stable shape for small geometries due to the oxide layer. This method, however, has not been fully successful due to unevenness in Ga-In alloy surface and its random spreading on the surface as shown in Fig. 10.

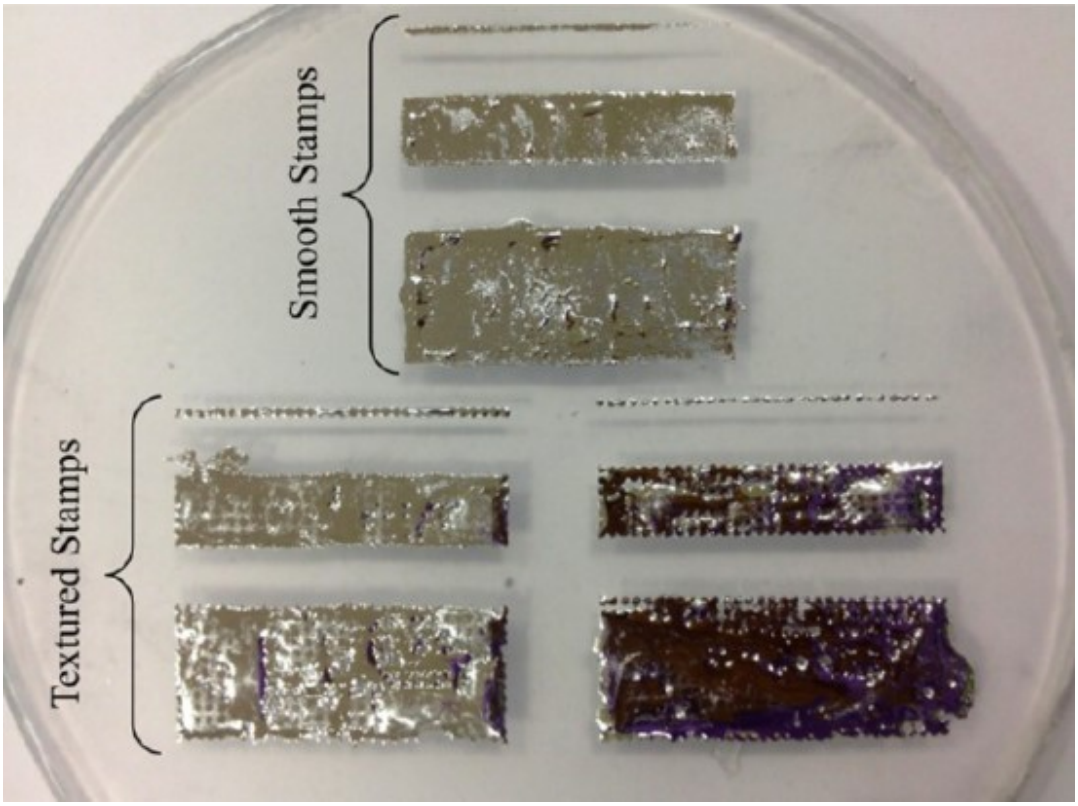

Fig. 10. Unevenness in LM patterns made with stamp lithography with smooth and textured PDMS stamps. [Reprinted from [101] Copyright 2013 American Chemical Society]

2.5.1.3 Micro-transfer Molding with Selective Surface Wetting

Micro-transfer molding is advanced by engineering surfaces to be lyophobic or lyophilic to LMs therefore there are wetting and non-wetting regions on the substrate when the LM is spread on the surface [102]. Kim et al. has selectively chemically

modified the wetting properties of PDMS with toluene, therefore when the PDMS mold is pressed against a LM film, the metal on the chemically modified parts can be easily transferred to a sacrificial layer [103]. Li et al. has discovered that HCl treated galinstan selectively wets patterned Au layer deposited on PDMS [104]. This approach provides a good resolution but it needs deposition of Au and Cr layers and pattering them (Fig. 11). If the surface is not selectively engineered to enhance or deduct wettability, the LM outside trenches needs to be cleaned afterwards by some methods such as acid treatment. This is the underlying principle for imprinting patterning technique [105]

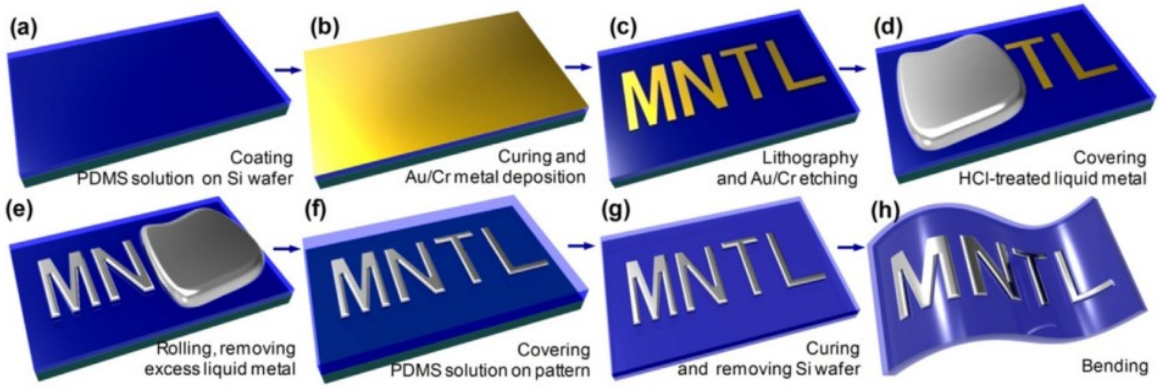

Fig. 11. Fabrication process of EGaIn structures in PDMS via Au selective wetting. [Reprinted from [104] with permission from Elsevier]

2.5.1.4 Direct Writing (2D and 3D Printing)

LM structures can be directly-written at room temperature with pressures lower than 5 kPa at micro-scale [106]. This method includes using advanced automatic 3-dimensional (3D) printers with precise control of the position of nozzle [107] or simply painting the LM on the substrate with a brush or a pen [108-109].

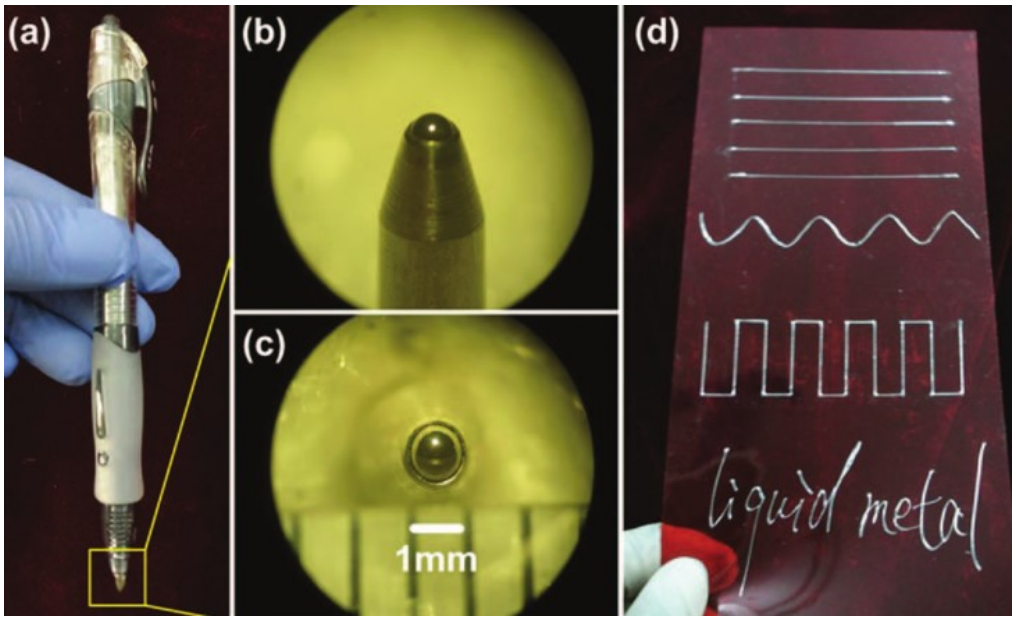

Fig. 12. A roller ball pen filled with GaIn24.5 alloy for direct writing. [Reprinted from [109] with the permission of AIP Publishing]

Printing 3D free-standing structures (which are not supported by an encapsulating layer) is more challenging and requires techniques such as piling droplets of LM or injection molding into an elastomer and etching it later on as explained in Fig. 13 [106]. Otherwise if LM traces need to be encapsulated in an elastomer, they are frozen and sealed with a curing polymer like in previous methods [110].

Yan et al. have developed a coaxial printing technique that simultaneously prints the substrate (PDMS) and the LM core [111]. Although this method can be optimized further for printing multi-dimensional shapes, it opens a new window for facile fabrication of flexible electronics [111].

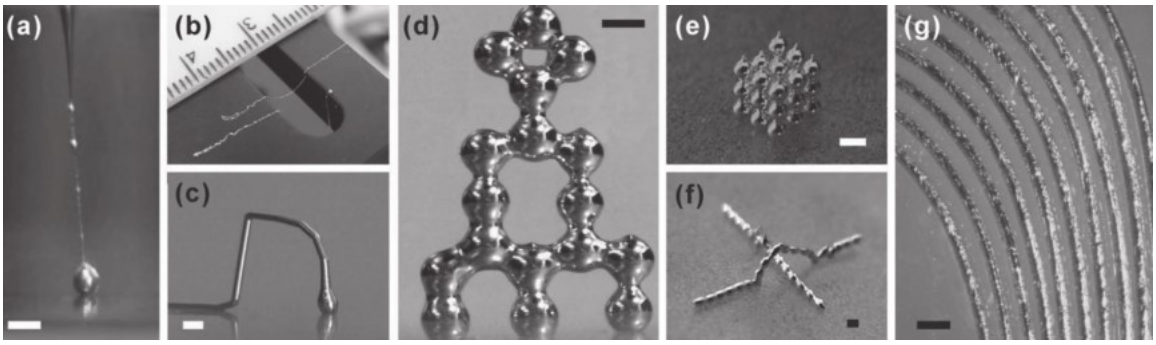

Fig. 13. Fabrication of LM free standing structures with: (a) Extrusion of LM from a needle to write free standing wires, (b) Expelling metal rapidly with bursts of pressure, (c), (d), (e), and (f) Stacking of droplets to form tall structures, (g) Injection molding to PDMS micro channels and etching the channels later on with tetrabutylammonium fluoride. Reprinted from [106] with permission from John Wiley & Sons, Inc..

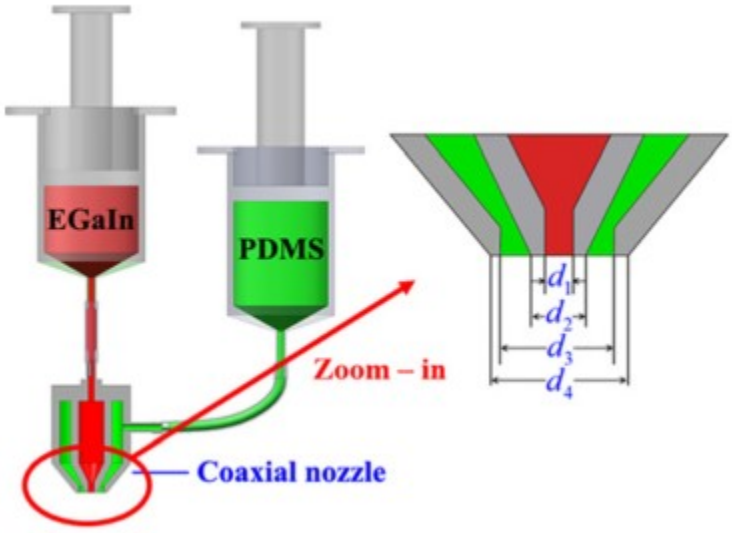

Fig. 14. Coaxial nozzle schematic for simultaneous print of conductor and substrate. [Adapted from [111] with permission of AIP Publishing]

Two opposing factors to quality and resolution of direct writing methods are low viscosity and large surface tension of LMs, however the oxide layer stabilizes the LM

structures to some extent if the size of the features are small enough [106]. On the other hand, there is not any means of robust and accurate control of the dimensions yet and the fabrication process is tricky [110]. The sizes of features that can be patterned in room temperature LMs also is in a small range where they are not too small or too large to be possible to print and to avoid yielding and collapsing [112]. Using additional steps along with 3D printing such as freezing the printed metals on the fly can facilitate achieving more stable 3D structures [113]. Furthermore, more research needs to be done on obtaining reliable nozzle and printing set-up that does not corrode when in contact with Ga alloys and can be cleaned.

2.5.1.5 Injection Molding and Vacuum Assisted Filling

Due to the very high surface tension of LM it is tricky to shape it in desired forms, therefore it can be inserted into already-formed arrangements [114]. To force LM into pre-sealed channels a positive pressure (injection molding) or negative pressure (vacuum filling) can be used. This pressure should be higher than the critical surface tension of Ga based alloys to break the oxide skin. For channels with larger widths this is a straightforward process and can be done with a simple needle. However, when there is a need for miniaturization of the system and to control the filling parameters (for instance in measuring filling pressure) a reliable and repeatable chip to world connection should be used. Despite its simplicity this method has limitations for complex 3 dimensional structures with multiple inlets and outlets [106].

Laplace pressure shaping is another filling technique that takes advantage of vacuum for patterning [6]. Cumby et al. fabricated devices by inserting a LM droplet

between two sheets of patterned polymer (poly-ethylene terephthalate or polyimide) and applying vacuum to evacuate the air and pulling the LM into holes [49]. For Ga based LMs an inert gas like nitrogen, or HCl vapor which reacts with metal oxide needs to be used to avoid formation of gallium oxide which makes this process less practical [49]. Another drawback is that as soon as the vacuum is released, LM retracts from the channels if not fixed in the traces by some approaches such as freeze-casting [6].

(a) (b)

Fig. 15. Patterning LM structures with Laplace pressure shaping method. (a) The LM droplet is placed between two elastomer layers. (b) When the vacuum is applied metal droplet is pushed into trenches. Inspired from [49].

2.5.1.6 Ink Jet Printing or Jetting

Despite several proposals for inkjet printing of Ga based metals, this patterning method is not trouble-free for these alloys. Jetting with Ga alloys, if not performed in an oxygen free environment, leads to accumulation of oxidized LM at the nozzle [101] [115]. To avoid clogging and oxidizing, the orifice of the printing system (made of PDMS) can be fabricated from HCl impregnated paper [116] but this method is far from a long-term and reliable method of patterning.

2.5.1.7 Tape Transfer Atomization Patterning

In this method liquid alloy is atomized and sprayed on a half cured PDMS substrate through a tape transferred mask and then encapsulated as shown in [117]. Semi-cured

PDMS will improve LM wetting on the PDMS surface so that the patterned metal remains in place when the mask is removed [118]. This method is a potentially large scale manufacturing method but it lacks resolution and the line roughness is high.

2.5.1.8 Freeze Casting: A Complementary Method in Additive Manufacturing

It is often necessary to maintain LM structures' shapes before sealing them within another layer of elastomer in additive manufacturing methods like direct writing, micro-contact printing, masked deposition, and Laplace pressure shaping. Due to the large area to volume ratio for micro-scale LM structures, the melting happens faster than usual and the size discrepancy between the nominal and final sizes is observed [6][99]. The elastomers that are molded after LM pattering need to be cured at low temperatures to minimize the distortion of LM patterns. Since curing of most of the polymers such as PDMS is temperature dependent, these methods work only for structures with low aspect ratios where the oxide layer can preserve the melted LM's shape to some extent [6]. For taller structures in freeze casting and when it is essential to precisely control the height, the frozen components should be placed manually in patterned molds as shown in Fig. 16 to avoid shape distortion [6]. However, if the structures are small, handling these small pieces is extremely tough and requires accurate means of alignment. Another solution is to use UV curable polymers to make the curing process faster while alloys remain solid. For these reasons the resolution for most of the manufacturing methods that are based on freeze-casting is as low as 200 micrometers [6].

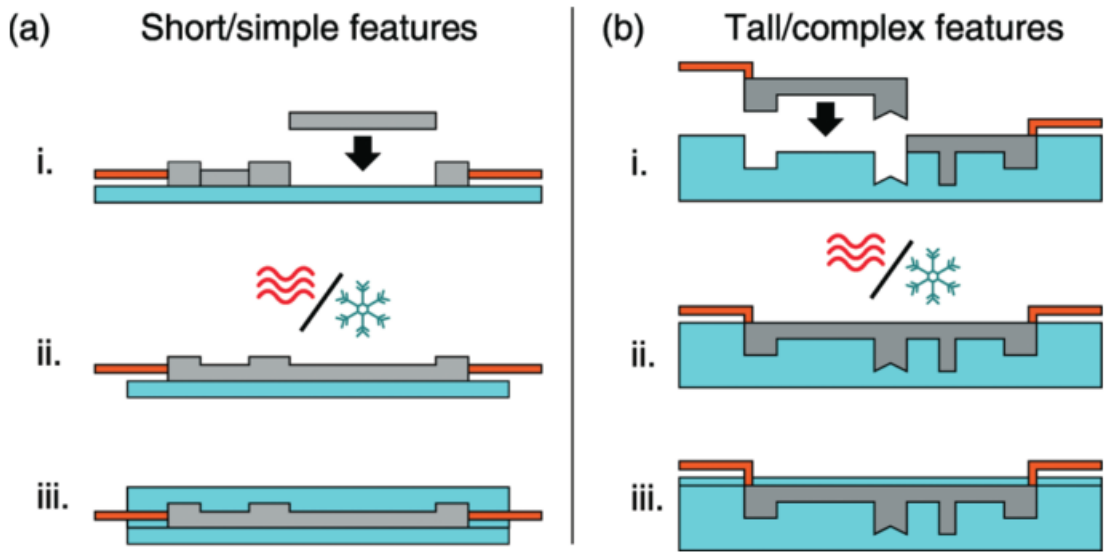

Fig. 16. (a) General freeze casting process and (b) freeze casting for tall/complex structures using patterned substrate and manually aligning pieces. [Reprinted from [6] with permission form Royal Society of Chemistry]

2.5.2 Subtractive Manufacturing

2.5.2.1 Direct Laser Patterning

In this method, LM (EGaIn) is encapsulated between two PDMS layers but it is not patterned until a CO_2 laser locally heats PDMS. The heat from the laser vaporizes PDMS in the bottom layer. This vaporized PDMS punctures the LM surface and displaces the LM as shown in Fig. 17 [119]. This is a rapid prototyping method in soft lithography however the resolution is about 150 micrometers, the roughness is considerable and in cases where the conductor occupies a small ratio of area or where the size of the device is large it is not efficient.

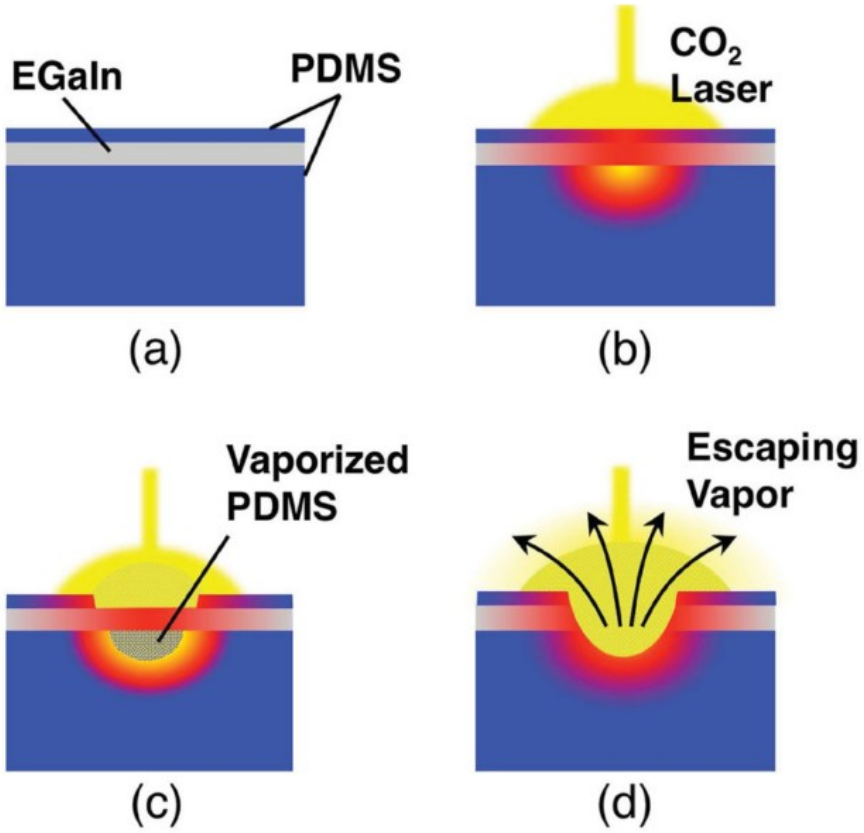

Fig. 17. Laser patterning fabrication process. (a) LM is sandwiched between PDMS layers, (b) Bottom PDMS layer is locally heated and vaporized, (c) When the vapour pressure exceeds the surfaces tension of metal ruptures the oxide layer and (d) relocated the LM. [Reprinted from [119] with permission of John Wiley & Sons, Inc.]

2.5.2.2 HCl Selective Erasure

In this method LM filled PDMS micro-channels are treated by inserting an HCl droplet on top of the sealing layer. HCl vapor penetrates through top layer and dissolves the oxide layer which causes LM to bead up and retract [120]. In spite of reconfigurability arising from the fact that these structures can be filled again with LM,

precise control of the LM location is almost impossible and the method is inherently slow.

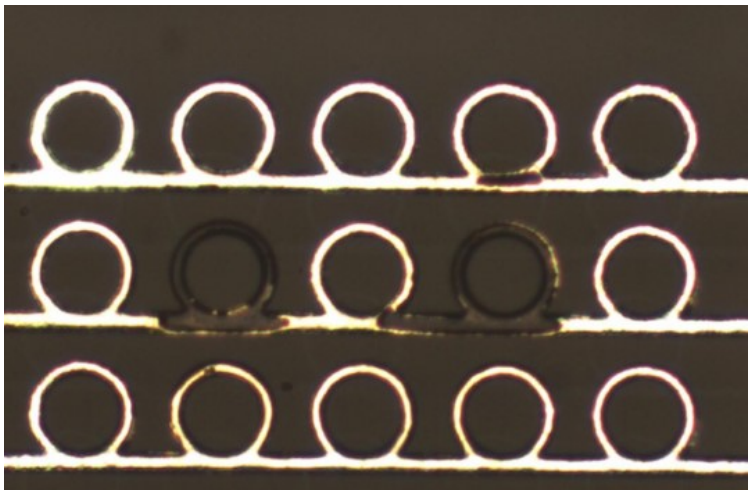

Fig. 18. Array of closed ring resonators made of LM embedded in micro-fluidic channels. Two rings have been emptied by HCl selective erasure method. [Reprinted from [120] with the permission of AIP Publishing]

2.6 Selection of Substrate in Soft Electronics

A typically insulating substrate is required for encompassing soft conductors and avoid their contamination. Synthetic and natural rubbers are the most used substrates in flexible electronics due to their flexibility and low-cost. These flexible substrates serve as dielectrics in radiating elements or just a packaging material in other applications.

2.6.1 Important Parameters in Selecting a Substrate for Soft Electronics

The most important properties in choosing an appropriate substrate for electronic devices are mentioned in Fig. 19.

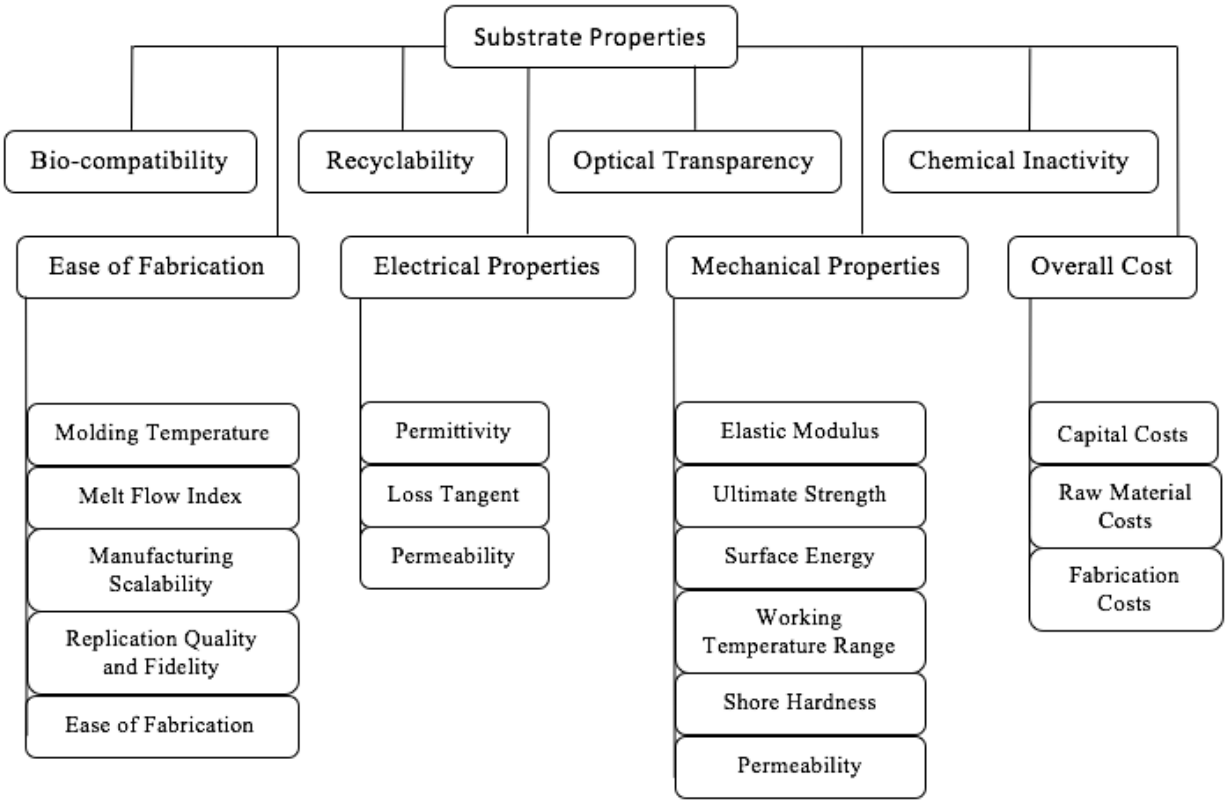

Fig. 19. Important properties in choosing an appropriate substrate for flexible electronics.

2.6.2 Common Polymers in Flexible/Stretchable Electronics

2.6.2.1 PDMS

PDMS is a silicon-based organic polymer developed during World War II in USA. The most predominant choice of PDMS for rapid prototyping is Sylgard 184 by Dow Chemicals [121]. Its interesting properties such as bio compatibility and optical transparency and easy handling makes it the most favorite substrate for rapid prototyping in microfluidics and later in flexible electronics [122]. Siloxane linkages in the PDMS

backbone gives it its great flexibility and stretchability. PDMS however, is a thermoset polymer which cross-links into a 3-dimensional structure while curing and cannot be heated to remold after being cured once. This makes it unsuitable for some industrial mass production manufacturing methods such as hot embossing [123]. Another issue with PDMS is its low surface energy which makes the bonding of PDMS layers challenging. In order to seal microfluidic systems made of PDMS, adhesion strength needs to be improved by some technologies such as oxidizing with oxygen plasma [124]. The extensibility of PDMS depends on its grade and preparation method [125]. Sylgard 184 for instance has a Young's modulus of 1.32-2.97 MPa, and an ultimate tensile strength of 3.51-7.65 MPa [126], but most of the devices composed of it fail well below 100% strain values [127]. There are complex methods to increase this value to about 200% by fabricating 3D nanonetworks in PDMS proximity field nanopatterning [128]. PDMS has a dielectric constant in the range of 2.77-3.69 depending on its working frequency [5]. At 100 kHz, its dielectric constant is 2.67 and it changes to 3 at 3.45 GHz [129]. Its loss tangent is 0.001 at 100 kHz [130] and shifts to 0.05 at 3.45 GHz [129].

2.6.2.2 Ecoflex®

Ecoflex® is a low viscosity bio compatible platinum catalyzed silicone and has been on market since 1998 [131]. Its elongation at break depends on its grade and is up to 1000% for some classes of ecoflex®. This high level of stretchability and its water resistivity makes it a fascinating substrate in fabrication of extra soft substrates especially in epidermal electronics [132]. Ecoflex® comes in a two part formulation (precursors) that need to be mixed for curing [133]. In spite of its attractive mechanical properties,

tough handling, optical opacity, high viscosity after mixing, and difficulty in bonding to itself, keeps Ecoflex® away from being a commercial substrate in electronics industry [134]. Ecoflex® has been used in academic labs for fabrication of antennas [135], sensors [136-137], and circuit elements [101], however there is no record of its electrical properties.

2.6.2.3 SEBS

Styrene ethylene butylene styrene (SEBS) is a triblock copolymer with high tensile strength and low modulus [138]. SEBS consists of ethylene-butylene chains with styrene domains on each end [123]. SEBS is available commercially (at lower costs than PDMS) with the trade name of Kraton® with different polystyrene content which shifts its mechanical properties and manufacturing parameters. SEBS is classified in a group of polymers named thermoplastic elastomers (TPE). Thermoplastic elastomers have the characteristics of both elastomers and thermoplastics and can be reversibly bonded to surfaces. In thermoplastics, polymer chains associate with intermolecular forces. These forces weaken dramatically above their melting temperature resulting viscous characteristics of thermoplastic. That is why thermoplastics are compatible with mass production methods such as extrusion or thermo-compressive molding and can be recycled and reused unlike thermosets. Elastomers have both viscosity and elasticity characteristics and very weak intermolecular forces which leads generally to low elastic moduli and high strain before failure. Despite these interesting properties, with PDMS as the dominating material for soft electronics, SEBS elastomer has been overlooked in this

industry. The application of SEBS has been limited to few cases where it is used as the wire coating for liquid conductor wires [139-140].

2.7 Bonding Technique

A microfluidic channel needs to be bonded to another blank or patterned substrate in order to keep the fluid/gas inside the chip. In spite of the advancements in microfluidics manufacturing methods, bonding of microfluidic chips has still remained a delicate and critical step [141]. Depending on the application, materials used, and desired mode of failure, various methods of sealing may be utilized. In general, bonding techniques can be categorized to reversible and irreversible bonding. A reversible bonding allows multiple assembly and disassembly of the chip without damaging it. This is beneficial for alignment purposes, temporary bonding applications, and recovering the valuable fluids. Irreversible bonding techniques on the other hand, usually provide higher adhesions and therefore can be used in high pressure applications [142]. This bonding includes indirect bonding techniques such as adhesive bonding [143], or direct bonding methods such as thermal fusion [144], localized welding [145], solvent bonding [146], and bonding with surface modification [141]. Surface energy modification methods such as plasma activated bonding are of the most common methods for bonding PDMS [147]. In plasma bonding, a plasma is created either with gases such as Ar, Ne, CO, He, N_2, NH_3, H_2O, CO_2, and O_2 or with air, or vacuum [148-149]. Plasma bonding however, is a costly and time consuming process [147]. Another widely used bonding method commonly used in polymeric electronics, is using an uncured or partially cured sealing

layer to achieve strong irreversible adhesion between the two layers yet the bonding results are inconsistent with this method [147].

Elastomers like PDMS or SEBS can be reversibly bonded to themselves or other materials by Van der Waals forces when they are in close contact. Van der Waals forces are relatively weak intermolecular forces which arise from interaction of transient or permanent dipoles. These forces can hold up to 5 psi fluid pressure and about 1 µl/min flow rate in PDMS microfluidic channels [150-151]. The energy required to separate two bodies which are in contact is called surface free energy and it depends on the effective contact perimeter rather than contact area [152]. This can also be seen in the equation for the pull off force for two elastic spheres in contact [153].

$$P = -\frac{3}{2}\gamma\pi R \qquad \text{Eq.10}$$

$$R = \frac{R_1 R_2}{R_1 + R_2} \qquad \text{Eq.11}$$

Where P is the pull-off force, γ is the energy per unit contact area, and R_1 and R_2 are the radii of spheres 1 and 2. Since the pull-off force is correlated with the effective contact perimeter, by splitting the contact surface dispersive adhesion can be increased. This phenomenon is called the "gecko effect" and is used in designing patterned surfaces with enhanced adhesion forces [154]. Geckos can adhere strongly to most of the surfaces by attractive Van der Waals forces due to the spatula shaped setae on their toes [155]. These hierarchical structures have inspired scientists to design biomimetic dry adhesives by micro-structuring various thermoplastics and thermosets [156-158]. Campo et al. have

tested different shapes of pillars to optimize the adhesion strength including pillars with flat, spherical, concave, spatular, and mushroom tips shown in Fig. 20 [159]. Their experiments showed that mushroom shaped and spatular tip pillars attain maximum levels of adhesion, which is about 30 times higher than the flat punch design [159].

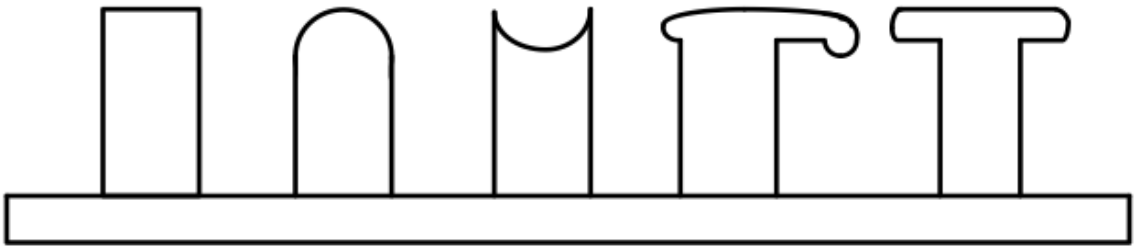

Fig. 20. Different pillar shapes in dry adhesive design including: (a) flat punch, (b) spherical tip, (c) concave tip, (d) spatular tip, and (e) mushroom shape tip. Inspired from [159].

Carbone et al. have suggested that this superior adhesive performance in case of mushroom shaped pillars is due to the elimination of stress singularity compared to flat punch design which changes the detachment mechanism. However, when the the pillar cap is too thin, a large stress concentration is observed, and when the cap thickness is too high, the stress singularity reappears [160]. The distribution of stress along the cap surface has been shown in Fig. 21. Wasay et al. used gecko-inspired dry adhesives for microfluidics application for the first time [161]. A gasket which is a sweep of the mushroom shaped pillars makes the microfluidics channels walls. Individual mushroom shaped pillars are surrounding this gasket for enhanced reversible adhesion. For microfluidic chips made of SEBS with a polystyrene backing layer, this bonding technique can sustain up to almost 100 psi pressure which is 10 times higher than a

standard reversible bonding of PDMS [161]. Developing a reliable and reversible bonding technique which does not put limit on stretchability of the substrate material, and can handle great fluid pressures, is critical in reconfigurable microfluidic electronics and is often the bottleneck point in evolution of super soft microfluidics electronics [162].

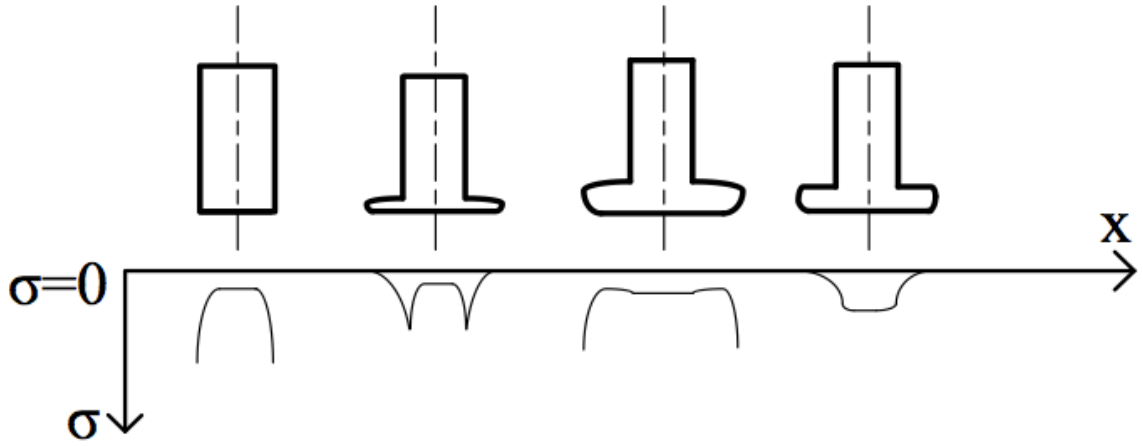

Fig. 21. Stress distribution for a (a) flat punch pillar, (b) mushroom shape pillar with thin cap, (c)mushroom shaped pillar with thick cap, and (d) mushroom shaped pillar with optimum thickness of cap. Inspired from [160].

Other methods for reversible bonding of polymers include using vacuum assisted bonding [163], bonding with magnetic clamping [164], and using external adhesives such as double sided tape to name a few, however, these methods limit the stretchability and versatility of the system.

2.8 Liquid Metal Based Devices

Ga-based liquid alloys can potentially be the next generation of conductors in soft electronics. They have been used in fabrication of reconfigurable communicational devices [39][130], interconnects [165], electrodes [166], RFID tags [167] and circuit

elements [101], to name a few. Soft electronic devices can be categorized to reconfigurable and non-reconfigurable devices. To attain reconfigurability, three main techniques are practiced:

- Repositioning the liquid conductor with hydraulic or pneumatic manipulation [168]
- Elongating the system axially or biaxially [169]
- Flexing and arching the system [170]

Actuating Ga-based liquid conductors in circuits is very challenging due to their stickiness arising from the oxide layer. Removing the oxide layer with other methods also causes unnecessary complications in the process. Arching/bending the device brings nonlinearity and unpredictable results and is not practical for all applications. Therefore, among the aforementioned reconfiguring methods, axial elongation is often preferred. In case of non-tunable soft electronics, the flexibility only serves for an enhanced conformal coating on curved or dynamically deforming surfaces especially in epidermal electronics [171].

2.8.1 Antennas

Antennas are arrangements of conductors or apertures that provide a platform for radiating or receiving electromagnetic waves by translating guided waves into free-space waves. Antennas are categorized to four major groups based on their sizes and their radiation mode:

- Electrically small antennas: Operating wavelength is much larger than physical size of the antenna.
- Resonant antennas: Their physical size is in order of half wavelength.
- Broadband antennas: Electrically large antennas which are continuously resonant.
- Aperture antennas: The radiating wave flows through a physical aperture.

For wireless communications, depending on the application, the antennas need to have certain properties in terms of distribution of power in space, polarization, impedance matching, bandwidth, and efficiency. By reconfiguring these properties, a single antenna can be used in different working points and this makes reconfigurable antennas extremely vital in compact wireless power transfer systems [172]. This tunability allows the designers to make multi-band antennas that have lower noise levels due to a better adaption to communication channel, have better matching, and potentially enable spectrum reuse [173].

2.8.1.1 Dipole Antennas

Dipole antennas are the simplest and the most widespread antennas in telecommunications. They consist of two identical conducting arms connected at their ends to an electromagnetic source. Dipoles are categorized based on the size and configuration of the conducting elements. Some of the most common types of dipoles are: Hertzian dipole (ideal dipole), short dipoles, electrically long dipoles, half-wave dipoles, and folded dipoles. Changing the dimensions of a dipole dramatically alters its radiation properties. Dickey et al. suggested using LMs for reconfigurable

communicational devices for the first time [39]. They fabricated two collinear EGaIn filled channels separated with PDMS in the middle and showed that by stretching it by 20% strain before it fails, the resonance frequency shifts by 14% Fig. 22.

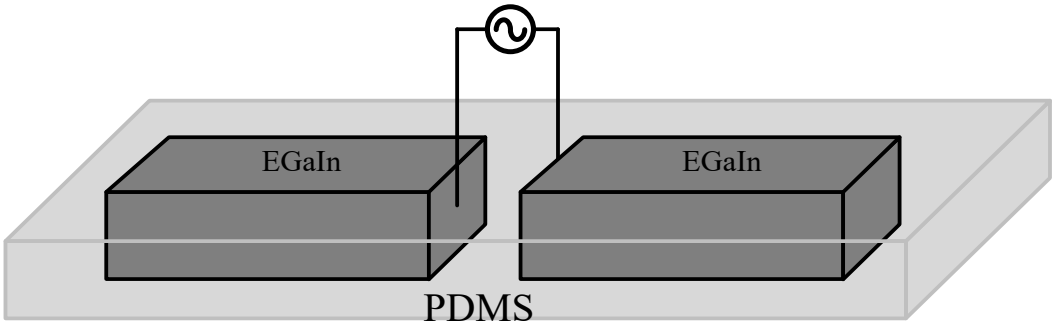

Fig. 22. Soft planar dipole antenna made of EGaIn filled channels in PDMS elastomer.

To enhance the degree of stretchablility, the integration of two polymers with different elastic moduli, can be used. Ecoflex which is a softer elastomer compared to PDMS is used for parts where large deformations are desirable and PDMS is used for in close proximity of rigid connections (Fig. 23) [135]. With this method strains up to 120% are possible. However due to variable stiffness of the substrate, the final shape would be uneven. This causes discrepancies between simulation and measurement results especially in other antenna configurations. Another drawback of this method is that there is not a high resolution consistent manufacturing method with this hybrid structure.

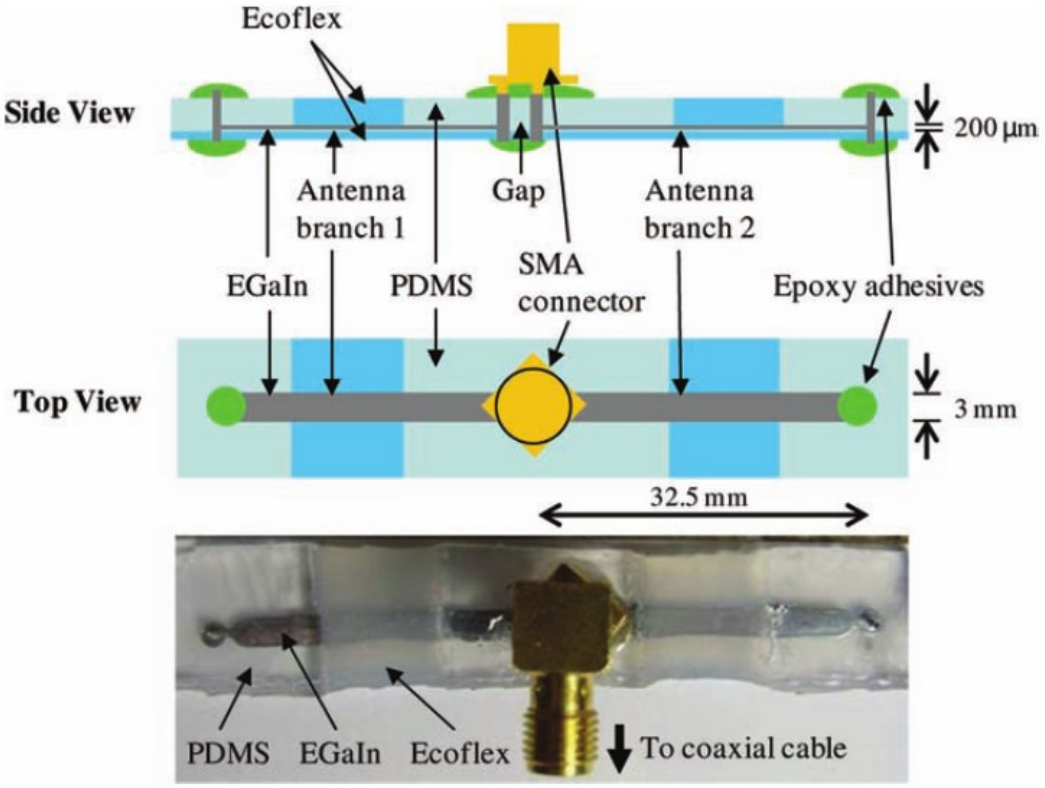

Fig. 23. Hybrid PDMS-Ecoflex® dipole Antenna. [Reprinted from [135] with permission of John Wiley & Sons, Inc.]

Apart from stretching, changing the electrical length of dipole by applying pressure to push LM through Laplace barriers (which were used to stop the LM flow previously) has been used as a reconfiguration method [174]. However, this method of tuning is irreversible and more optimization needs to be done for consistency and reliability of this method.

2.8.1.2 Monopole Antennas

Monopole antennas consist of a conductor rod which act as an open resonator over a large ground plane which is ideally a perfect electric conductor. These resonant

antennas were first invented in 1895 for radio communications by Guglielmo Marconi. Ideal monopole antennas like dipole antennas have omni-dimensional radiation patterns but this is not the case for planar antennas since the medium is not homogenous. An example of reconfigurable monopole is a continuously moved mercury column in a single microfluidic channel on top of a ground plane [175]. Since Ga alloys will stick to the surface, they cannot be used with this configuration. The continuous actuation of mercury is ensured with a number of micro-pumps which makes the antenna footprint large. To employ Ga alloys instead of hazardous mercury, theses metals can be actuated within an electrolyte solution with a DC voltage for the same monopole antenna [176]. However, this electro-chemically reconfigurable antenna, has very low efficiency due to the presence of lossy electrolyte. It also needs a separate DC circuit for actuation purpose, which makes the structure more sophisticated.

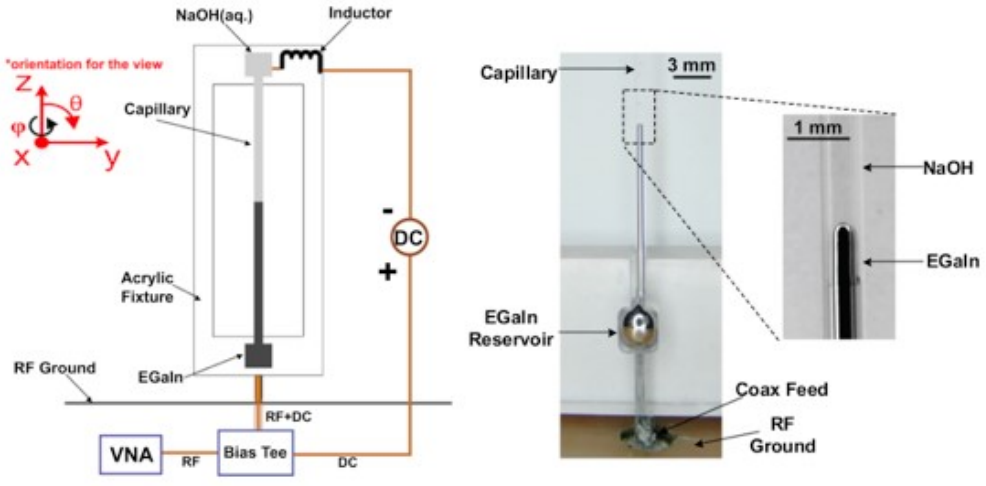

Fig. 24. Electrochemically driven LM monopole antenna. [Reprinted from [176] with the permission of AIP Publishing]

Another method of reconfiguration for this monopole antenna is to treat LM with HCl and actuate it pneumatically instead of using DC bias [177]. On the other hand, having HCl in close contact of other elements causes problems such as corrosion, unreliability of device, and environmental hazards.

2.8.1.3 Other Planar Antennas

The plnar patch antenna is the most common microstrip antenna used in communication devices such as cellphones due to their low profile and simplicity [162]. A microstrip patch is a resonant antenna that can be modeled as a leaky cavity resonator. Despite their low cost, light weight, simple and low profile, and easy integration with integrated circuits (IC) and non-planar geometries, these antennas usually have high quality factors (narrow-band). If there is a method to physically change the patch dimensions, the antenna can possibly work in different frequencies, basically behaving like a broadband antenna but with discrete working frequency ranges. Furthermore, by changing the relative width and length of a patch, its radiating mode and electric field plane (E plane) and magnetizing field plane (H plane) directions can be shifted. Reconfigurable soft patch antennas are fabricated by patterning a rectangular LM patch on a soft substrate on top of a ground plane. This patterning technique involves one or more of the patterning methods introduced in section 2.5 such as microtransfer molding and freeze casting. Injecting LM into structures has been one of most accurate and straightforward fabrication method for one dimensional arrangements (when other dimensions are relatively negligible). However, when it comes to 2 or 3 dimensional figures, due to the random filling and trapped air, this filling method is very challenging.

For this reason, most of the 2D shapes (for instance patch antennas and ground planes) are realized by a meshed surface with discrete conductor traces connected at specific locations. The patch antenna shown in Fig. 25 is made based on this concept. This antenna is used as a strain sensor with maximum elongation of 15% and has an efficiency of 3% to 37% in different elongations [178]. Fig. 25 (a) shows a stretchable (40% max. strain) planar inverted cone antenna [130] and Fig. 25 (b) is a stretchable unbalanced loop antenna (40% max. strain) [179] with meshed ground planes for frequency tuning in PDMS. Hayes et al. used photolithography methods to fabricate a mold for a high resolution continuous microstrip patch antenna [129]. This multi-layer device is fully flexible with a monolithic conductor structure unlike previous patch antennas but due to the its high thickness and the substrate material it is not stretchable. Mazlouman et al. fabricated a super soft (up to 300% strain) microstrip patch antenna from TC5005 silicone (Fig. 27) [162]. The standard molding process for fabrication of this silicone does not provide an accurate and homogenous substrate. The deformation of these polymers is highly dependent on their thickness and therefore, when stretched, the antenna would be wrinkled (Fig. 27). To prevent the conductor reservoir from sagging and blocking prior to LM injection, a plastic isolating layer has been used and LM is injected while the spacer still exists. For other configurations than a simple patch antenna using such isolators is not practical. For simplicity and better efficiency, they have also used a solid copper ground plane and the patch is mounted on that via a middle layer plastic spacer which compromises the overall flexibility.

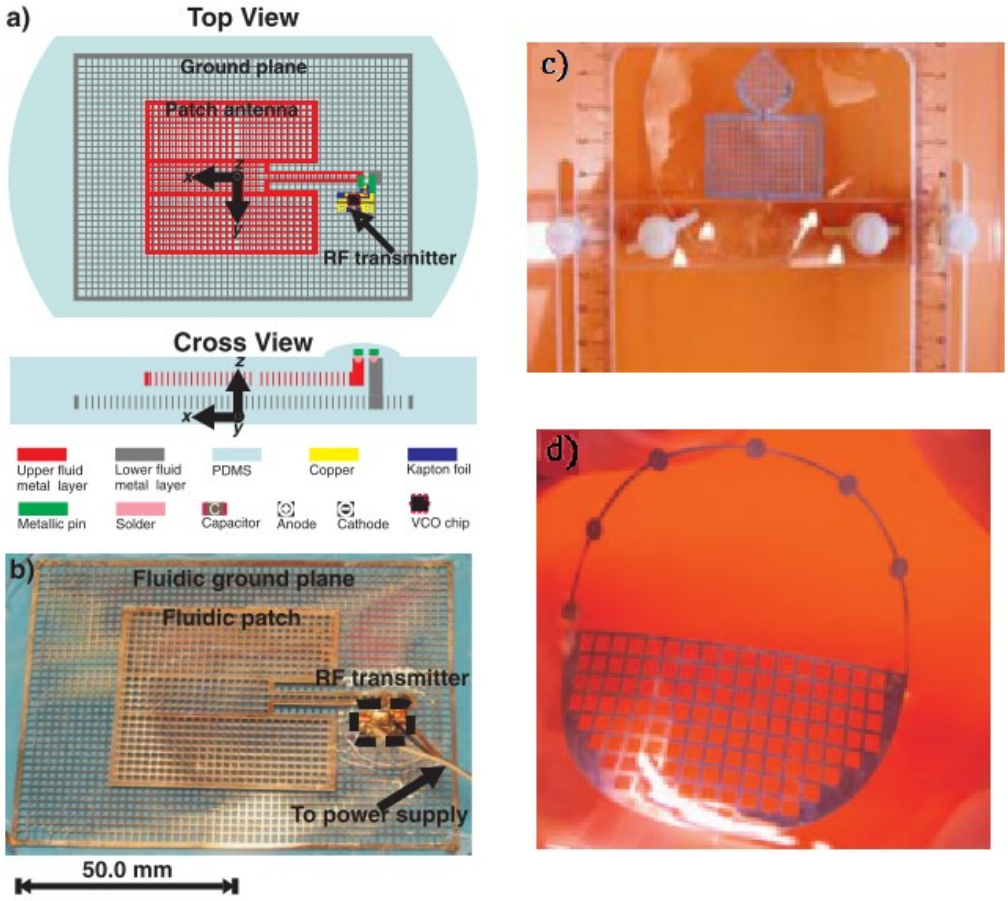

Fig. 25. Stretchable patch antenna with meshed structure (a) schematic, (b) optical image of antenna and its transmitter (Reprinted from [178] with permission of John Wiley & Sons, Inc.), (c) planar inverted cone antenna [Reprinted from [130] © 2009 IEEE] and (d) unbalanced loop antenna [Reprinted from [179] with the permission of AIP Publishing]

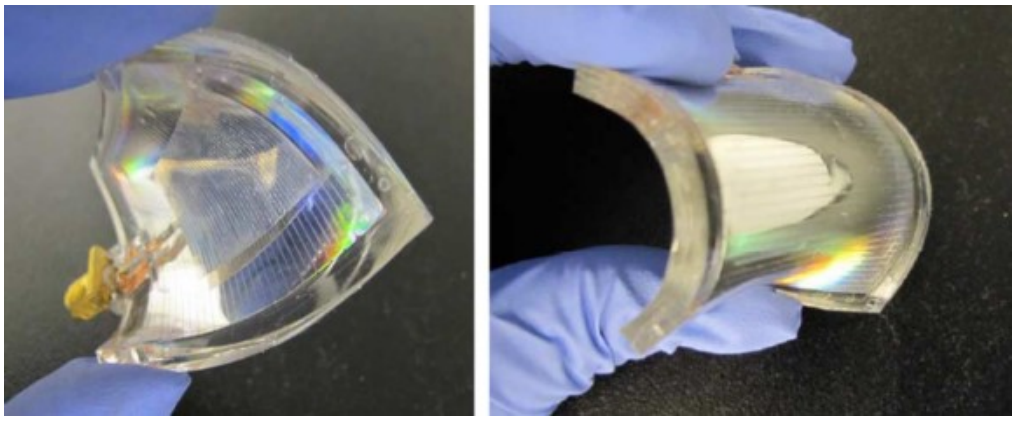

Fig. 26. Multi-layer patch antenna. [Reprinted from [129] © 2012 IEEE]

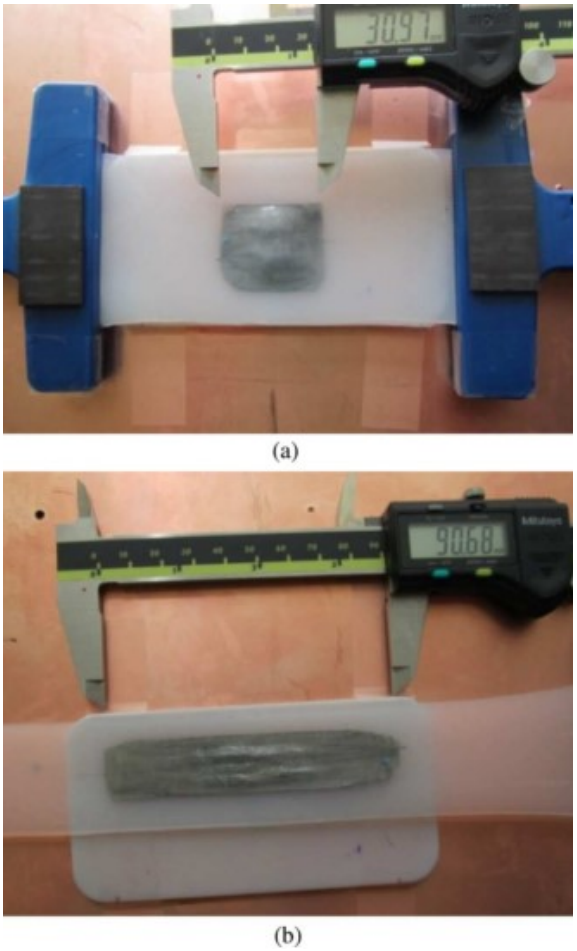

Fig. 27. (a) Unstretched and (b) stretched microstrip patch antenna. [Reprinted from [162] © 2011 IEEE]

Instead of a single antenna as the final device, antennas can be integrated with other soft or rigid circuit elements. Cheng et al. integrated rigid active elements fabricated in flexible substrate (flexfoil) with a stretchable passive RF antenna made of galinstan in PDMS to create a 900 MHz stretchable radiation sensor [180] which is an integration of a planar microfluidic antenna with active components.

2.8.2 Sensors

Elastomeric electronics have been widely used in skin sensors since these substrates are soft enough to conform to human bodies and track their movement. Strain gauges [87][110][136-137][181], direct curvature sensors [182], normal/shear force sensors [97][183-184], pressure gauges [97][136][185] are the most common soft sensors used in microfluidic electronics. These sensors are fabricated from liquid Ga alloys in PDMS or Ecoflex® substrates. The resistance (R), capacitance (C), and inductance (L) of a conductor changes when deformed upon application of strain or stress and this concept has been used in fabrication of such sensors. Based on the desired output signal (AC/DC), targeted sensitivity of device, and conductors shape (straight line, meandered, spiral) one or more of these parameters (L, R, C) may be considered for sensing. In simple DC sensors, measuring R is usually preferred for simplicity. According to resistivity equation, the resistance of a given material is proportional to its length, and inversely proportional to its cross-sectional area.

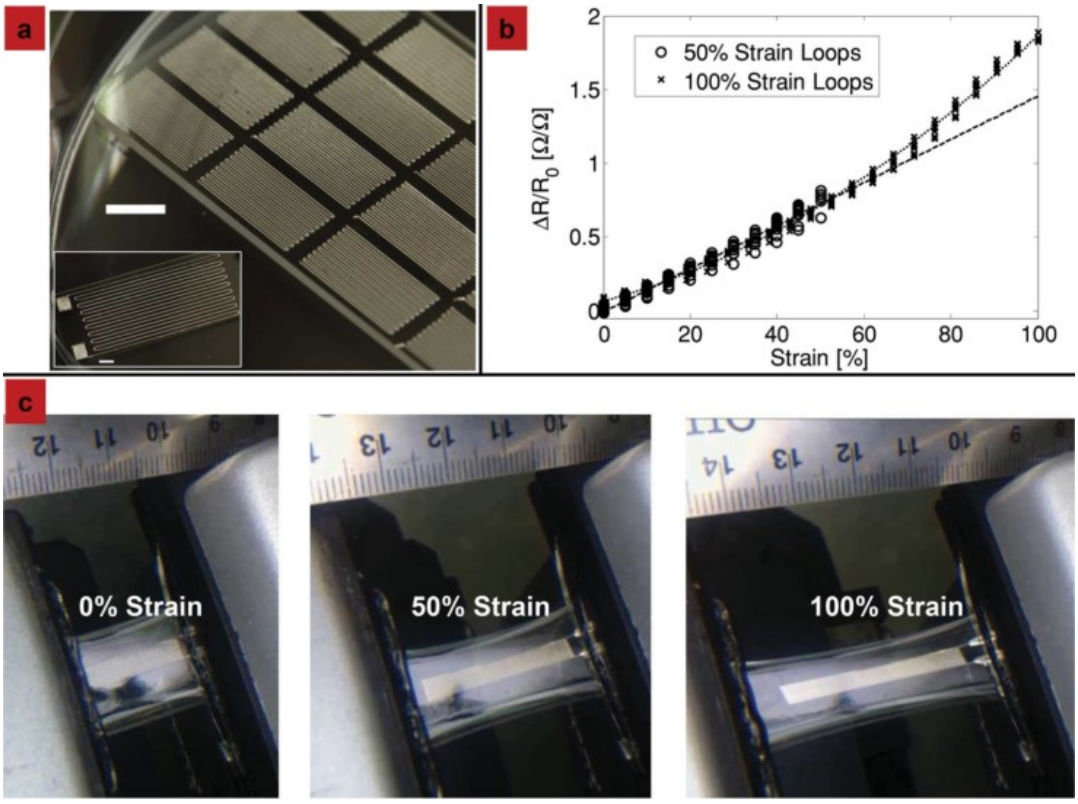

Fig. 28. (a) Meandered EGaIn lines used as a strain sensor. (b) Applying strain changes the resistance of the conductor. (c) the sensor can be stretched up to 100%. [Reprinted from [110] with permission from John Wiley & Sons, Inc.]

2.8.3 Transmission Lines and Interconnects

Transmission lines are interconnects capable of carrying RF AC signals for connection propose. Some of the most common transmission lines are coaxial cables, rectangular waveguides, microstrip line, and coplanar waveguides (CPW). In a soft electronic device, the wiring needs to be stretchable to match other parts' deformations. Fabrication of stretchable wires started with rigid metals (like gold) with diamond shape structure to reduce stresses in soft substrates [165][186]. Using LM as the conductor for interconnections increases the stretchability of the system greatly. Zhu et al. used SEBS

(Kraton® G1643) to extrude ultra-stretchable (700%) hollow fibers later filled with EGaIn [139] and Mineart et al. fabricated a gel by dissolving SEBS and mineral oil in toluene to make 600% stretchable fibers with a LM core [127]. For coaxial transmission lines extruded SEBS (Kraton® G1643) wires filled with LM are woven together as shown in (Fig. 25) [140]. If a self-healing polymer is used for interconnects, it can be cut and reassembled in desired configurations [187].

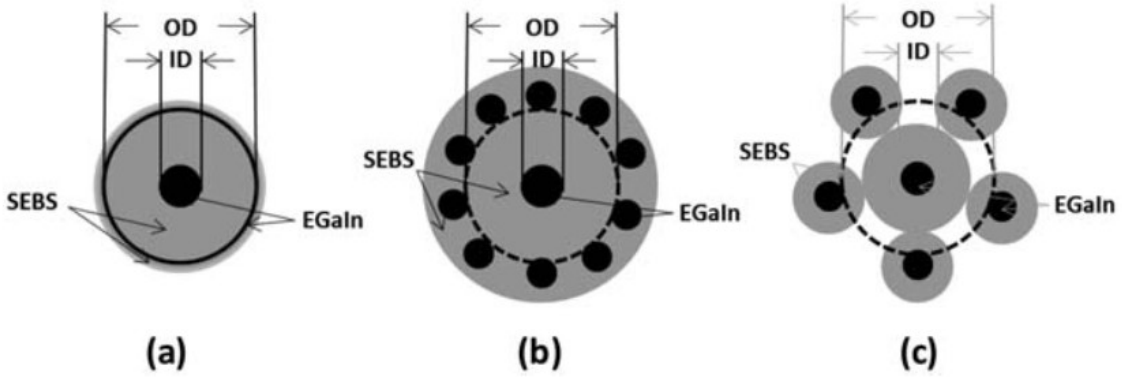

Fig. 29. (a) Ideal coaxial transmission line, (b) a simplified configuration of coaxial wire, (c) Real hand woven configuration of the fabricated coaxial line. [Reprinted from [140] with permission from John Wiley & Sons, Inc.]

2.8.4 Electrodes

LM can be used just as an electrode for the rest of the device instead of traditional solid electrodes [188-189]. Thanks to the monolithic fabrication process, these electrodes are “inherently aligned” in the circuit [166]. So et al. investigated their mechanical stability relationship with flow rate and pressure of nearby fluid, pH range, and bias DC and AC levels [166].

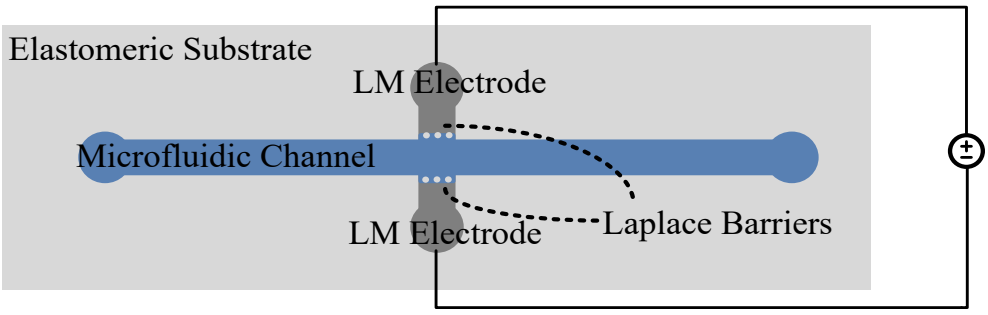

Fig. 30. Hybrid microfluidic LM electrode system. This concept has been used in micro-coulter counter design [188]. Inspired from [166].

2.8.5 Arrays of Conductors

Arrangement of periodic multiple unit cells of conductors can function as antenna arrays, frequency selective surfaces (FSS), or metamaterials. Frequency selective surfaces (FSS) are designed to block or pass electromagnetic fields depending on their bandwidth. Li et al. has designed an FSS with embedded galinstan filled Teflon tubes [168]. By moving the LM droplets in the channels, the equivalent capacitance of FSS changes, and this shifts the transmission coefficient for different frequencies [168]. Another example of tunable fluidic FSS, is Yang's et al. design of a cloaking meta-skin which is made of LM filled split ring resonators in Ecoflex® substrate and can dynamically change its resonance frequency by stretching [169]. Metamaterials are engineered structures with properties which are not normally found in nature such as negative refractive index [190]. Kim et al. has fabricated a wideband metamaterial absorber by injecting LM in PDMS channels which works in different frequencies with or without the presence of LM [191].

2.8.6 Unusual Applications of Liquid Metal Alloys

2.8.6.1 Speaker and Microphone

A neodymium magnet attached to a spiral micro-channel of galinstan in PDMS has been used for a stretchable acoustic device working as a loudspeaker and microphone simultaneously [192]. This loudspeaker/microphone remains functional even after stretching to 30% biaxial strain which is very important in fabricating conformal and body attachable acoustic devices.

2.8.6.2 Soft and Reconfigurable Photo-Mask

Galinstan, unlike PDMS, is UV opaque. Therefore, PDMS channels filled with LM can act as a photo-mask for photolithography with a minimum feature size of 5 micrometers [193]. This mask can be stretched to reconfigure the mask pattern however due to the imperfect contact in this mode, the patterns would be blurry to some extent.

2.8.6.3 Heater

Meandered traces of galinstan in acrylic VHB elastomer substrate has been used as a flexible Joule heater to heat a nearby embedded Field's metal or shape memory polymer [98]. Due to high length of galinstan trace, by applying electrical current to it the temperature of fields metal or shape memory polymer goes up and this is used for rigidity tuning of the system.

2.9 Electrical Connection

A key downside with gallium is that it attacks most metals aggressively even at low temperatures and dissolves them [10][45]. Therefore, realizing a reliable interconnect between the liquid alloy and conventional solid circuits and power sources is challenging but essential for the fabrication of integrated devices. Ga reacts more aggressively with some metals such as aluminum, copper, zinc, and platinum but it takes more time to damage brass, nickel, and gold [10][194-195]. Tungsten, titanium, and graphene are compatible with LMs [45]. Stainless steel has also tremendous corrosion resistance to Ga [194]. Galinstan is less chemically reactive compared to gallium to other metals (except to aluminum and copper) [196]. Ahlberg et al. has used deposited graphene as a diffusion barrier for aluminum electrodes to prevent direct Ga-Al contact [197].

2.10 Conclusion

In this chapter, the present research in soft electronics and its components including the conductors, substrates, patterning methods, and bonding techniques have been reviewed. Although, LM based technology is a promising solution for the next generation of soft electronics, there are still significant uncertainties and challenges in designing complex and highly accurate structures, precise control over the LM filling of microfluidic channels, chip-to-world interconnection, efficient and temporary bonding techniques, and the scope of potential applications in electronics. These issues will be addressed in the following chapters.

CHAPTER 3: TEST STRUCTURES (FABRICATION AND CHARACTERIZATION)

3.1 Introduction

Injection molding and vacuum assisted filling of LMs into microchannels is a crucial step in co-fabrication of high resolution miniaturized microfluidic or microsolidic electronics [43]. Such co-fabricated circuits have potentially lower fabrication costs and minimal required equipment [198]. Co-fabrication of a fluidic microelectronic system contains several steps including: 1) fabrication of the elastomeric channel templates with basic microfluidic or soft lithographic techniques, 2) sealing of microfluidic channels with different bonding methods, 3) injection of liquid conductor into the hollow arrangements, and 4) placing world-to-chip mechanical and electrical inter-connections. Driving LM into small microsystems with multiple divisions and complex shapes is a very challenging process [106] and there is a need for extensive research on flow control of LM in micro-channels due to the complex viscoelastic characteristics of Ga-based liquid alloys.

The critical pressure for filling a channel is equal to the pressure drop across the liquid-solid interface and is calculated from Laplace law as shown in equation 8. This pressure is proportional to the surface tension, contact angle between the liquid and channel walls, and is inversely proportional to the hydraulic diameter of channels. In general, the filling of microchannels can occur with capillary action, or active

injection/suction. In case of LMs such as Ga alloys and mercury, due to extremely high interfacial forces, capillary action does not work in favor of filling, therefore an active positive or negative pressure source is required to surpass their relatively large critical Laplace pressure. For Ga based metals such as EGaIn specifically, an oxide layer with elastic characteristics, forms on their surfaces in presence of oxygen and the bulk LM needs to break through this oxide skin with a critical surface stress to flow. Dickey et al. tested rheological parameters of oxidized EGaIn with parallel plate rheometer, and measured its surface tension to be approximately 0.5 N/m [66], however Zrnic et al. reported this value to be close to 0.63 with the pendant drop method [56]. Dickey et al. simplified the critical pressure for EGaIn to be injected to PDMS channels [66]:

$$P_c \times CD \propto 1.1(N/m^2) \quad \text{Eq.12}$$

Where P_c is the critical pressure in Pa and CD is the critical dimension or channel's cross section in meters. In spite of this study, design of LM filled electronics have not reached its full potential due to the practical limitations in the filling process. Quantifying the filling parameters for different materials provides the opportunity to design microfluidic components such as phase-guides and valves to control the filling precisely and will be investigated in this chapter.

Fabrication of large/wide planar structures, and structures with multiple branches and intersections have been very challenging and sometimes impossible in the past [101] and that is why most of the previous devices are made of very simple geometries with only two terminals [6]. One of the solutions practiced in order to entirely fill structures with multiple outlets and inlets and intersections is electro-recapillarity. In electro-

recapillarity the interfacial tension is changed (deduction or deposition of the oxide layer) by applying a voltage in order to fill or empty a channel in a desired direction [65]. To guarantee the electrical connection in this method, the channels need to be filled with an electrolyte solution prior to metal filling or while emptying which is one of the complications of this method. Also, the location of the flow front and its directional advancement is not accurate as shown in Fig. 31. Also, in this method and the system will not stay stable upon disconnecting the biased voltage [199].

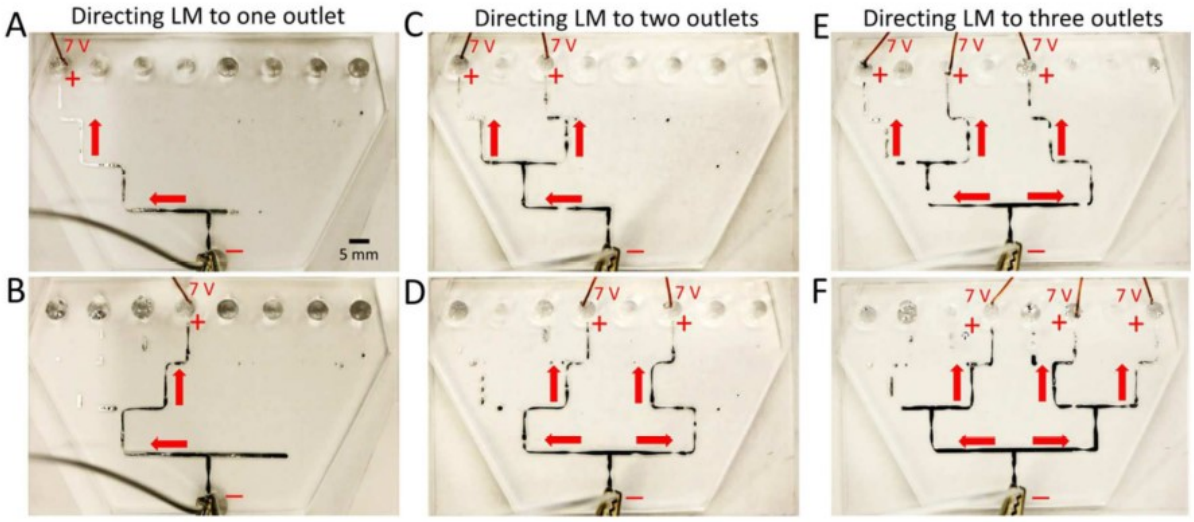

Fig. 31. Directing LM to: (A) and (B) one outlet, (C) and (D) two outlets, and (E) and (F) three outlets with electrorecapillarity. Precise control of LM flow is not possible. [Reproduced from [200] with permission from Royal Society of Chemistry]

Another method to control the flow advancement is using hydrophobic valves to stop the flow progress below a certain level of pressure. These valves work by creating a pressure gradient as the result of the system geometry that makes the LM stop when it reaches them. Cylindrical or cubical Laplace barriers have been used for this purpose in

forming inherently aligned electrodes in microsystems [166][188], resonators and [201], and antennas [129][174]. While employing pressure barriers seem to be a promising method for flow control, more in-depth quantitative research is needed to be able to develop hydrophobic valves with optimized configurations and dimensions that result in minimal number of valves in the system, minimum trapped air, and a safe pressure margin that ensures an efficient and controllable filling.

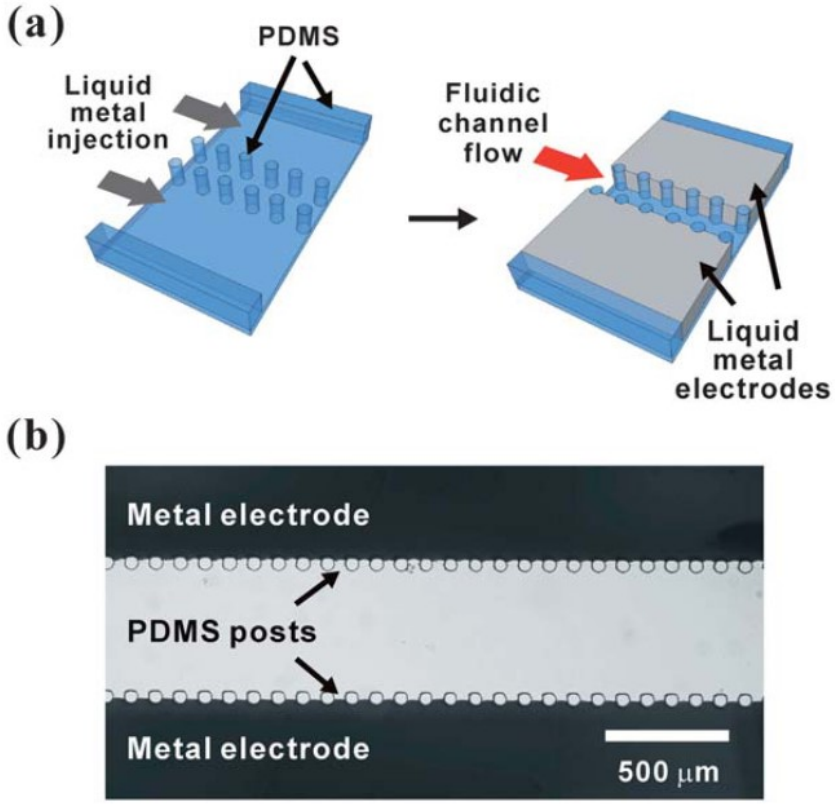

Fig. 32. (a) Fabrication process of LM electrodes with cylindrical posts, and (b) an optical image of the actual electrode. [Reproduced from [166] with permission of Royal Society of Chemistry]

Wide planar arrangements of LM are needed in realization of microstrip antennas, ground planes, and other coplanar circuit elements. Fabricating large continuous

microfluidic structures with very low aspect ratios (height : width) has been extremely challenging [6][101][129]. The collapse of channels' back layers which seals the traces is a common cause of failure. Using a thicker backing layer or a stiffer material would compromise the flexibility of the final structure. Another difficulty with wide microchannels is the inconsistent filling towards the outlet which leaves air gaps behind instead of fully filled LM structures and this affects the electromagnetic performance. Hayes et al. has used cylindrical PDMS posts for fabrication of a broad-area patch antenna. In this design, the LM fills a meandering track leaving air bubbles in between PDMS posts as shown in Fig. 33 and when this process is finished the substrate is pressed with a finger to increase the pressure for filling the air gaps between the posts with LM [129]. This innovative filling method however, suffers from a number of uncertainties. The additional step of manually pressurizing the substrate, is a randomly uneven procedure that leads to non-uniform pressures in different locations. This can damage the posts or seal the channels in case of elevated pressures and causes air bubbles to remain where the pressure is lower than expected. Trapped air between the posts forces the electrical current to turn around in a spiral path instead of its intended distribution. Such challenges are critical especially in more delicate and complex designs and therefore, it is beneficial to avoid this step if possible. Another issue with this tactic is that by pushing the air bubbles out when the other sections are filled entirely, they most likely cannot get to the outlet but instead are relocated inside the patch structure. We investigate the optimization of the shape, size, and distances of Laplace barriers in order to fill the LM in meandering pathway that pushes away the air bubbles on the fly.

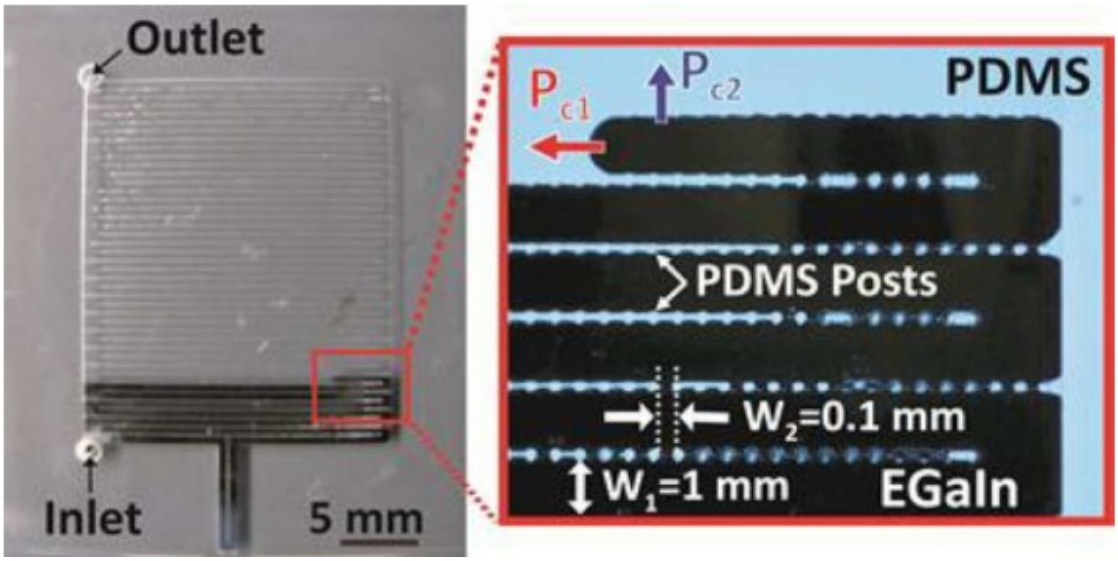

Fig. 33. LM filling of a microstrip patch antenna. Most of the spacing between PDMS posts are not filled with LM. [Reprinted from [129] © 2012 IEEE]

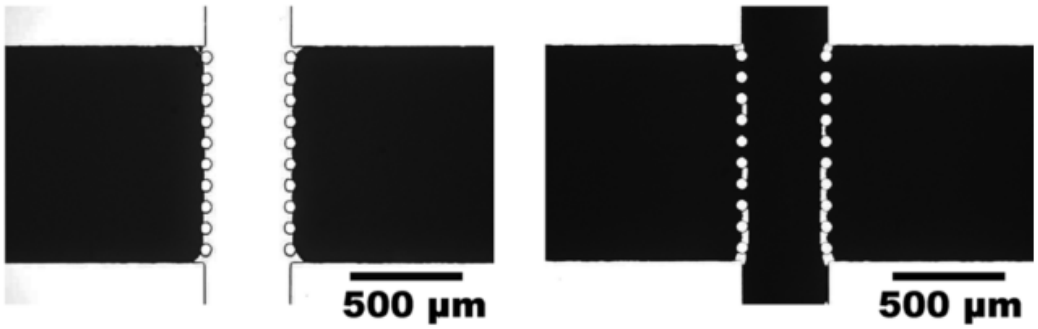

(a) (b)

Fig. 34. (a) LM flow stopped at valves' entrances, and (b) passes through the valves. Although the pressure has reached its critical value for valves, most of the gaps between posts are not filled with LM. [Reproduced from [174] with permission of AIP publishing]

3.2 Materials and Methods

3.2.1 Fabrication Method

3.2.1.1 Fabrication of Gecko-adhesive Based Structures

A versatile, reliable, and repeatable fabrication method is used for manufacturing micro-structures in SEBS (Kraton® G1657 and Kraton® G1645) which will later be filled with EGaIn. For biocompatibility purposes, it is crucial to have a reliable bonding so that the metals do not leak out of the system [202]. Mushroom shaped pillars and gaskets with undercuts which provide the system with the natural reversible bonding, are created by uncollimated exposure of 254 nm light to PMMA master mold. In traditional microfluidics, PDMS forms the final device, but here it is a mold for SEBS and it works perfectly even after 100s of working cycles [161]. The fabrication process is explained in the following [91]:

1. A Thin (~2 μm) layer of SU-8 2002 MicroChem® photoresist is spin coated on a PMMA substrate with an elevated speed up to 3000 rpm.

2. The substrate is soft-baked in a convection oven at 85°C for 2 minutes to evaporate the solvent in SU-8.

3. The system is exposed to UV light through a chrome coated glass mask (with 450 mJ/cm^2 exposure dose and 365 nm wavelength).

4. The system is post exposure baked in a convection oven at 85°C for 3 minutes. At this point a pale image of patterned SU-8 is visible.

5. Unexposed SU-8 is developed in SU-8 developer with mild agitations for one 1 minute, rinsed with IPA, and dried with nitrogen. The substrate is observed under microscope to make sure every section with un-crosslinked SU-8 is removed. The process is repeated if necessary (total development time is about 80 seconds).

6. PMMA is patterned with 254 nm wavelength uncollimated UV light for 12 hours with an intensity of approximately 4.4 mW/cm^2 . In this step cross-linked SU-8 works as a mask for patterning PMMA and the under-cuts are created underneath the SU-8 layer.

7. To release any residual stress the substrate will be baked in oven for 24 hours at 85°C. This step minimizes future cracks and substrate fracture.

8. Remaining SU-8 and PMMA underneath are developed in SU-8 developer for 1 hour followed by development in IPA-SU-8 developer solution (1:1) for 4 minutes and 20 seconds to slow down the development process. The height of the features in PMMA are now measured with an optical profilometer to make sure they are accurate (70 μm). At the end, the substrate is rinsed with IPA and water and dried with nitrogen.

9. A PDMS master mold (TC-5030 from BJB Enterprises) is molded against PMMA and the patterns are replicated in this silicone rubber.

10. SEBS is compressed with 150 lb force against the PDMS mold on a hot plate at 220°C so that all the features are replicated in SEBS.

11. The patterned SEBS is put in contact with another flat SEBS layer to bond and seal the channels.

It is important to note that steps 1 to 8 which require clean-room facilities are only done once for a single design and the rest of the steps for manufacturing multiple devices can be done in normal laboratories with an inexpensive and fairly straightforward procedure.

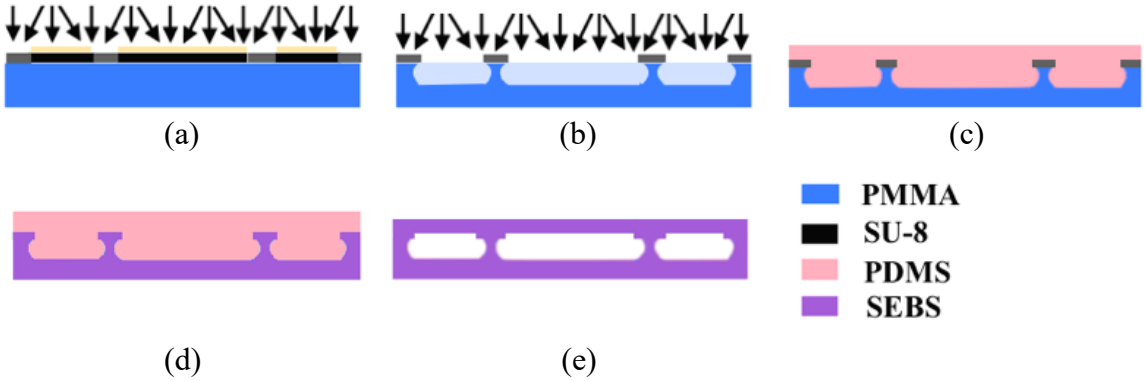

Fig. 35. Fabrication procedure: (a) UV exposure of SU-8 with chrome mask, (b) UV exposure of PMMA with SU-8 as a mask, (c) replicating PMMA patterns in PDMS, (d) thermo-compressive molding of SEBS against PDMS, and (e) sealing SEBS channels.

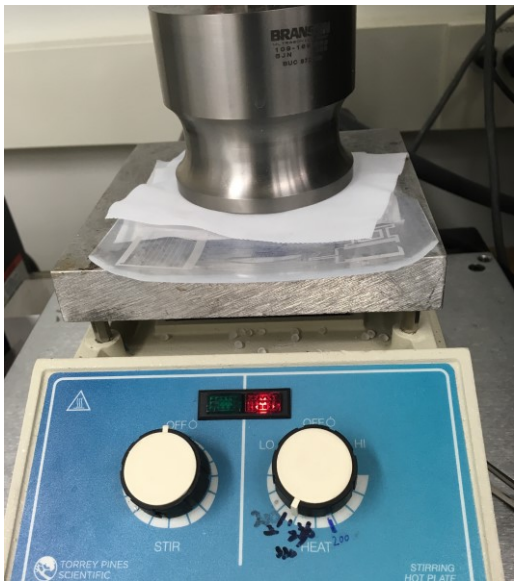

Fig. 36. Replicating PDMS patterns in SEBS with thermo-compressive molding process using an embosser on a hotplate.

3.2.1.2 Fabrication Procedure for Structures with Straight Side-walls

When there is no need for reversible bonding, or the mushroom-shaped profile of the gecko-based gaskets may bring inaccuracy into calculations, a silicon based photolithographic method is used for making micro-channels. Two methods have been tried to make high aspect ratio micro-channels which are explained in this section. These two methods are different from section 3.2.1.1 only in the method of making the master mold however the steps 9 to 11 in the previous section are repeated once the master mold is prepared.

In the first method, two layers of SU-8 are coated on silicon in order to get the desired height in SU-8 (100 μm). After Piranha cleaning of silicon wafer, it is spin coated with an increasing speed up to 2500 rpm for 30 seconds to create a thin (12 μm) layer of SU-8 2010. Afterwards, the wafer will be baked on a hot plat at 50ºC for 2 minutes and then at 80 ºC for 3 minutes. The first spin coated SU-8 acts as an adhesive for the next layer. Then, SU-8 2050 is spin coated followed by a pre-bake step on a hot plate for 2 minutes at 65 ºC and then for 8 minutes at 95 ºC. The wafer is then exposed to 200 mJ/cm^2 dosage of UV light with 365 nm wavelength. The post exposure baking time is 9 minutes at 85 ºC and it is followed by 7 minutes of development with SU-8 developer. The final height measured with a profilometer is about 101 μm. Releasing PDMS from the wafer is problematic due to their very high adhesion and can lead to breaking of silicon wafer. Therefore, the SU-8 covered silicon wafer is silanized in a vacuum chamber with trichlorosilane to air releasing the PDMS mold later on. Once the PDMS

mold is prepared, it is used to make structures in SEBS. For bonding of SEBS channels made with this method, they are thermally bonded on a hot plate at 85 ºC for 30 minutes.

In the second fabrication method, the final structures are built in silicon wafer itself. A 3 μm thick SU-8 2002 layer is spin coated on silicon at 1000 rpm for 40 seconds, prebaked at 95 ºC for 2 minutes, exposed to 80 mJ/cm^2 UV light (365 nm), baked again at 95 ºC for 150 seconds, and developed in SU-8 developer for 1 minute. This patterned SU-8 works as a mask for etching silicon with Inductively Coupled Plasma Reactive Ion Etching (ICPRIE) process. To get 40 μm depth, 160 cycles of high rate 1 stage modified Bosch cycles are performed. The SU-8 then is stripped with a plasma barrel etcher and the remaining silicon is silanized with the same procedure used before.

3.2.2 Filling Characterization

In order to obtain the critical filling pressure for microfluidic channels, a series of channels with various dimensions are fabricated and their filling pressure is measured. The channels are made of a class of SEBS polymer (Kraton® G1657) with thermo-compressive molding and are filled with EGaIn LM. Kraton® G1657 has 750% elongation at break, 3400 psi tensile strength, a melt index of 22 grams/10min, and its 300% modulus is 350 psi [138]. In order to ensure that the expansion of channels has minimal influence on the filling pressure, these tests are done with a temporary bonded rigid backing layer made of polypropylene and SEBS. The measurement set-up consists of a pressure regulator and a digital pressure sensor (Measurement Specialities-M5100) placed upstream of the channel's inlet to measure the air pressure applied to the LM. The

pressure sensor is powered with a programmable DC power supply (NI PXI 4110) and the pressure data is read with a digital multimeter (NI PXI 4070) in volt.

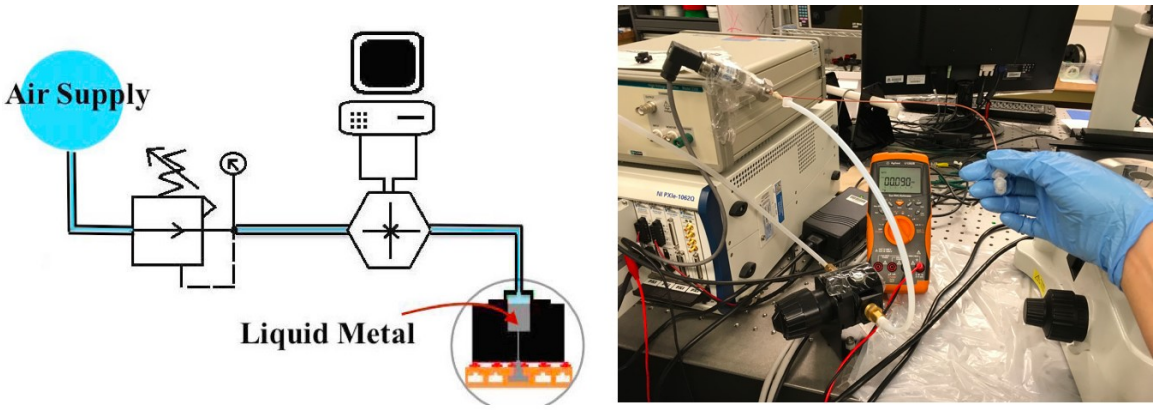

Fig. 37. The pressure measurement test set-up.

Suction of LM into the microchannels with a negative pressure can lead to the collapsing of the low aspect ratio structures especially in softer SEBS classes such as Kraton® G1645 (Fig. 38) which is harder to fill and has lower replication quality compared to Kraton® G1657 [123]. This is why using a positive pressure is preferred in most of the cases.

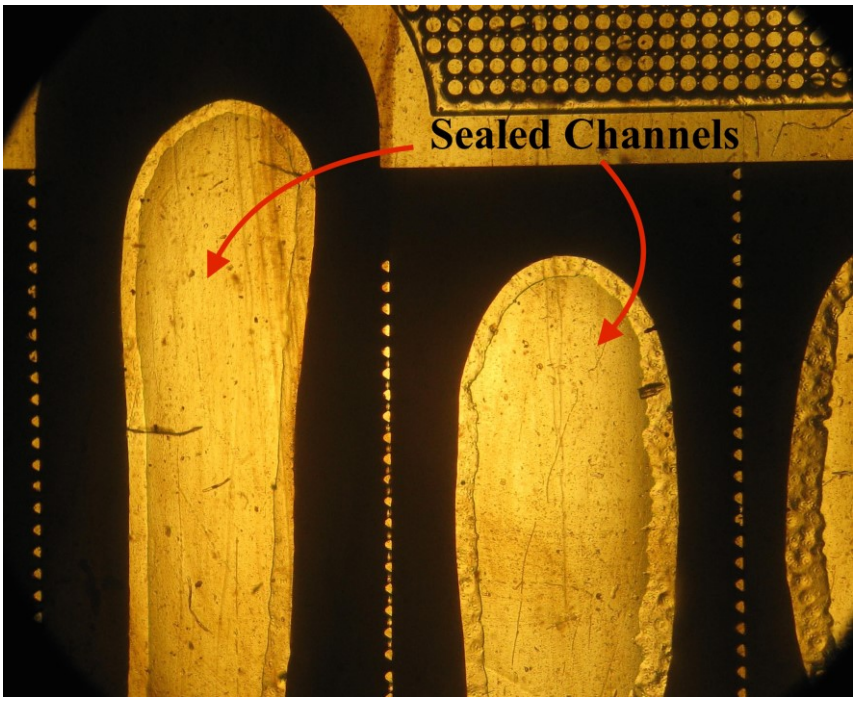

Fig. 38. Sealing of microfluidics channels upon applying the required negative pressure for filling.

In order to standardize the filling process, a polymethyl methacrylate (PMMA) reservoir with an attached SEBS gecko-blister is used to create a strong temporary bonding to the channel's inlet. This SEBS gecko-blister can endure pressures as high as 40 psi (and up to 100 psi in presence of a rigid backing layer) [161] which is far beyond the required pressure for filling micro-scale channels. The use of this world to chip interface, prevents any air leakage which is also confirmed by reading the calibrated pressure sensor. After the injection is complete, the LM reservoir can be detached and reused for 100s of cycles.

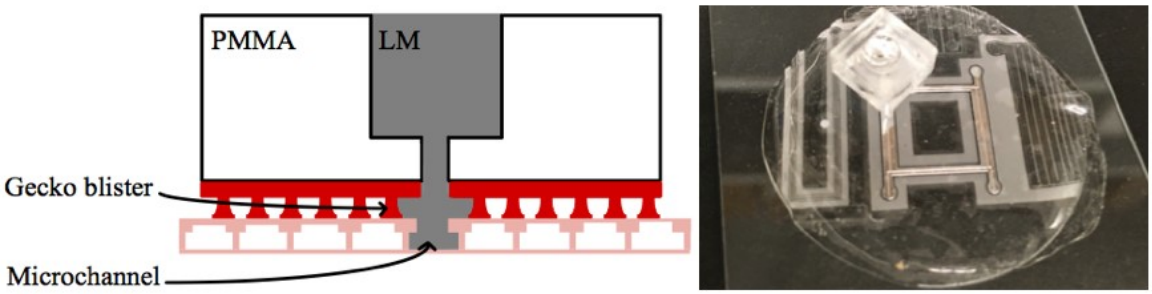

(a) (b)

Fig. 39. (a) Schematic view of the stick-n-play PMMA chip with attached gecko blister, and (b) filling of a power divider with this temporarily bonded filling chip.

For realizing low aspect ratio structures in LM, meandered parallel channels are separated with posts which have trapezoidal, circular, or rectangular bases with various entrant angles, various spacing and different sizes. These posts represent the inner channel's wall. It is expected when the LM is filling the main channel, it pins to the posts but does not pass through them. The LM adhered to the pillars, merges with the metal flow from the following parallel channel and pushes the air out at the same time (Fig. 40). The constant creation of the oxide skin due to the existence of oxygen stabilizes the LM and does not allow it to flow readily through the posts.

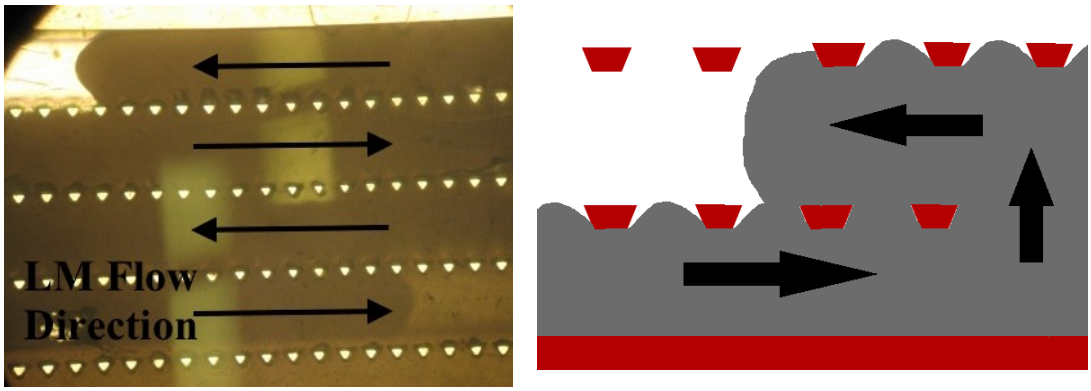

Fig. 40. Optical photograph of the microchannels while filling with LM. The flow merges the LM pinned between the posts in the nearby channel.

Another challenge with injection molding is its limitation in fabricating isolated features. Discrete arrays of conductors are extensively used as antenna arrays, frequency selective surfaces, and metamaterials and are fabricated either with injecting every unit cell independently which is a time consuming and costly procedure [169] or by using other manufacturing techniques such as 3D printing [106] which suffers from drawbacks such as rough surfaces and encapsulating complications [118]. In this work, we use a combination of hydrophobic valves and diluted HCl in order to accurately split a continuous LM trace to smaller isolated features.

3.3 Result and Discussion

3.3.1 Pressure Measurement

Fig. 41 is a plot of air inlet pressure as a function of (D'=1/W+1/H) which is inversely proportional to the hydraulic diameter for a rectangular channel. A regression line can be fitted to the points in Fig. 41 with a high coefficient of determination

(R^2=0.998). The randomly distributed residual plot in Appendix B verifies this linear fit. The line relates pressure to channels dimensions with the following equation.

$$P = 160\ (\frac{1}{W} + \frac{1}{H}) \qquad \text{Eq.13}$$

Where, P is the critical pressure applied to LM at the entrance of channels in Psi, and W and H are the width and height of the channel's cross section respectively in micrometers. Based on equation 9, the slope of this line indicates the product of the surface tension and contact angle of LM on the channels walls. The contact angle of EGaIn on SEBS surface can be estimated to be 150˚ as shown in Fig. 42. This will result in a value of ~0.637 N/m for the surface tension of EGaIn which is very close to the reported value of 0.63 N/m in [56].

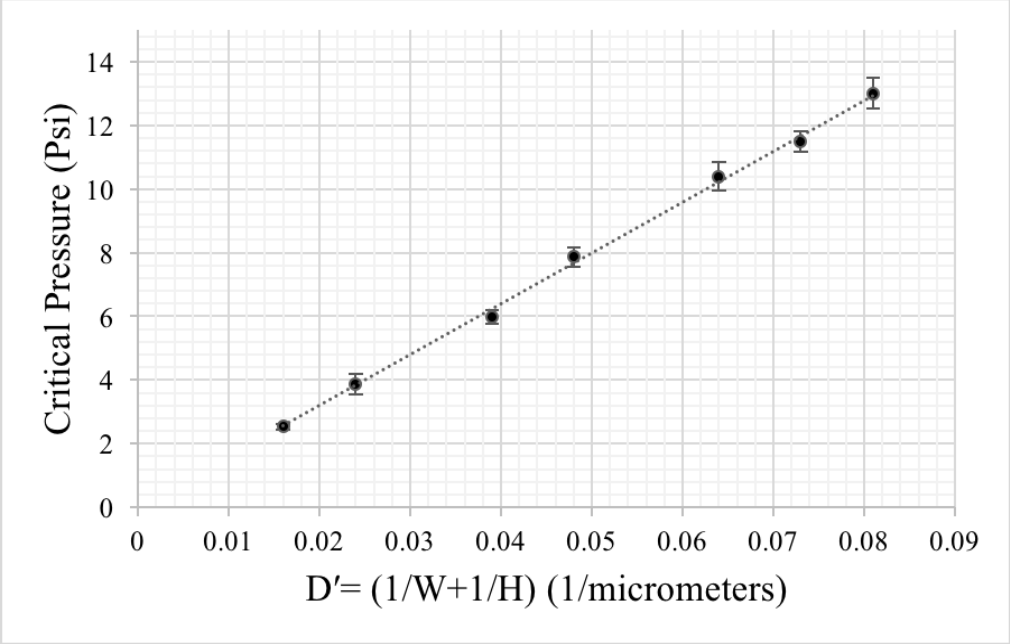

Fig. 41. The average critical pressure of EGaIn for filling microchannels made of SEBS (Kraton® G1657) as a function of channel dimensions.

Fig. 42. Top-down optical image of EGaIn with SEBS channel walls for determining the contact angle.

3.3.2 Hydrophobic Valves

Based on the relationship between the pressure and the dimensions of the channels, hydrophobic valves can be optimized to direct the flow in desired directions. To test the proficiency of these valves, a series of circular and triangular micro-valves are utilized for directional distributing of LM in complex structures. Fig. 43 shows a SEBS made microstructure consisting of a straight channel and a delay channel filled entirely with LM thanks to two sets of Laplace barriers placed near the outlet of the channel.

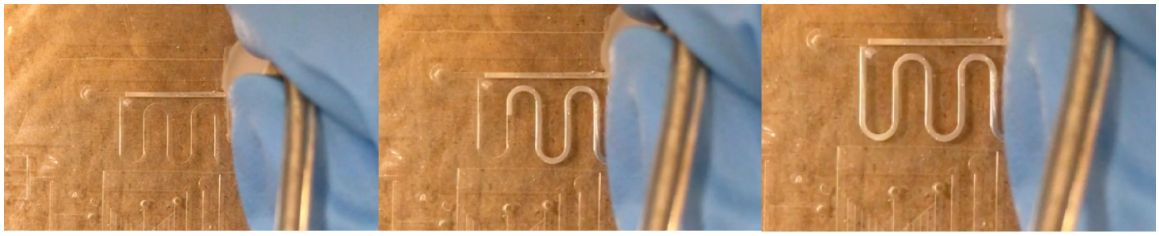

(a) (b) (c)

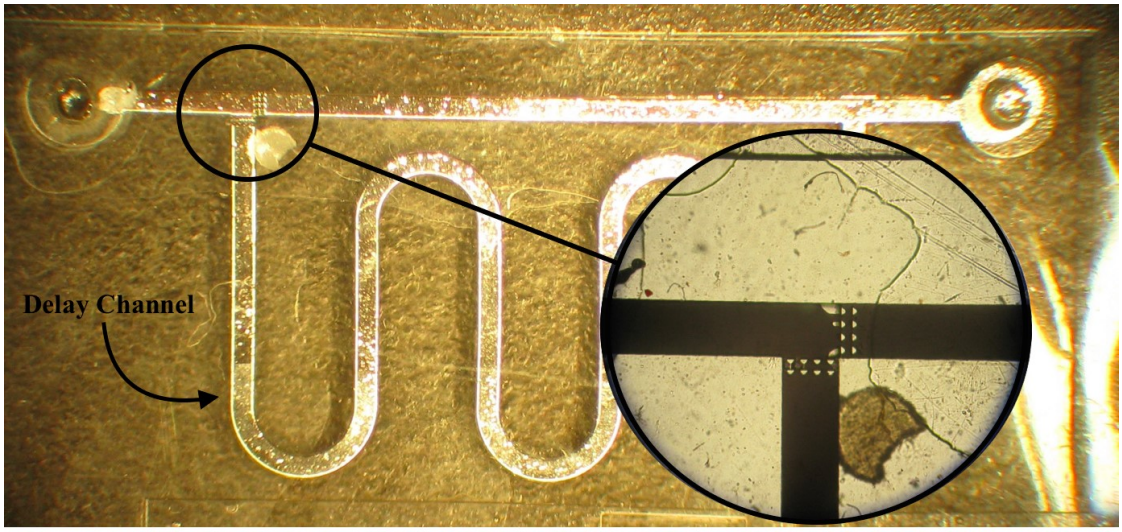

(d)

Fig. 43. LM filled microstructure consisting of a straight channel and a delay channel. (a) LM fills the straight channel and stops at the micro-valves, (b) and (c) delay channel fills, and (d) fully filled structure and magnified view of micro-valves.

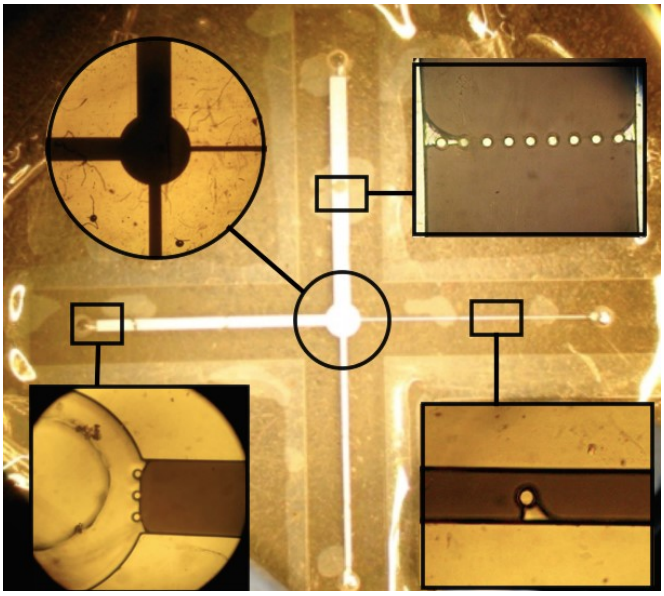

Fig. 44. Channels with different widths filled from a single central inlet due to the hydrophobic valves and magnified image of these valves.

A more complicated design of branched structures can be seen in Fig. 45 where LM from a single inlet distributes into eight outlets simultaneously. This is possible with three sets of valves located throughout the channels. The first, second, and third sets of valves impose a critical pressure gradient of 5.9 Psi, 15.5 Psi, and 26.2 Psi, respectively, compared to the critical pressure at the main channel. This means in order to force the metal out through the exits, the applied pressure needs to increase up to about 10 times of its initial value required for getting the metal inside the main channel. The configuration of this design has been explicitly displayed in Fig. 45.

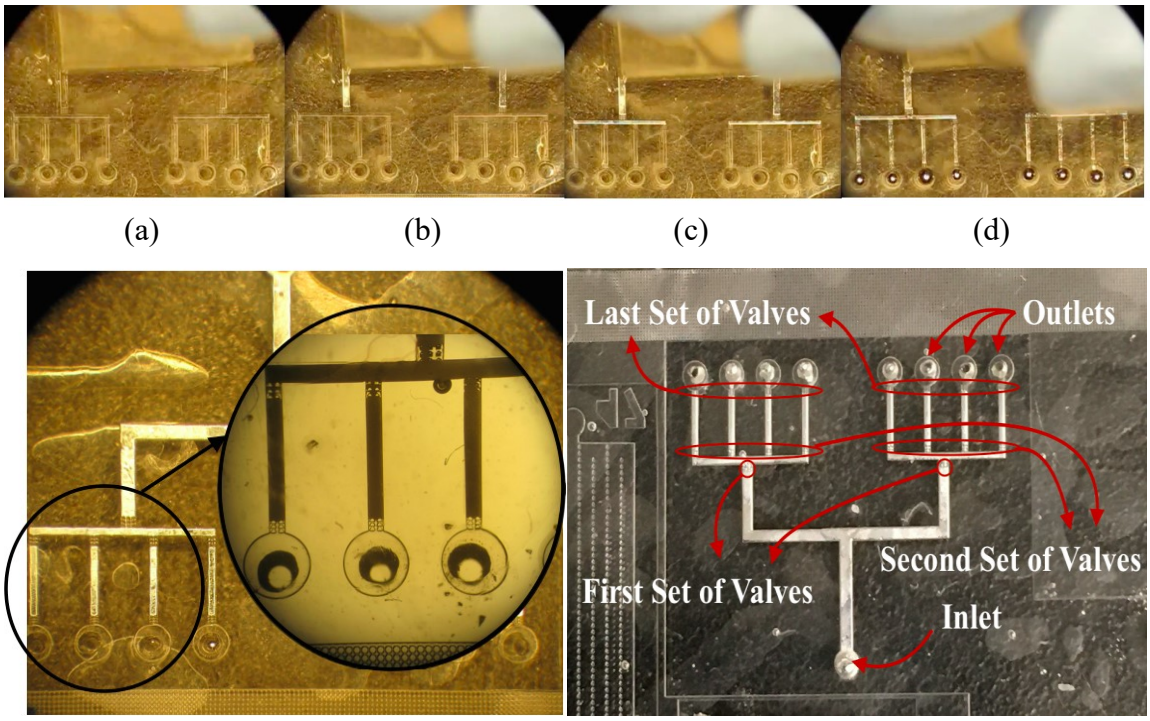

(a) (b) (c) (d)

(e) (f)

Fig. 45. (a) Empty channels, (b) first round of barriers block the flow of LM after being divided between two arms, (c) LM stops at the second arrangement of triangular posts, (d) all the eight outlets are filled with EGaIn, (e) magnified photo of the triangular pillars preventing LM flow, and (f) locating the valves within the system.

3.3.3 Low Aspect Ratio Structures

As mentioned before, sheet-like low aspect ratio structures of LM are challenging to manufacture due to sagging of micro-structures, uneven filling process, and trapped air. The objective of this section is to design an arrangement where extremely low aspect ratio structures are split into smaller structures with smaller widths separated by micro-posts. Such posts direct the LM to go through a meandered path as shown in Fig. 46 as well as supporting the channels' sealing layer. The goal is to optimize the distance of the

posts so that the LM can easily enter the gap and pin to the posts, but it does not exit until it joins the flow in the next channel. Ideally, minimizing the number of posts is desirable, however, if these posts are too far away from each other the sealing layer may sag, or LM may flow perpendicular to the desired direction. Once LM breaks through its oxide layer and starts to flow, it is possibly easier to flow in the normal direction as well although the inlet pressure is kept below the critical pressure for passing through posts at all times. Therefore, it is beneficial to design a system that will not allow for perpendicular flow within a safe pressure margin. Trapezoidal posts have shown the most promising results compared to rectangular and circular based posts since they provide a tapered cross section where the critical pressure changes along the gap. In Fig. 47 the effect of this tapered cross section on the LM profile can be observed.

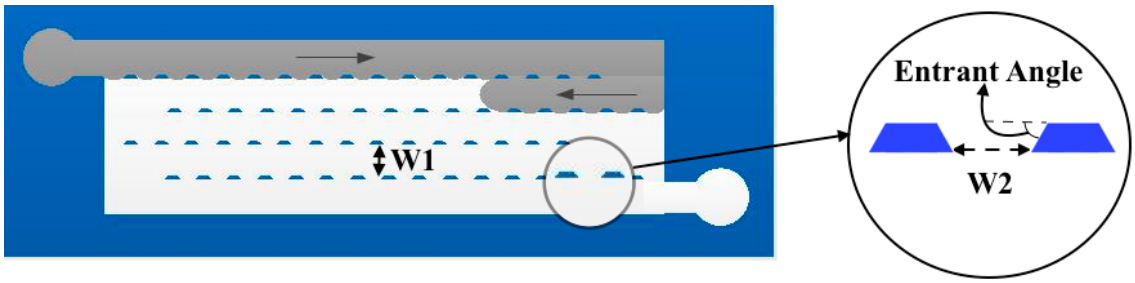

Fig. 46. Filling strategy for low aspect ratio structure divided to narrower traces. W1 is the width between two parallel channels and W2 is the spacing between the pillars.

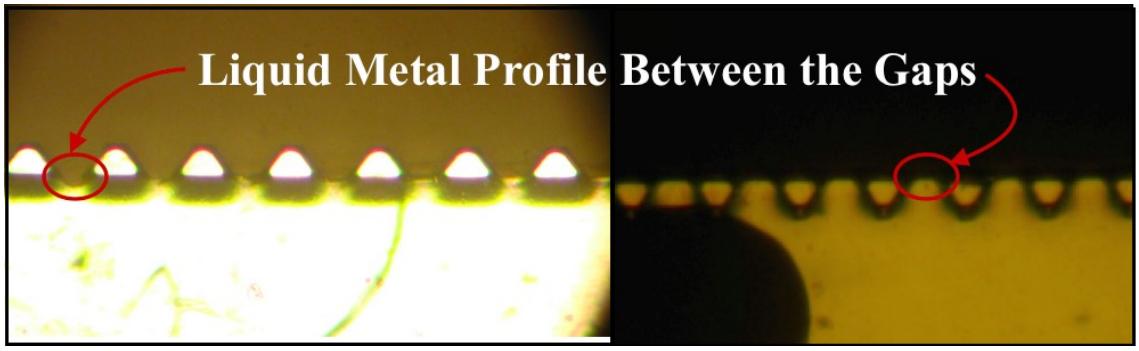

(a) (b)

Fig. 47. Same channel filled in the designed and reverse direction: (a) LM enters the gap between posts when it is filled in the designed direction, (b) air pockets are trapped when system is filled in the reverse direction (The channel next to the narrow part of the gaps is filled first).

Three scenarios have been observed while filling these low AR structures: (a) The gap fills perfectly, (b) there is an air pocket trapped in the gap but it is covered with a layer of LM, and (c) the gap has not been filled with LM as shown in Fig. 48. For electrical connection, case (b) can be considered "success" since the skin depth at GHz frequency range is only a few microns. However, this case looks more like a random incident rather than an intended auto-filling therefore it is considered as a failure. The filling percentage is defined as the ratio of the gaps between posts filled with LM perfectly (scenario a) to the overall number of gaps between posts.

(a) (b) (c)

Fig. 48. (a) An entirely filled gap, (b) the gap is filled but the air pocket exists underneath the metal, (c) the gap has not been filled with LM.

Fig. 49 shows the results for two sets of channels made of pillars with different entrant angles (30° and 45°). The gap's spacing is tested at 7 levels which and is identical for both channel sets. This spacing imposes a higher critical filling pressure in the normal direction rather than the main channel's direction. The difference between these two values is called the pressure gradient and calculated from equation 13. Although pressure gradients under 3.5 Psi have shown very promising results (filling percentages over 99%), the structures failed 70% of the times due to a normal flow towards outlet which resulted in incomplete filling of the device. The pressure gradient of 6.4 Psi has shown the best results in terms of repeatability (no failure) and reliability (low deviation) with an average filling percentage of 95%.

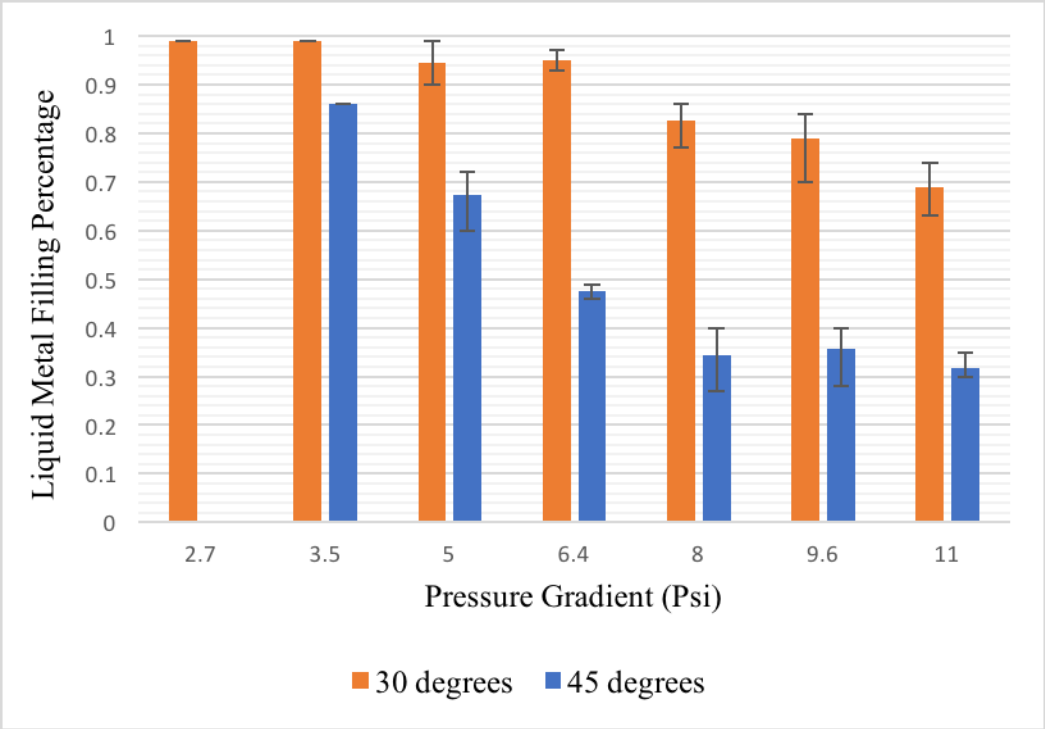

Fig. 49. Percentage of the gaps filled with lm versus the pressure difference for filling the gaps' space compared to the main channel.

3.3.4 Isolated Features

The difficulty in fabricating isolated features has been one of the drawbacks of injection molding for LM based circuits, and that is why researchers have proposed more complex fabrication methods for manufacturing discrete components [99]. Here, we propose a method for realizing discrete elements from a continuous injection molded pattern. In this technique, micro nozzles inject diluted hydrochloric acid (20% wt) into the interconnections which are separated from the main elements with micro-valves. These valves prevent further withdrawal of LM when the deoxidizing acid is injected. In this method, however, the inlets and outlets should be completely closed and the HCl flow should be limited and controlled otherwise the LM beads up driving out of the channels.

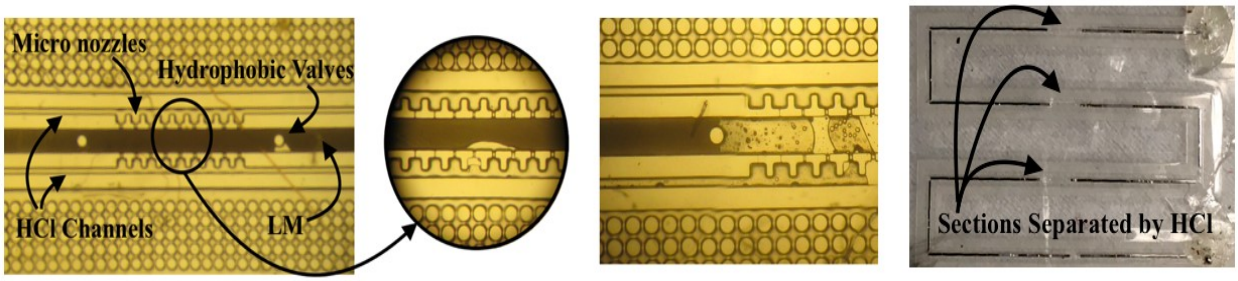

(a) (b) (c) (d)

Fig. 50. Creating isolated features from a monolithic LM trace with diluted HCl injected from micro nozzles. (a) the trace before injecting HCl, (b) magnified view of metal retracting due to the presence of HCl, (c) LM is pinned to the circular post where further withdrawal of LM is avoided, and (d) final arrangement after 24 hours.

As a proof of concept, a wideband antenna named a bow-tie antenna is fabricated which consists of two metal portions shaped like butterfly wings. These wings are fabricated

with a single step injection and are later separated using the procedure explained in this section.

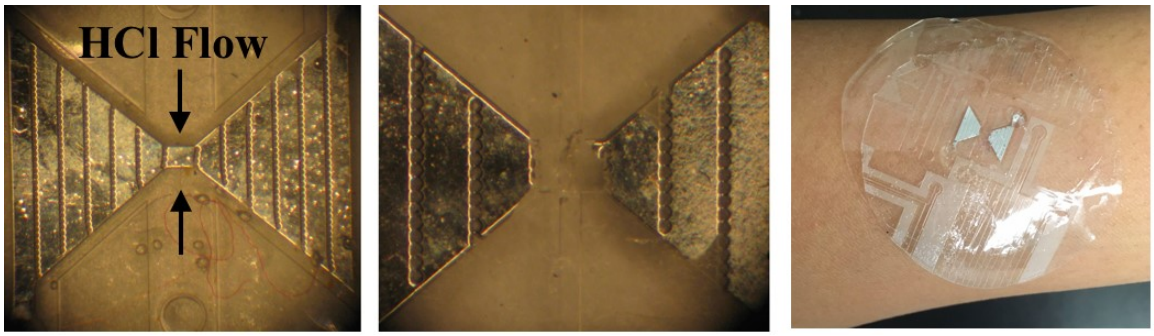

(a) (b) (c)

Fig. 51. (a) Bow-tie antenna structure before HCl injection, (b) using HCl and micro posts, the device has been cut in half to create a bow-tie antenna, and (c) the final device placed on human's skin.

One major difficulty in fabricating LM structures with injection molding is filling very sharp corners and turns due to the high surface tension of EGaIn [102]. In order to enhance the sharp angles' filling, the guiding posts are curved to make the angles larger and air escape openings are located at the corners. The critical pressure for LM to exit through air escape is approximately 10 times larger than the induced pressure, therefore, only air can pass through these exits.

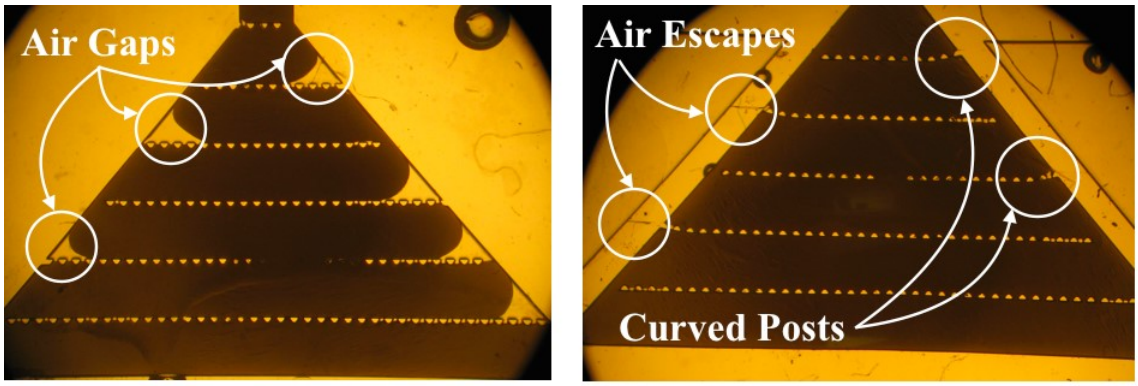

(a) (b)

Fig. 52. Half bow-tie: (a) with straight guiding posts, and (b) with curved posts to reduce sharp angles and air escapes.

3.4 Conclusion

In this chapter, a cost-effective reliable fabrication method is introduced for manufacturing gecko-adhesive based microstructures or microchannels with straight sidewalls. The filling characteristics of these channels with EGaIn LM is studied and optimized. In the first section, it is shown that the critical filling pressure depends on the dimensions of the channel's cross section with a linear function. The slope of this line which depend on the contact angle between the metal and channel's walls and its surface tension are calculated from the fitted regression line. By estimating the contact angle, EGaIn surface tension is calculated and verified with literature. Utilizing the results in the first section, hydrophobic valves are designed to make the control of flow direction and sequence possible. Channels with multiple outlets are then fabricated and tested as a proof of concept. Designing optimized Laplace barriers has made the fabrication of wide planar structures possible due to the stabilizing nature of oxidized EGaIn. Realization of such low aspect ratio structures has remained a limiting factor in using microfluidics for

electronics. These results will be used in the next chapter for making different antennas and ground planes. As the next part of our project, we sought to solve one of the main issues with injection molding in fabricating numerous isolated features. We have used a combination of HCl flow and micro-posts to control the splitting process of a monolithic LM structure into smaller sub devices.

CHAPTER 4: ANTENNAS AND DEVICES

4.1.1 Introduction

In wireless communication technology, the demand for reconfigurable antennas and other communicational devices which can alter their characteristics dynamically is emerging [173]. Some electronic phase shifting methods such as using solid-state or micro-electro-mechanical system (MEMS) switches have been used in the past for reconfigurability [203], but due to reliability issues, lower efficiencies, complexity, and higher costs, mechanically tunable electronics can be an alternative substitute [204]. Here we present compact, lightweight, and mechanically flexible reconfigurable antennas made of EGaIn encapsulated in different classes of SEBS based on the fabrication method and characterizations done in the previous chapter. All the designs are first simulated and optimized in FEM electromagnetic software (ANSYS HFSS) and then fabricated.

In radio frequencies (30-3000 MHz), the electrical current flows through the surface of a conductor rather than its volume. The depth of the conductor in which the electrical currents have penetrated is called the skin depth and can be calculated from the following equation:

$$\delta = \sqrt{\frac{\rho}{\pi \mu f}} \qquad \text{Eq.14}$$

Where, δ is the skin depth, ρ is the electrical resistivity [56], μ is the magnetic permeability, and f is the working frequency, all in SI unit systems. The magnetic permeability of EGaIn can be calculated from the magnetic susceptibility:

$$\mu = \mu_0(1 + X_V) \quad \text{Eq.15}$$

Where, μ_0 is the vacuum permeability ($\mu_0 = 4\pi \times 10^{-7}$ (H/m)) and X_V is the volumetric magnetic susceptibility (dimensionless). The value of the mass magnetic susceptibility for the alloy of 24% In and 76% Ga at room temperature is CGS unit system has been reported to be -0.22×10^{-7} CGSM/g [205].

$$\frac{X_V}{\rho} = X_{mass} \quad \text{Eq.16}$$

$$X_V^{SI} = 4\pi\, X_V^{CGS} \quad \text{Eq.17}$$

Where X_{mass} is the mass magnetic susceptibility and $\rho = 6.25 \times 10^3$ (kg/m^3) is the density of EGaIn. From the aforementioned equations, the skin depth of EGaIn at 2.5 GHz is equal to 5.46 micrometers and it changes to 8.64 microns at 1 GHz. The height of these features is about 70 micrometers which is more than 5 times of the skin depth of EGaIn in 2.5 GHz.

In this chapter after measuring the electrical properties of the substrate, antenna configurations are shown and their properties are measured and compared to theory.

4.1.2 Devices and Measurement method

4.1.2.1 Electrical Properties

Two of the most significant propagative properties of a substrate includes its relative permittivity (dielectric constant or ε_r) and its loss tangent ($\tan\delta$). The dielectric constant is the ratio of permittivity of the substrate to the permittivity of free space which is $\approx 8.85 \times 10^{-12}$ $m^{-3}kg^{-1}s^4A^2$ and the loss tangent represents dielectric losses (electromagnetic energy dissipation). These two properties are frequency dependent so they need to be measured around the working frequency to be valid. In order to do these measurements, a 2 cm thick sample of Kraton® G1657 is fabricated and measured with KEYCOM dielectric measurement kit (model number DPS16). The values for ε_r and $\tan\delta$ at 3.5 GHz are 2.3 and 0.07, respectively. Although the loss tangent of SEBS is a little higher than the values reported for PDMS (≈ 0.04) [204], thanks to the gecko-based adhesive architecture, a considerable volume of the dielectric is made out of air (unlike solid PDMS microfluidics systems) which reduces the effective loss of the system.

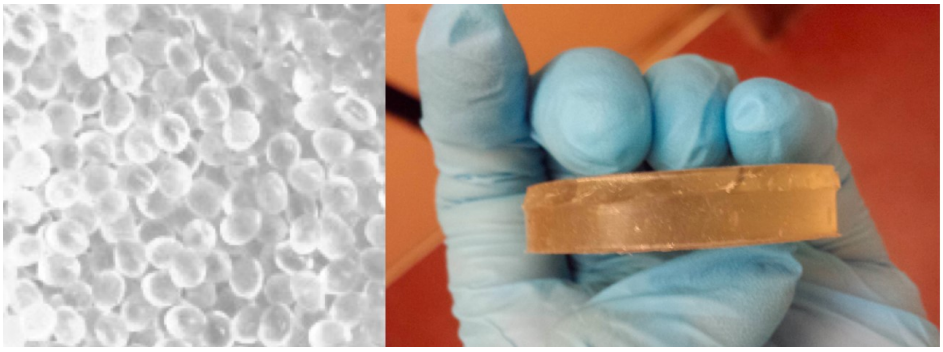

(a) (b)

Fig. 53. (a) Kraton® G1657 pellets and (b) molded SEBS sample for measuring electrical properties.

4.1.2.2 Devices

As the first proof of concept, a stretchable folded dipole antenna is fabricated which can tune its working frequency by changing its electrical length. Folded dipole is a half-wavelength resonant antenna in which the dipole arms are folded back to connect to each other and form a closed loop. Its radiation pattern should ideally be like a half-wave dipole which has the maximum direction at a right angle to the main radiator. Since folded dipoles are resonant dipoles (with narrow bandwidth), it is very beneficial to have the ability to tune their frequencies which depend on their electrical length. In free space for an infinitely thin conductor, the electrical and mechanical lengths are equal. In reality, however, the electrical length is slightly larger with a modification factor [206]. Here, for the dipole antennas, by increasing the physical length (stretching the antenna), the electrical length increases as well and the working frequency shifts down. The dimensions and a scanning electron microscopic (SEM) photo of the fabricated dipole antenna are shown in Fig. 54 and Fig. 55.

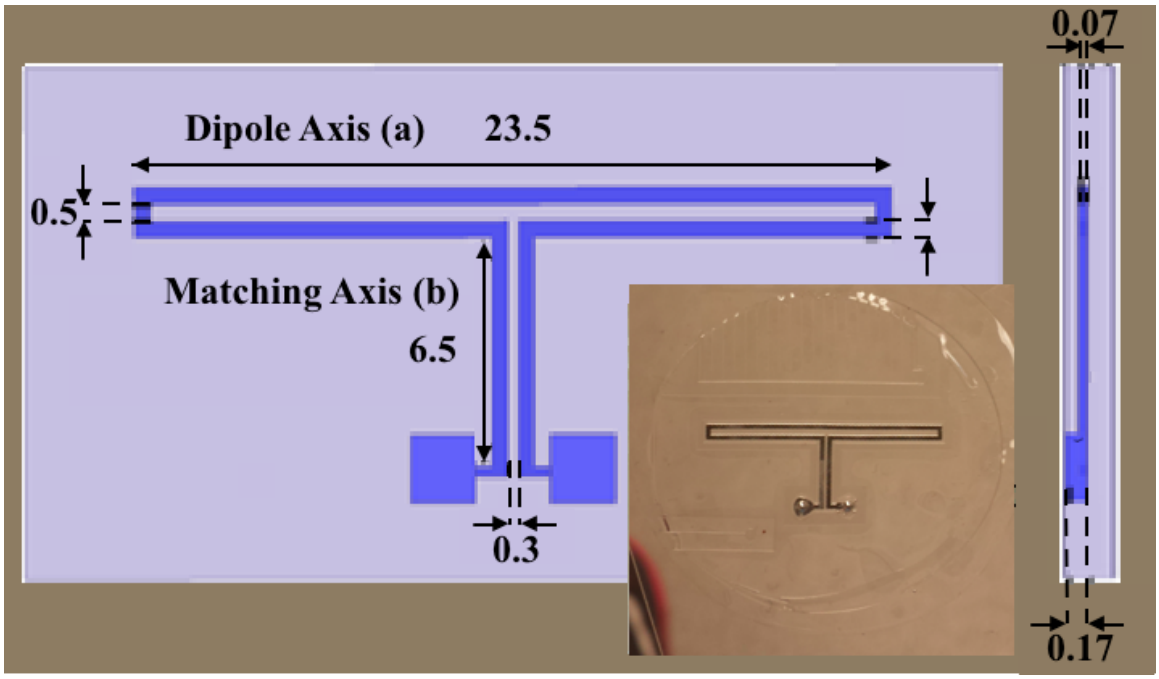

Fig. 54. Top view and side view of the folded dipole antenna. All the dimensions are in millimetre. [Reprinted from [91] © 2016 IEEE]

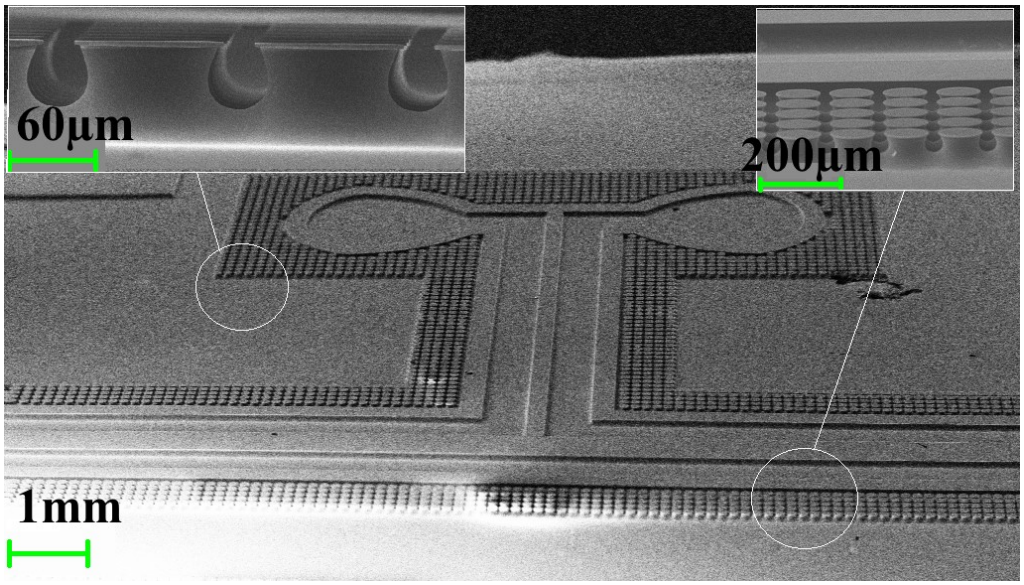

Fig. 55. SEM image of the folded antenna micro-channels along with the magnified view of the adhesive micro-pillars surrounding the channels' gasket. [Reprinted from [91] © 2016 IEEE]

In multilayer printed circuit board (PCB) and integrated circuit (IC) designs, different levels are electrically connected with vias (vertical interconnect access). These electrically conductive traces are critical in antenna design for signal connectivity across layers. Fabricating vias in rigid substrates require methods such as mechanical or laser drilling which can be a costly and complex procedure especially in miniaturized or high density devices. One of the drawbacks of microfluidic electronics often mentioned is being limited to only one layer [106]. Also, using a rigid conductor integrated into the system (such as a connector [135], or a via), is often a source of failure due to the disparities between the rigid and soft materials.

We have designed a multilayer flexible dipole antenna with an embedded soft micro-via. The upper and lower layers containing micro-channels and the middle dielectric layer are fabricated and then aligned under microscope. Afterwards, the LM enters from the inlet in the upper layer, fills a half arm of the dipole, passes through the via to the lower layer and exits from the outlet. The reversible gecko-bonding is strong enough so that metal will not leak out while transferring between the layers. With this method, the micro-via has the same stiffness of the rest of the structure and can reform itself to adjust to the changing shape of the antenna. The reversible nature of the gecko-adhesive bonding makes the alignment process much simpler.

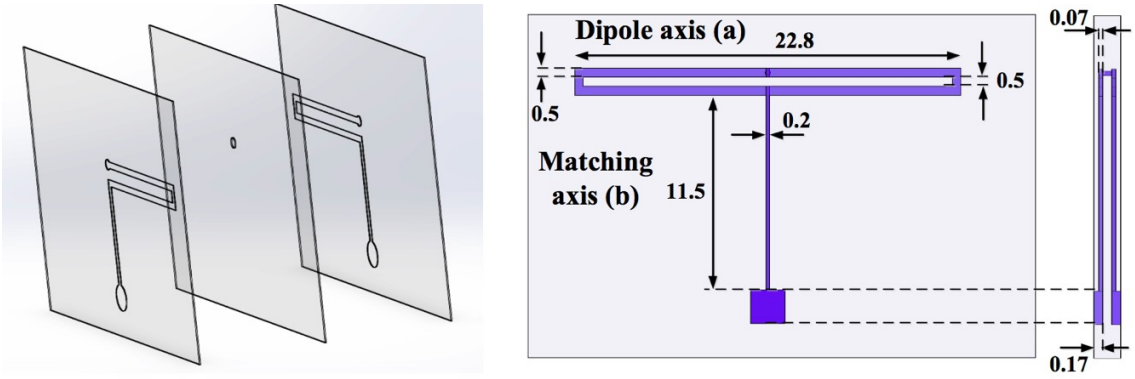

(a) (b)

Fig. 56. (a) Exploded view of the flexible multilayer dipole fabricated with a single injection step and (b) its dimensions.

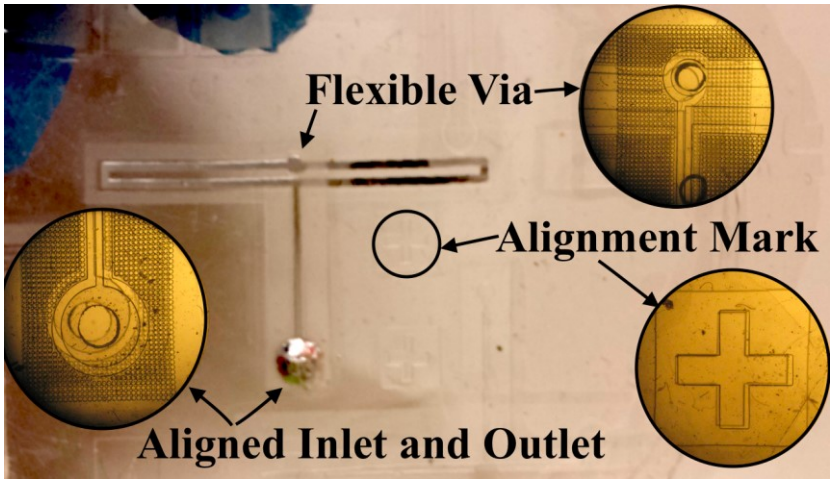

Fig. 57. Optical image of the multi-layer folded dipole and magnified images of its alignment marks, inlet and outlet, and via before LM injection.

A microstrip patch antenna is one of the most highly used antennas in industry, however due to its sheet-like configuration it is challenging to fabricated a flexible patch antenna with the existing tools. Here, a thin stretchable patch antenna and its ground plane are fabricated using gecko-adhesive bonding in SEBS (Kraton® G1657 or Kraton® G1645) based on the results in section 3.3.3 on using Laplace barriers to make low aspect ratio structures. Fig. 58 displays the top and side views of a patch antenna with all the

dimensions. It consists of a rectangular radiator with the length L_P and width W_P fed by a transmission line with length L_f and width W_f located on the top layer and a ground placed on the bottom layer. The feed points in the patch and the ground plane are aligned in order to feed the antenna as shown in the side view of Fig. 58. From feed points, a coaxial cable with the impedance of 50 Ohm may feed the antenna.

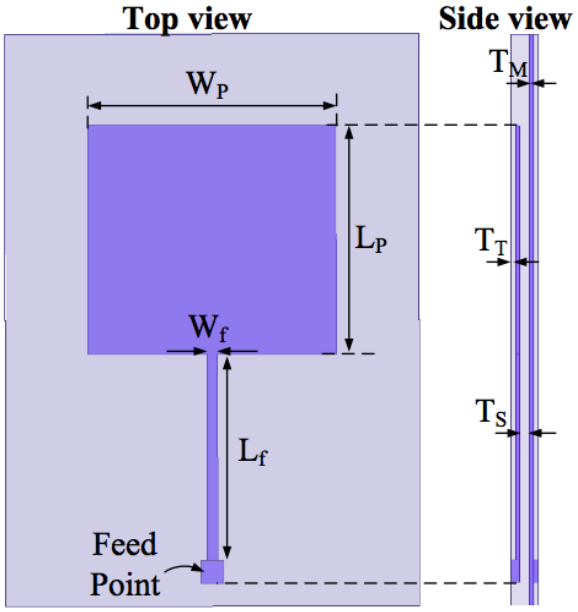

Fig. 58. Configuration of the patch antenna, (T_S= 0.4mm, T_T= 0.1 mm, T_M= 0.07 mm, W_P= 12 mm, L_P= 20 mm, W_f= 0.9 mm, L_f= 10 mm).

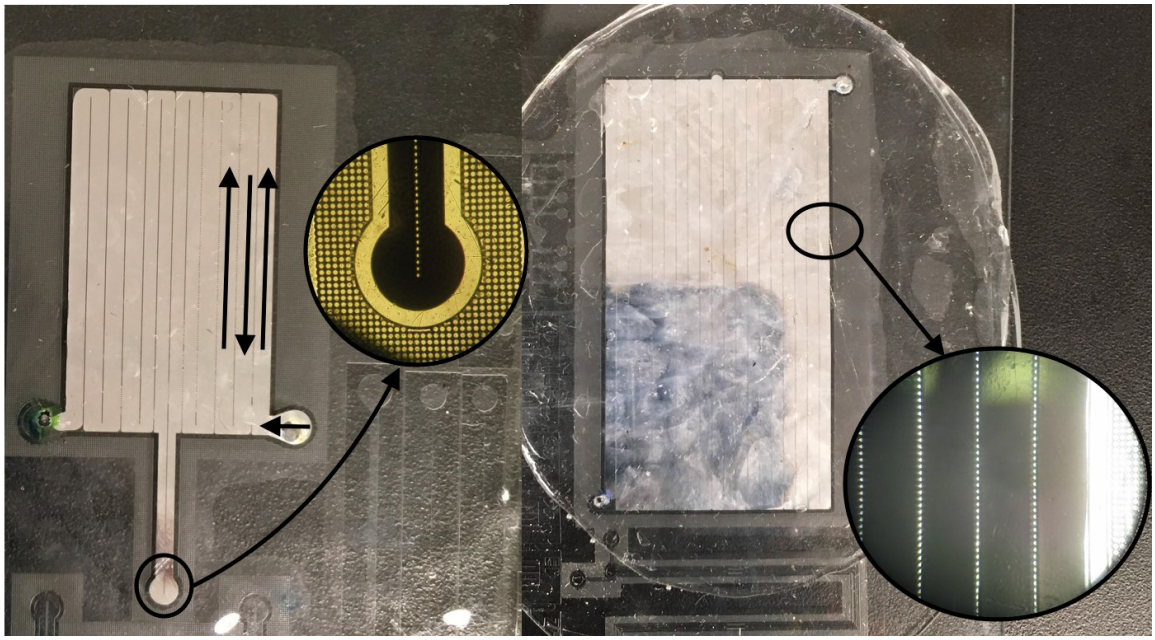

(a) (b)

Fig. 59. (a) The patch antenna (the place where the antenna is fed electrically is magnified), and (b) its ground plane.

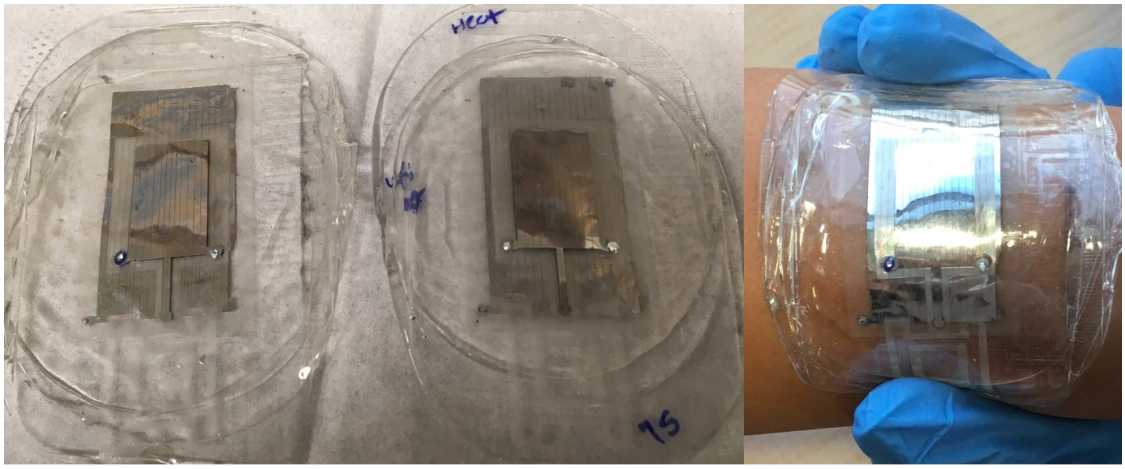

(a) (b) (c)

Fig. 60. Assembled patch antenna on the ground plane made of (a) Kraton® G1657, and (b) Kraton® G1645. (c) The Kraton® G1657 patch antenna is conformed to human's arm.

In fabrication of the patch and ground plane, a temporary glass back layer has been used in order to prevent collapsing of the channels. Due to the high adhesion between this support layer and SEBS, while detachment the metal is pushed out of the channels (Fig. 61). In order to prevent this, acetone is used as to provide a slip layer between glass and SEBS.

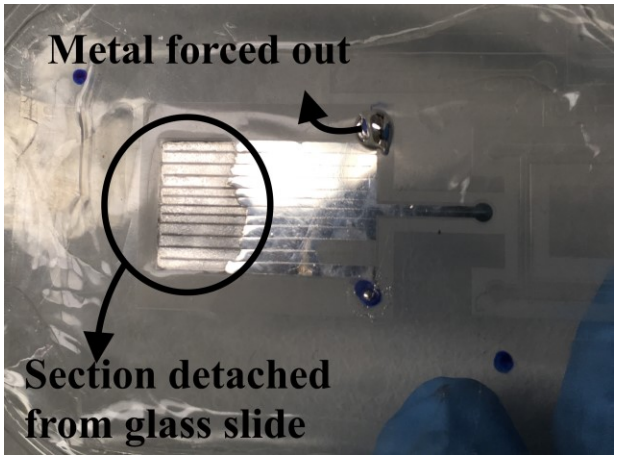

Fig. 61. Releasing LM filled SEBS from glass without using acetone

4.1.2.3 Measurement Method

In order to evaluate these antennas, their reflection coefficient, radiation pattern, and maximum gain are measured. The radiation pattern is the angular distribution of power density or field intensity at a distance from the antenna and is usually normalized to the antenna boresight amplitude and is stated in dB. The reflection coefficient represents the reflected back rather than radiated due to mismatching. The reflection coefficients are measured with an R&S® ZVL Network Analyzer and the radiation pattern is measured using RFxpert by measuring the near-field propagation and projecting the results in the far-field region [207].

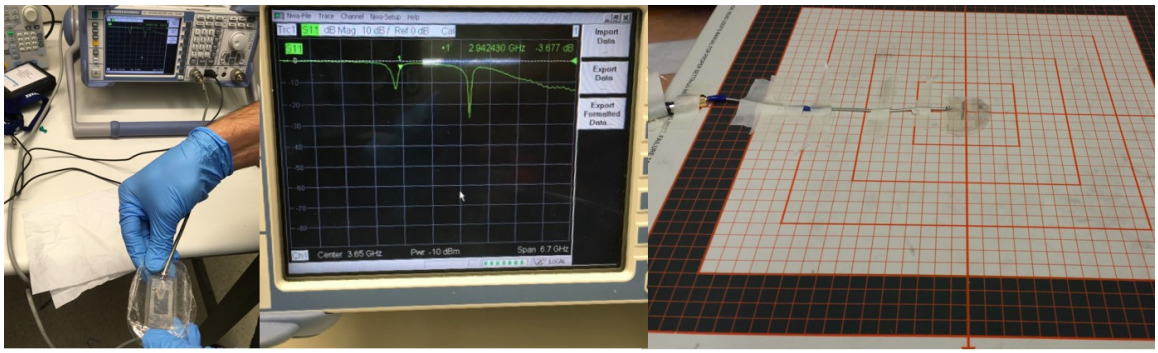

(a) (b) (c)

Fig. 62. (a) Measuring the reflection coefficient on network analyzer, (b) zoomed in image of the patch response on the screen, and (c) measuring the near field of radiation pattern.

4.1.3 Results and Discussion

4.1.3.1 Folded Dipole

By stretching this antenna along its dipole axis, its working frequency is tuned. Simulation results of the reflection response is shown in Fig. 63 and the measurement results compared to simulations can be seen in Fig. 64.

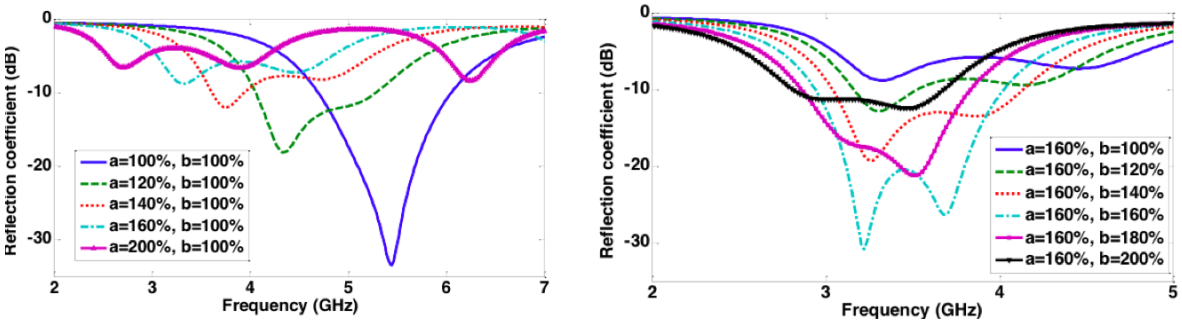

(a) (b)

Fig. 63. Simulated reflection response of the antenna for (a) variable length of dipole axis when the matching axis has a constant length, and (b) variable matching axis when the dipole axis is stretched to 160% of its original size. [Reprinted from [91] © 2016 IEEE]

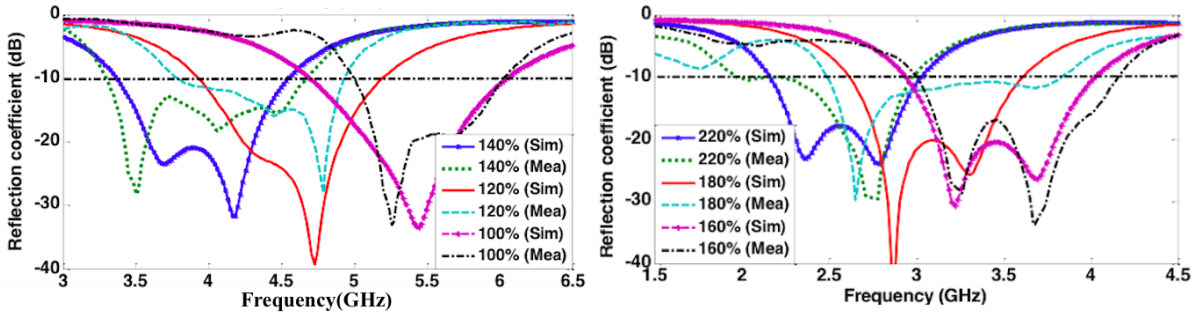

Fig. 64. Simulated and measured reflection response for different antenna sizes. [Reprinted from [91] © 2016 IEEE]

As seen in Fig. 63 (a) elongating the dipole along its axis shifts the frequency to lower values, however this results in larger reflection coefficients which confirms bad matching to the feeding system. In order to improve the matching, elongating the matching axis at the same time is essential. For a fixed elongation of dipole (60% strain), the best matching occurs when the matching axis is stretched to the same strain (Fig. 63, b). The antenna works at 5.5 GHz at its original size with 18% bandwidth. Biaxial stretching of this dipole up to 120% strain has been tested and measured. At this length, the antenna has 40% bandwidth from almost 2 to 3 GHz. This antenna has an approximately omni-directional radiation pattern in the H-plane and a donut-shape radiation pattern in its E-plane with a maximum gain (at center frequency) of 0.7 dB (Fig. 65). The E-plane is the plane containing the electric field vector and direction of maximum radiation intensity, and H-plane is the plane that contains the magnetic field vector and the maximum radiation intensity.

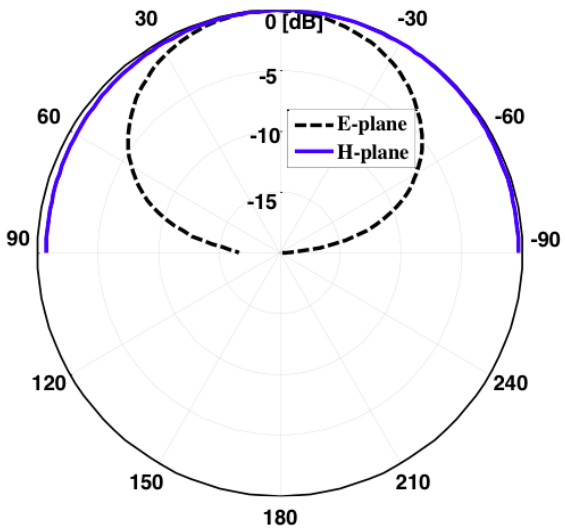

Fig. 65. Measured radiation pattern of the folded dipole at its center frequency (5.5GHz). [Reprinted from [91] © 2016 IEEE]

4.1.3.2 Multi-layer Folded Dipole

This antenna has two transmission lines along its matching axis one on top of the other, and its dipole arms are symmetrical about the matching axis. Its measured and simulated reflection coefficients when strained, and its measured radiation pattern at center frequency is shown in Fig. 66 and Fig. 67, respectively.

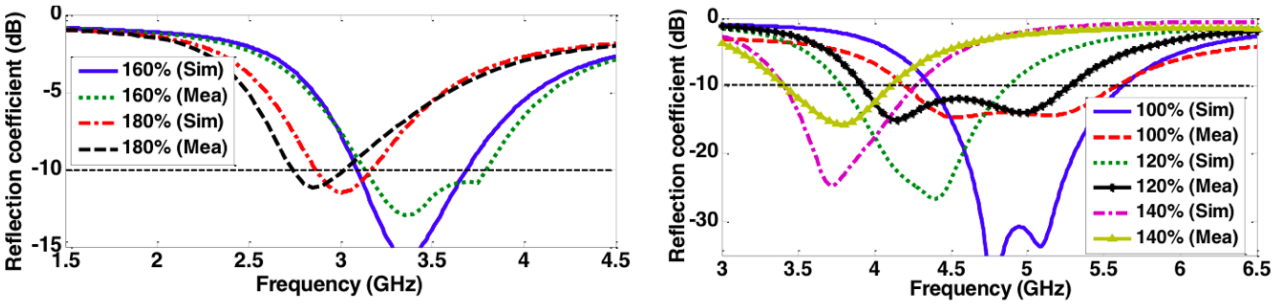

Fig. 66. Reflection coefficient of dipole for different biaxial strains along the matching and the dipole axes.

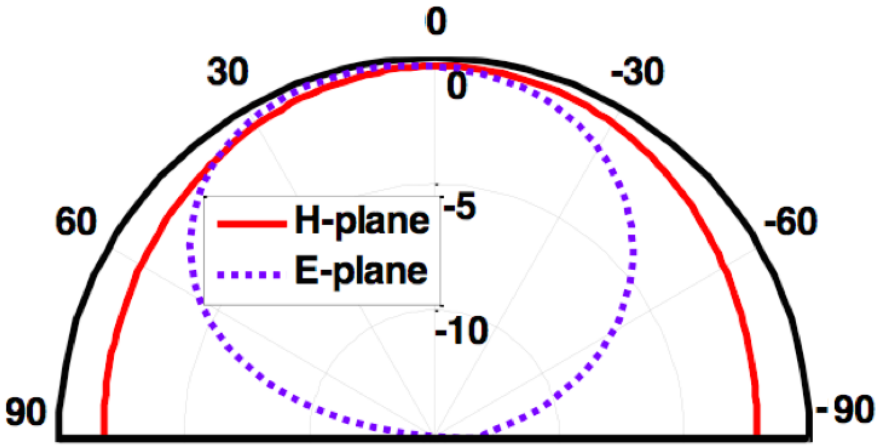

Fig. 67. The measured radiation pattern at the center frequency of 4.875 GHz

According to simulation results, the reflection coefficient is at its optimum value when the stretching is homogeneous at both sides. As shown, at zero strain, based on the measurement, the antenna works over 30% bandwidth from 4.15 to 5.6 GHz with the center frequency of 4.875 GHz. The operating bandwidth shifts to the lower frequencies when the antenna is stretched. The maximum stretching is around 80% strain which corresponds to the measured center frequency of 2.8 GHz. It is seen that as the antenna gets stretched more, the operating bandwidth decreases further. The radiation pattern has a fairly omni-directional pattern in H-plane and donut shaped pattern in E-plane as expected.

4.1.3.3 Microstrip Patch Antenna

In this antenna, the length (L_P) in Fig. 58 determines the operating frequency of the antenna and the width W_P affects the antenna radiation characteristics. When the antenna gets stretched longitudinally, the resonant frequency shifts toward lower frequencies due to larger electrical length of L_P. The width of the feed line (W_f) is

designed to provide the same characteristic impedance of the coaxial line which is a 50 Ω line. This way, the feed line length (L_f) does not affect the operating bandwidth of the antenna. Therefore, when the antenna gets stretched, the increase in the feed line length will not affect the total impedance significantly. Fig. 68 depicts the measured reflection coefficient of the fabricated antenna for different stretching values. The bandwidth is defined as the frequency range for which the antenna's reflection coefficient is under 10 dB in terms of percentage of the center frequency of this range. The resonant frequency at the original size is 4.8 GHz with a bandwidth of 19% (frequency range of 4.35 to 5.25 GHz), however, when the antenna gets stretched around 110%, the resonant frequency goes to 2.3 GHz and the bandwidth increases to 36% from 1.8 to 2.6 GHz. Fig. 68 shows how stretching the antenna can shift the operating frequency to lower frequencies.

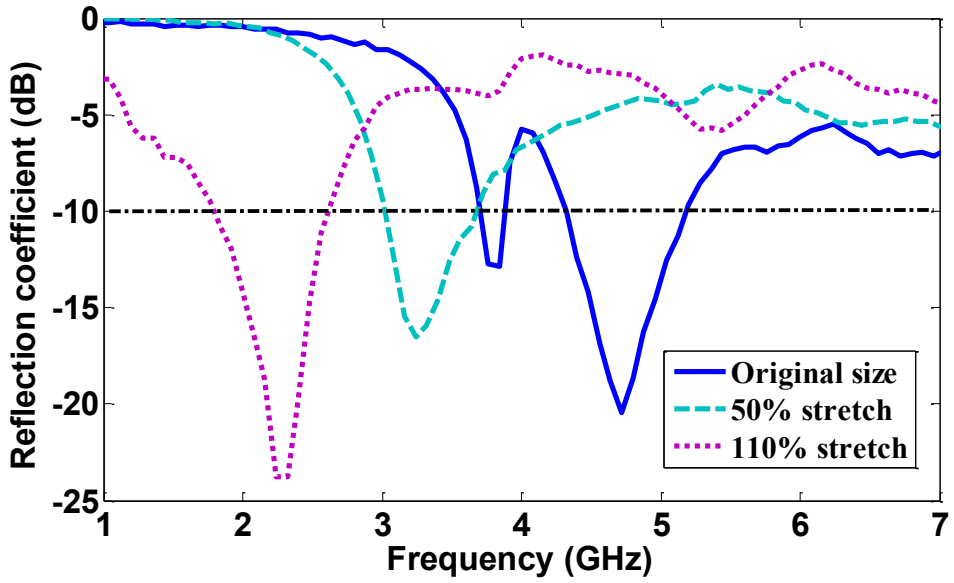

Fig. 68. Measured reflection coefficients of the stretchable antenna for different strains.

For a stretch of 110%, we have measured the effect of bend radius on the operating frequency of the antenna. As shown in Fig. 69, for different bending radii, the reflection coefficient response does not change greatly. This result verifies that the antenna is bendable and stretchable and its functionality in terms of radiation characteristics such as reflection coefficient and radiation pattern would not change upon bending. Therefore, the antenna can be used in many applications where a flexible feature is needed and can be mounted on curved features.

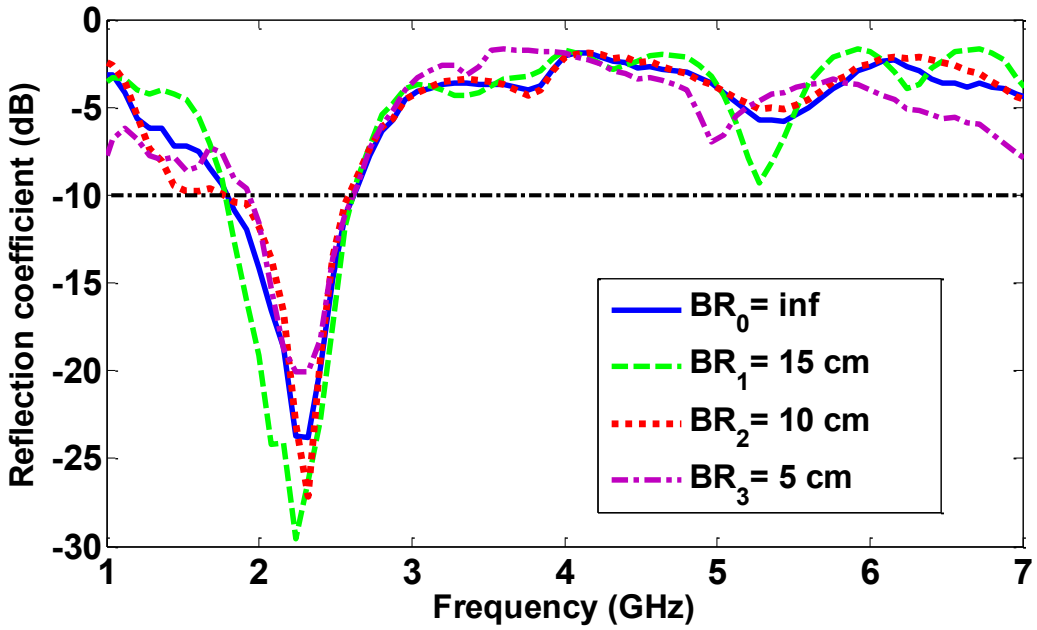

Fig. 69. Measured reflection coefficients of the stretchable patch antenna for 110% stretch and different bending radii (BR).

Fig. 70 shows the simulated and measured E-plane and H-plane of the antenna at 4.8 GHz. The antenna propagation is at broadside and there is a good agreement between simulation and measurement results of the antenna.

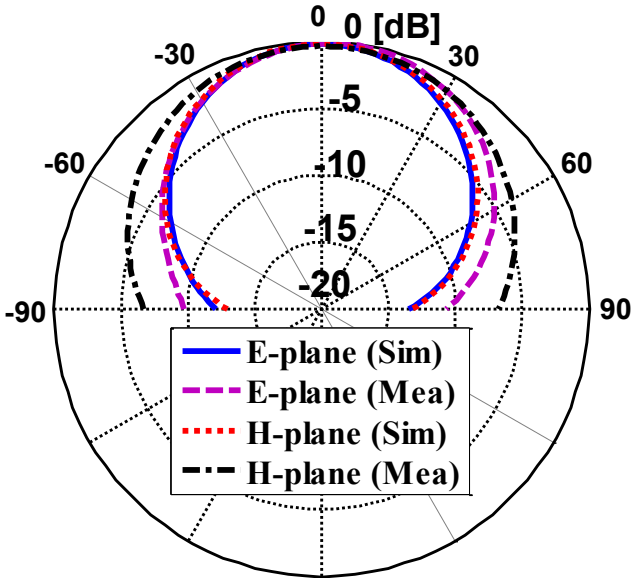

Fig. 70. Simulated and measured co-polarization of E- and H-planes of the patch antenna at its center frequency (4.8 GHz)

4.1.4 Conclusion

The feasibility of fabricating functioning radio frequency antennas with the techniques explained in previous chapters are demonstrated by designing various antennas and measuring their propagation properties. These antennas are bendable, flexible, and stretchable which make them very beneficial in many applications such as pressure sensing, reconfigurable antennas, and wireless communications.

Overall, the simulation and measurement results are in good agreement. There are small discrepancies between the measurement and simulation results however these discrepancies seem logical since the reflection coefficient is always below 10 dB at working frequencies and the radiation patterns are very close to the ideal patterns. Uneven thickness of substrate, inhomogeneous or inaccurate biaxial stretching, substrate thickness reduction during stretching due its high Poisson's ratio, and poor or

inconsistent connection to the feed are some of the factors that can possibly cause divergence from the predicted results.

CHAPTER 5: RECONFIGURABLE FREQUENCY SELECTIVE SURFACES

5.1.1 Introduction

Beam-reconfigurable high-gain aperture antennas such as reflect arrays, transmit arrays, and partially reflective surfaces are in high demand due to their applications in microwave to millimeter-wave bands [208-214]. These periodic apertures are usually tuned electronically by integration with switches or varactors. However, electronic tuning suffers several drawbacks which result in a high cost and confine them to military applications, especially in large scale [215]. These drawbacks are as follows; first, a huge number of similar switch/varactors have to be fabricated and integrated into the surface. This is a complicated task especially in case of hybrid integration using wire-bonds [208]; second, it needs an extensive DC bias line network for the dynamic control of switch/varactors which should be routed over the surface and requires special design so the lines are transparent to RF signals and avoid interference of RF/DC signals [210]; third, the nonlinearity of semiconductors limits the power handling capacity of tunable surfaces [214].

As an alternative to electronic tuning technique, recently, mechanical tuning has been offered [91][135][216-217]. The mechanical tuning incorporates the physical movement, deformation, inflation, stretching, or periodic folding of a surface. With its simplicity and reduced cost, mechanical tuning presents acceptable performance especially in large scale, without the need for bias network. Nevertheless, the actuation

speed of mechanical tuning is lower than electronic tuning which is acceptable for many applications. Despite the high potential of mechanical tuning, it has not been fully explored on aperture antennas and the literature on mechanical tuning is confined to controlling the passband of frequency selective surfaces [217] or tuning the operating frequency or broadside directivity of single element antennas [91].

This section presents a three-state beam-reconfigurable aperture antenna composed of a mechanically-tuned flexible periodic surface. The flexible surface is an array of dipoles realized by liquid-metal filled micro-channels inside a polymer and it is excited by an Open Ended Waveguide (OEW). Two beam-reconfiguration techniques are used here: 1. stretching: pattern shape is controlled by the elongation percentage, 2. reshaping: pattern shape is controlled by changing the shape of the surface to concave/convex using a special setup.

5.1.2 Surface Structure and Fabrication Method

The fabricated periodic surface is shown in Fig. 71 (a) and (b) at relaxed and stretched states. The surface is a 9×5 array of metal dipoles of size 0.5×10 mm with a periodicity of 5×11 mm, realized by liquid-metal-filled microfluidic channels inside platinum-cured thermoset silicone (TC-5101 from BJB Enterprises) with dielectric constant and loss tangent of 2.2 and 0.08, respectively. The room-temperature-LM alloy (Eutectic Gallium Indium) is injected into the channels to form the dipole array. The fabrication process is simple and low cost as follows (Fig. 72); (a) to fabricate a mold, the microfluidic patterns are engraved in PMMA using a VLS 3.50 laser; (b) Then, the

silicone is cast, degassed, and cured for 2 hours at room temperature against this mold and baked overnight at 85º C. (c) In order to seal the channels, after demolding the channels from PMMA, they are bonded to a semi-cured layer of silicone that has been baked for 2 min at 85º C. The entire system has then been baked for 2 hours to fully cure in an oven heated to 85º C. (d) Finally, the LM is injected into the channels and the entrances are sealed with more silicone. The features are large enough so there is no need for photolithography patterning and clean-room facilities. The flexible surface makes a superstrate antenna which is fed by an OEW (Fig. 73 (a)). In order to control the surface, a special setup is used (Fig. 73 (b)); Poly-Methyl-Methacrylate (PMMA) frames with 8 plastic screws hold the surface firmly on two sides. Another PMMA sheet with an array of holes hosts the screws, enabling variations in the surface along the x-axis. The fabricated antenna setup is shown in Fig. 73 (c). The next two sections elaborate the realization of a beam-reconfigurable antenna utilizing the flexibility of the superstrate by stretching and also reshaping.

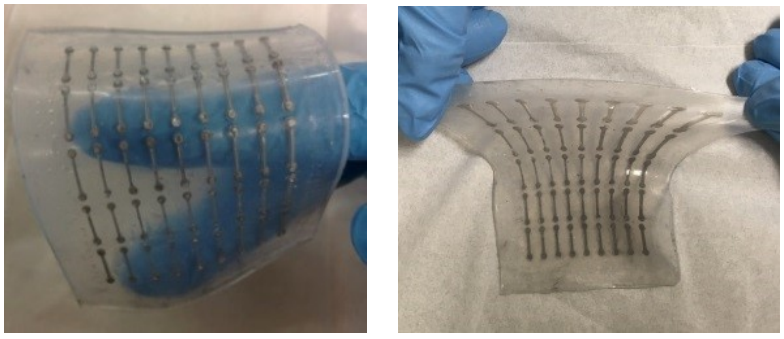

(a) (b)

Fig. 71. Flexible surface: (a) relaxed, and (b) stretched from two corners.

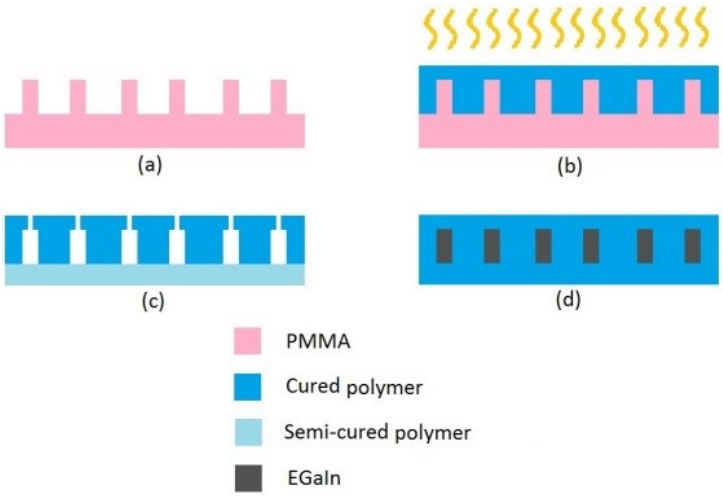

Fig. 72. Fabrication Process: (a) Fabricating PMMA mold, (b) Casting silicone against PMMA, curing, and baking, (c) Punching the entrances and bonding the channels to a semi-cured back layer, (d) filling the structures with LM and sealing the channels.

The periodicity of a surface is an important factor in its frequency response. The periodicity of dipoles in this surface can be controlled along the x-axis by elongation. To study this, an array of dipoles is simulated in ANSYS Designer. The Ku-band reflection response of the surface is shown in Fig. 74. The elongation of the surface is an effective means of tuning its reflection. To design the antenna at the target frequency of 15.5 GHz based on partially reflective surface antenna principles, the distance between OEW and surface (h) is calculated using ray tracing method [208] as:

$$h = \frac{c}{4f}\left(2N + \frac{< \Gamma_1}{\pi} + \frac{< \Gamma_2}{\pi}\right) \quad \text{Eq. 18}$$

where c is the light speed in vacuum, f is the frequency, $< \Gamma_1$ is the reflection phase from flexible surface, $< \Gamma_2$ is the reflection phase from the back metal sheet, and N is an

arbitrary integer. At no elongation, in order to have a broadside beam ($\theta = 0$), h should be 17.8 mm. As the surface is stretched, its reflection changes and the broadside beam is split to two beams off-broadside ($\pm\theta_0$).

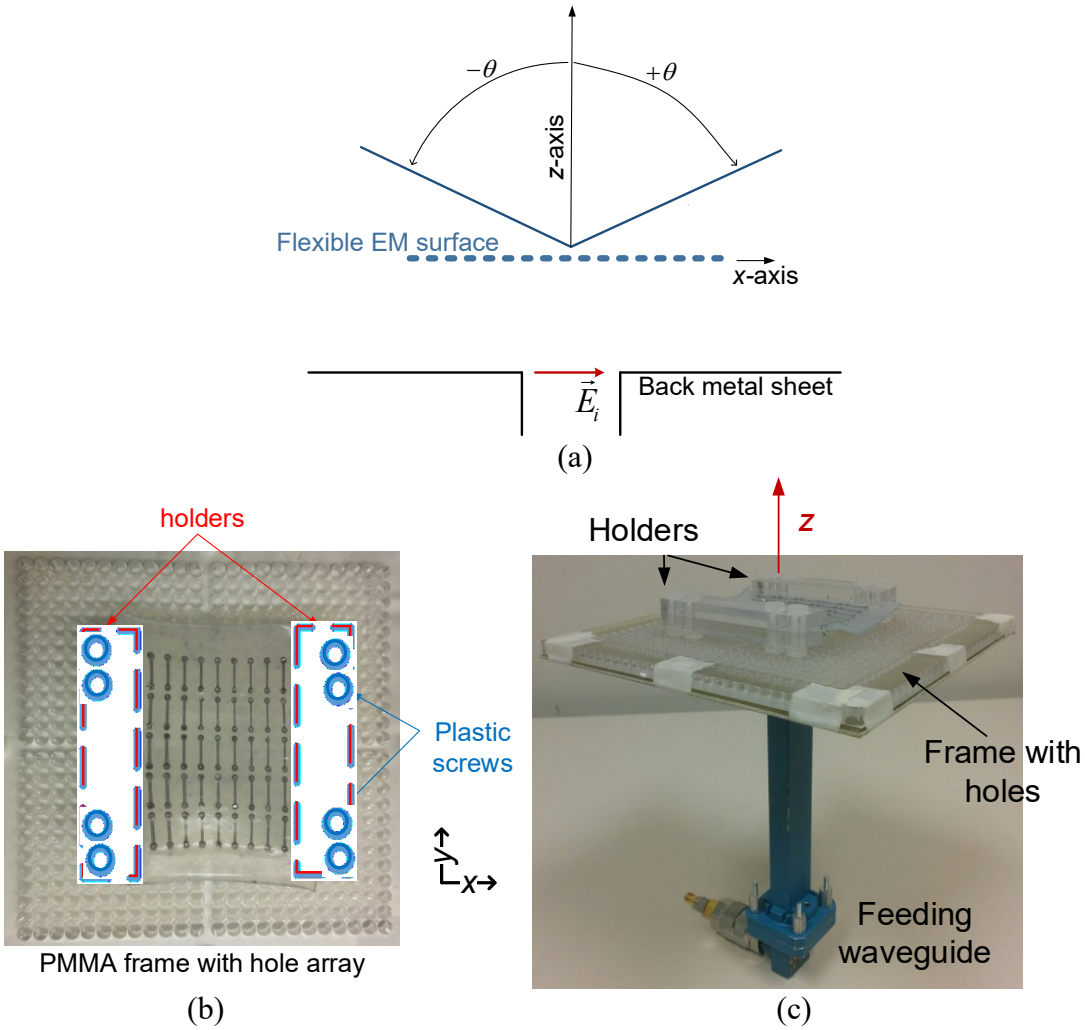

Fig. 73. (a) Antenna structure. (b) Setup for surface profile control. (c) Complete antenna with feed and connectors.

Using this technique, a three-state beam-reconfigurable antenna is implemented where the pattern is controlled by elongation percentage. Fig. 75 (a) depicts the antenna inside NSI anechoic chamber. The patterns are measured (Fig. 75 (b)) and summarized in Table 2. The antenna S-parameter is shown in Fig. 76 for all different surface states.

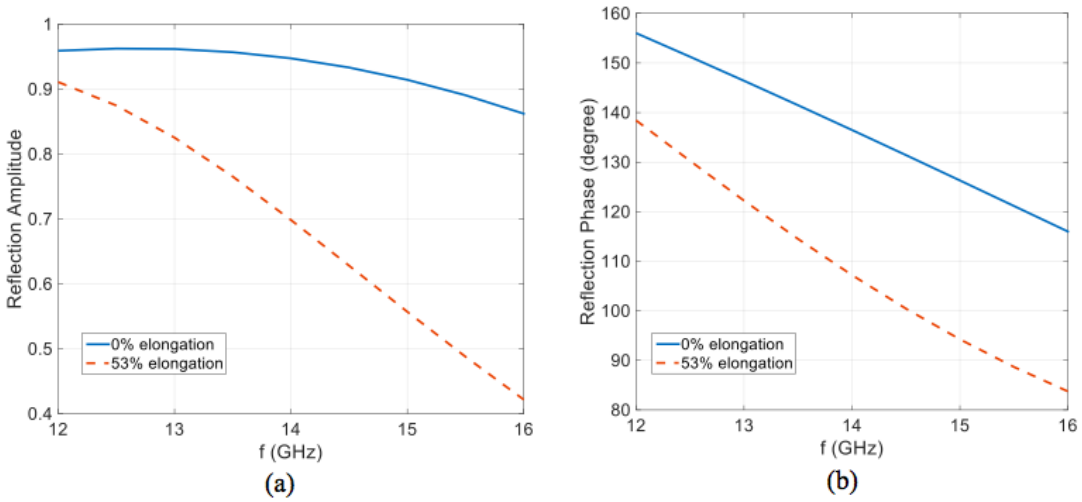

Fig. 74. Tuning the reflection of surface by elongation along x-axis. (a) Reflection amplitude. (b) Reflection phase.

5.1.3 Beam Reconfiguration by Reshaping

Reshaping the flexible surface can also allow the reconfiguration of the radiation pattern. The 2D cross section of the surface controlled with the setup is shown in Fig. 73.

Table 2. Beam reconfiguration by stretching the surface.

Elongation (%)	θ_0
0	0
14	±27°
53	±55°

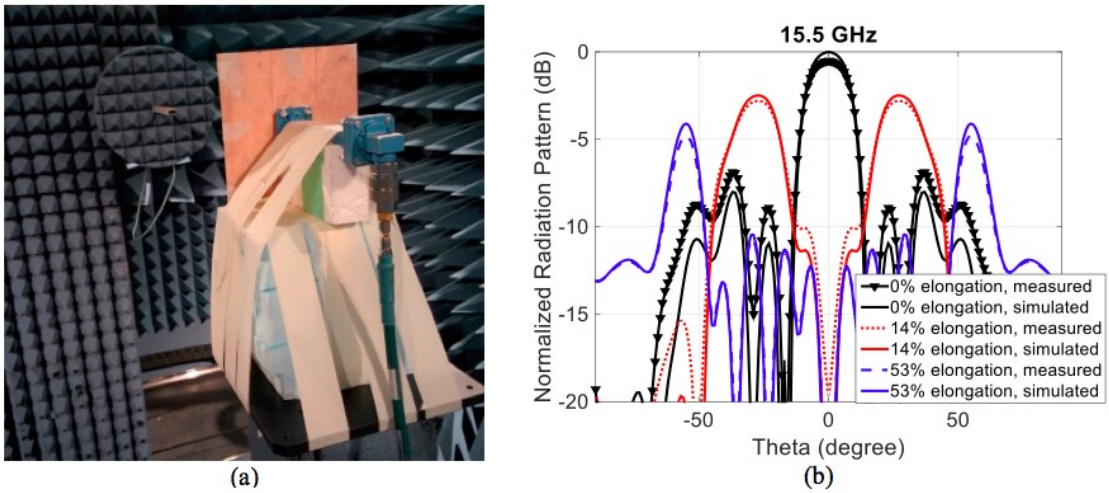

Fig. 75. (a) Antenna inside NSI anechoic chamber. (b) Reconfiguration of radiation pattern by stretching the surface.

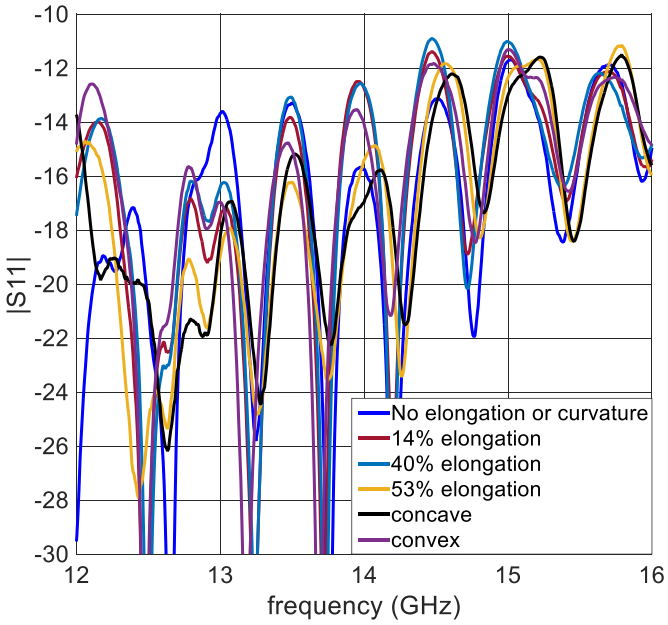

Fig. 76. |S11| of the antenna at different states mentioned above.

Here, two convex/concave surface states are tested (Fig. 77) which are described by this mathematical rational function

$$z = \pm \frac{0.01}{1+4\times10^{6}|x^{3}|} \quad \text{Eq.19}$$

where both x and z are in meter and the ± sign indicates the two states of concave/convex. To design the antenna at the target frequency of 12.5 GHz based on partially reflective surface antenna principle, the distance between OEW and surface is calculated using ray tracing method. Without reshaping, in order to have a broadside beam (θ = 0), the height should be 23 mm. The simulation model of the convex state surface is shown in Fig. 77 (b) and (c) from the side and top view, respectively. Fig. 78 depicts the side view of the surface in concave (a) and convex (b) states and also the top view of the surface in concave (c) and convex (d) states.

Using this technique, a three-state beam-reconfigurable antenna is implemented where the shape of the flexible superstrate can control the pattern. The radiation pattern is shown in Fig. 79 and summarized in Table 3. For all of the above-mentioned states, the OEW port is well matched, as shown in Fig. 76.

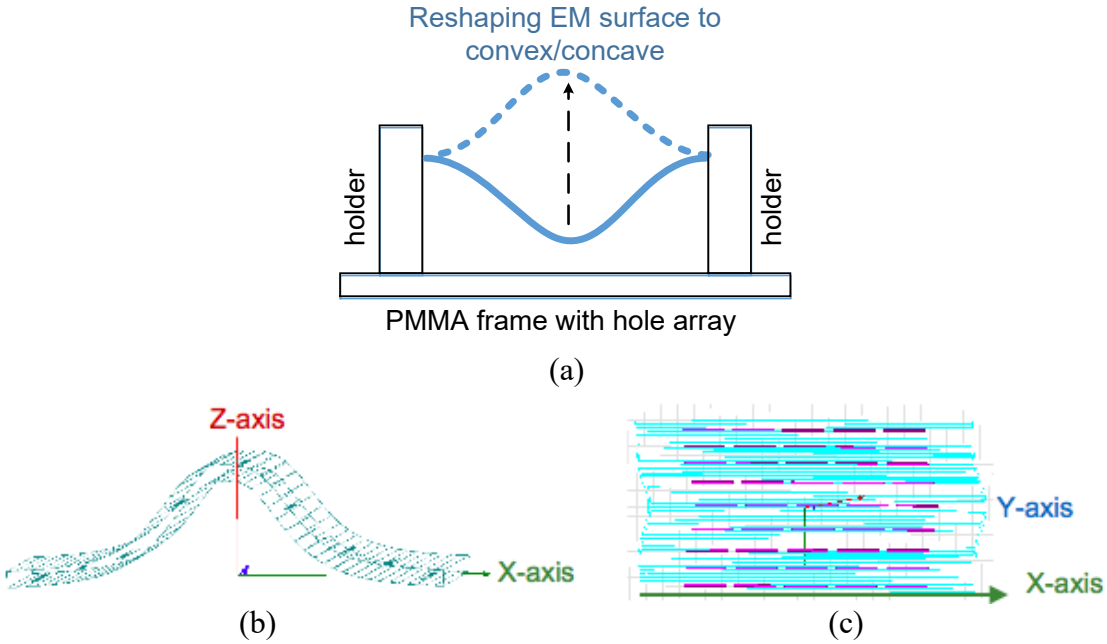

Fig. 77. (a) Reshaping the surface. (b) Convex state simulation model from side view. (c) Convex state simulation model from top view.

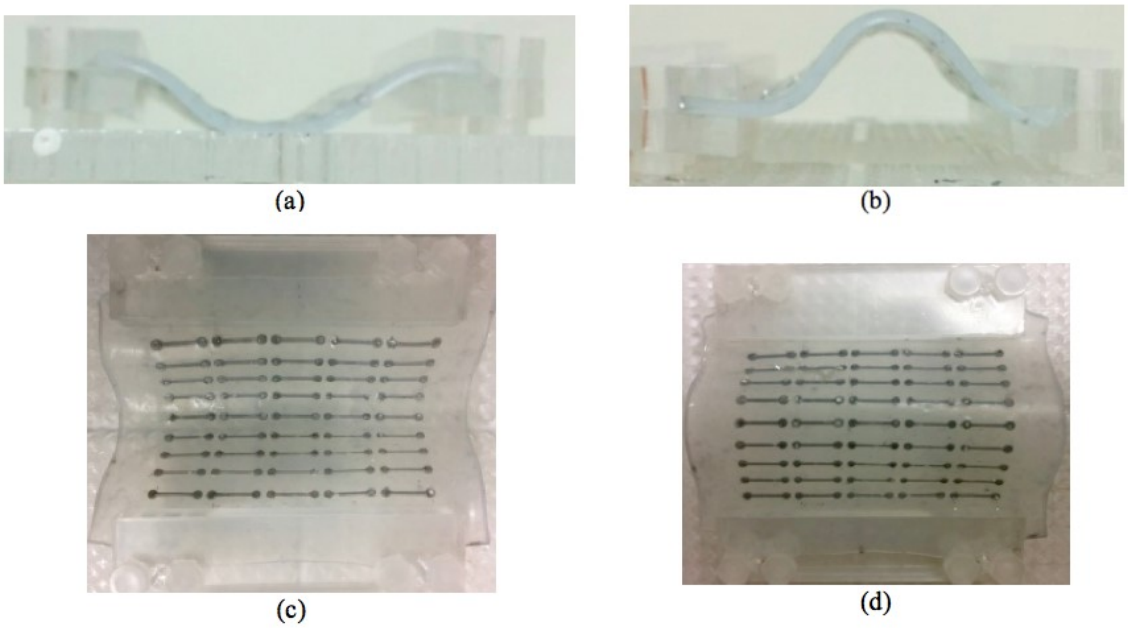

Fig. 78. Flexible surface in different reshaped states (a) concave side view; (b) convex side view; (c) concave top view; (d) convex top view.

Table 3. Beam reconfiguration by reshaping the surface.

Reshape	θ_0
No	0°
Convex	±37°
Concave	±58°

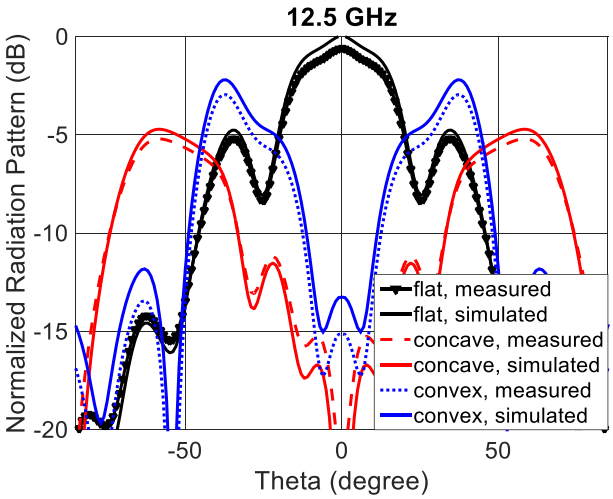

Fig. 79. Reconfiguration of radiation pattern by reshaping the surface at 12.5 GHz.

5.1.4 Conclusion

This chapter demonstrated the potentials of flexible periodic electromagnetic surfaces in reconfiguration of radiation pattern of the aperture antennas, as a simple and low cost alternative to electronic tuning by switches and varactors. The surface was composed of a 2D periodic array of dipoles implemented by liquid-metal filled microchannels inside a flexible polymer which could be stretched or reshaped to

convex/concave. The control of radiation pattern was demonstrated by both methods of elongation percentage or concave/convex shaping.

CHAPTER 6: CONCLUSION

6.1 Conclusion

In this work, we propose a tuning approach based on mechanical manipulation of soft-matter electronics by distorting their geometry to change their radiational properties. In the proposed method, the tuning of working frequency of electromagnetic systems such as antennas is possible while maintaining their original radiation pattern. This can potentially eliminate the need for wide-band antennas and have numerous applications in intelligent wearable sensing systems.

In this thesis, EGaIn LM structures in micro-scale are fabricated and efficiently manipulated. Two classes of SEBS elastomers (Kraton® G1657 and Kraton® G1645) are introduced as a soft dielectric material due to their interesting manufacturing, mechanical, and electrical properties. In Chapter 3, the dielectric constant and loss tangent of SEBS are measured (2.3 and 0.07 at 3.5 GHz, respectively) to be used as an electrical insulator for wireless devices. For fabrication of these soft antennas, the gecko-fluidics concept developed in our group is employed. The temporary gecko-adhesive bonding provides us with the opportunity for easier assembly/disassembly and recovery of liquid conductor and substrate without damaging the entire system. Although the loss tangent value for SEBS is slightly greater than PDMS, the gecko-adhesive architecture consists of large volumes of air unlike solid PDMS microfluidics, which brings down the energy dissipation of the system. This fabrication process reduces the manufacturing costs. The

reason is that unlike the conventional microfluidic methods, in which PDMS is mostly the final device, here PDMS is used for replica molding of SEBS for many cycles without failure. The features in PDMS can be easily transferred to SEBS thermoplastic with thermo-compressive molding in an ordinary laboratory. In some experiments, where exact dimensions of channel's cross section are needed (like filling pressure measurements), the micro-channels are fabricated with a traditional silicon based photolithography to obtain straight sidewalls.

Chapter 3 continues with measuring the critical pressure to fill micro-channels made of SEBS with specific dimensions, and then the critical surface tension of EGaIn is verified after estimating its contact angle on SEBS (≈150º). In order to gain control over the filling of complex structures, hydrophobic valves are employed to enforce a critical pressure for filling the channels. Thanks to stabilizing nature of EGaIn's oxide layer, fabrication of low aspect ratio structures with implanted Laplace barriers is realized. These planar structures are split into meandered channels separated by Laplace barriers. The shape, size, angle, and distance of these barriers are optimized to prevent collapsing of the channel's top layer as well as ensuring a reliable LM "auto-filling" with minimum trapped air within a safe inlet pressure margin. Furthermore, a method for fabrication of discrete array of unit cells is proposed to create isolated features from a monolithic structure made in a one-step LM injection process. In this process, a combination of an oxide reducing solution (20% diluted HCl) and hydrophobic valves (to prevent further retraction of LM) are employed. As a proof of principle, a bow-tie antenna is fabricated using this technique.

In Chapter 4, various antennas are designed with FEM simulator and fabricated, and their working proficiencies are tested. These designs include a single layer folded dipole antenna, a multilayer dipole with an inherently aligned soft via made of a vertical short microfluidic channel, and a micro-strip patch antenna. The patch antenna and ground plane structures are based on the optimized trapezoidal based Laplace barriers in Chapter 3. By elongating antennas axially or bi-axially and changing their mechanical and therefore electrical sizes, their working frequencies shift. Bi-axial stretching results in better impedance matching for dipole antennas. The folded dipole showed 55% frequency tuning with 20% to 40% bandwidth in different frequencies. The multilayer dipole shifts its center frequency from around 5 GHz to 2.8 GHz with a strain of 80%. Near-field measurements of both dipoles depicted an ideal radiation pattern. The three-layer patch antenna and its ground plane are measured up to a maximum 110% strain which shifts its frequency from 4.8 GHz (with a 19% bandwidth) to 2.3 GHz (with an increased 36% bandwidth). Moreover, the measurement results show a stable radiation pattern when the antenna is bent to various curves. This offers a potential application to be mounted on curved or complex surfaces. It should be emphasized that the gecko-adhesive bonding guaranteed no LM leakage even with high levels of strain (220%).

In Chapter 5, an extremely soft beam reconfigurable FSS is made from an array of periodic LM filled dipoles in a platinum-cured silicone (TC-5101). This electromagnetic surface shifts its broadside beam to two off-broadside beams up to ±55° when it is stretched and ±58° when it is curved to a concave shape.

Overall, this work demonstrates the potentials and advantages of mechanically reconfigurable electromagnetic devices made of EGaIn conductor in soft elastomeric substrates over electrical tuning techniques.

6.2 Future Works

- The thermo-compressive molding process can be standardized to make an SEBS layer with controllable and uniform thickness and achieving thinner than 100 micrometers substrates with small thickness variations.
- Research can be done on replacing the first fabrication phase in making the PMMA master mold (which needs costly cleanroom facilities) with some simpler alternative (such as lamination technique).
- The strong gecko-adhesive bonding technique can be used to fabricate molds in SEBS for LM, similar to freeze casting method [6]. Since the gecko-adhesion is a reversible bonding, after injecting the LM and freezing it, the layers can be detached to remove the frozen LM structure.
- More research can be done on splitting a single LM structure to isolated features to fabricate larger arrays with numerous elements.
- An on-chip pump for LM actuation can be designed and integrated with the system.
- Other reconfigurable and soft electromagnetic or circuit elements can be manufactured for different applications.

BIBLIOGRAPHY

[1] K.Y. Lien, W.C. Lee, H.Y. Lei, G.B. Lee, Integrated reverse transcription polymerase chain reaction systems for virus detection. *Biosens. Bioelectron,* 22 (2007) 1739–1748. DOI:10.1016/j.bios.2006.08.010.

[2] F.K. Balagaddé, L. You, C.L. Hansen, F.H. Arnold, S.R. Quake, Long-term monitoring of bacteria undergoing programmed population control in a microchemostat. *Science,* 309 (2005) 137–140. DOI:10.1126/science.1109173.

[3] A. Groisman, M. Enzelberger, S.R. Quake, Microfluidic memory and control devices., *Science*, 300 (2003) 955–958. DOI:10.1126/science.1083694.

[4] G.M. Whitesides, The origins and the future of microfluidics, *Nature*, 442 (2006) 368–73. DOI:10.1038/nature05058.

[5] Z. Wu, K. Hjort, S.H. Jeong, Microfluidic Stretchable Radio-Frequency Devices, *Proc. IEEE*, 103 (2015) 1211–1225. DOI:10.1109/JPROC.2015.2395716.

[6] A. Fassler, C. Majidi, 3D structures of liquid-phase GaIn alloy embedded in PDMS with freeze casting, *Lab Chip*, 13 (2013) 4442–50. DOI:10.1039/c3lc50833a.

[7] C.H. Chen, D. Peroulis, Liquid RF MEMS wideband reflective and absorptive switches, *IEEE Trans, Microw. Theory Tech*. 55 (2007) 2919–2929. DOI:10.1109/TMTT.2007.910011.

[8] M.D. Dickey, R.C. Chiechi, R.J. Larsen, E. A. Weiss, D. A. Weitz, G.M. Whitesides, Eutectic gallium-indium (EGaIn): A liquid metal alloy for the formation of stable structures in microchannels at room temperature, *Adv. Funct. Mater.* 18 (2008) 1097–1104. DOI:10.1002/adfm.200701216.

[9] Q. Zhang, Y. Zheng, J. Liu, Direct writing of electronics based on alloy and metal (DREAM) ink: A newly emerging area and its impact on energy, environment and health sciences, *Front. Energy.* 6 (2012) 311–340. DOI:10.1007/s11708-012-0214-x.

[10] S. Cheng, Z. Wu, Microfluidic electronics, *Lab Chip*. 12 (2012) 2782. DOI:10.1039/c2lc21176a.

[11] B. Soltannia, D. Sameoto, Strong, reversible underwater adhesion via gecko-inspired hydrophobic fibers, *ACS Appl. Mater. Interfaces*. 6 (2014) 21995–22003. DOI:10.1021/am5075375.

[12] J.A. Rogers, T. Someya, Y. Huang, Materials and Mechanics for Stretchable Electronics, *Science* (80). 327 (2010) 1603–1607. DOI:10.1126/science.1182383.

[13] D.S. Gray, J. Tien, C.S. Chen, High-Conductivity Elastomeric Electronics, *Adv. Mater*. 16 (2004) 393–397. DOI:10.1002/adma.200306107.

[14] S. Ḃfahy, S. Yunus, T. Pardoen, P. Bertrand, M. Troosters, Stretchable helical gold conductor on silicone rubber microwire, *Appl. Phys. Lett.* 91 (2007) 10–13. DOI:10.1063/1.2793185.

[15] D. Brosteaux, F. Axisa, M. Gonzalez, J. Vanfleteren, Fabrication and Performance of Elastic Interconnections for Stretchable Electronic Circuits, *IEEE Electron Device Letters,* 28 (2007) 552–554.

[16] S.P. Lacour, D. Chan, S. Wagner, T. Li, Z. Suo, Mechanisms of reversible stretchability of thin metal films on elastomeric substrates, *Appl. Phys. Lett.* 88 (2006) 2004–2007. DOI:10.1063/1.2201874.

[17] S.P. Lacour, S. Wagner, Z. Huang, Z. Suo, Stretchable gold conductors on elastomeric substrates, *Appl. Phys. Lett.* 82 (2003) 2404–2406. DOI:10.1063/1.1565683.

[18] S.P. Lacour, J. Jones, S. Wagner, T. Li, Z. Suo, Stretchable Interconnects for Elastic Electronic Surfaces, *Proc. IEEE.* 93 (2005) 1459–1466. DOI:10.1109/JPROC.2005.851502.

[19] D.H. Kim, J.A. Rogers, Stretchable electronics: Materials strategies and devices, *Adv. Mater.* 20 (2008) 4887–4892. DOI:10.1002/adma.200801788.

[20] W.M. Choi, J. Song, D.Y. Khang, H. Jiang, Y.Y. Huang, J.A. Rogers, Biaxially stretchable “wavy” silicon nanomembranes, *Nano Lett.* 7 (2007) 1655–1663. DOI:10.1021/nl0706244.

[21] A.J. Baca, J.H. Ahn, Y. Sun, M.A. Meitl, E. Menard, H.S. Kim, W.M. Choi, D.H. Kim, Y. Huang, J.A. Rogers, Semiconductor wires and ribbons for high-performance

flexible electronics, *Angewandte Chemie* - Int. Ed. 47 (2008) 5524–5542. DOI:10.1002/anie.200703238.

[22] E. Menard, K.J. Lee, D.Y. Khang, R.G. Nuzzo, J.A. Rogers, A printable form of silicon for high performance thin film transistors on plastic substrates, *Appl. Phys. Lett*. 84 (2004) 5398–5400. DOI:10.1063/1.1767591.

[23] J.H. Ahn, H.S. Kim, K.J. Lee, Z. Zhu, E. Menard, R.G. Nuzzo, J.A. Rogers, High-speed mechanically flexible single-crystal silicon thin-film transistors on plastic substrates, *IEEE Electron Device Lett.* 27 (2006) 460–462. DOI:10.1109/LED.2006.874764.

[24] V. Der Marel, V. Der Beek, P.H. Superconducting, High-performance thin-film transistors using semiconductor nanowires and nanoribbons, *Nature*. 425 (2003) 274–278. DOI:10.1038/nature01978.1.

[25] D.-Y. Khang, H. Jiang, Y. Huang, J.A. Rogers, A Stretchable Form of Single-Crystal, *Science* (80). 311 (2006) 208–212. DOI:10.1126/science.1121401.

[26] Y. Sun, J.A. Rogers, Inorganic semiconductors for flexible electronics, *Adv. Mater.* 19 (2007) 1897–1916. DOI:10.1002/adma.200602223.

[27] L. Song, A.C. Myers, J.J. Adams, Y. Zhu, Stretchable and reversibly deformable radio frequency antennas based on silver nanowires*, ACS Appl. Mater. Interfaces*. 6 (2014) 4248–4253. DOI:10.1021/am405972e.

[28] M. Gonzalez, F. Axisa, M. Vanden Bulcke, D. Brosteaux, B. Vandevelde, J. Vanfleteren, Design of metal interconnects for stretchable electronic circuits, *Microelectron. Reliab.* 48 (2008) 825–832. DOI:10.1016/j.microrel.2008.03.025.

[29] C. Kuo, C. Lin, Y. Huang, Plastic deformation mechanism of pure copper at low homologous temperatures, *Materials Science and Eng.,* 396 (2005) 360–368. DOI:10.1016/j.msea.2005.01.052.

[30] J. Xie, M. Pecht, D. Dedonato, A. Hassanzadeh, Investigation of the mechanical behavior of conductive elastomer interconnects, *Microelectron. Reliab*. 41 (2001) 281–286. DOI:10.1016/S0026-2714(00)00214-6.

[31] T. Tamai, Electrical Properties of Conductive Elastomer as Electrical Contact Material, *IEEE Trans. Components, Hybrids, Manuf. Technol.* 5 (1982) 56–61. DOI:10.1109/TCHMT.1982.1135954.

[32] R. Kumar, S. Singh, B.C. Yadav, Conducting Polymers : Synthesis , Properties and Applications, *J. of Intell. Mater. Sys. And Struct.,* 2 (2015) 595–604. DOI:10.17148/IARJSET.2015.21123.

[33] H. Rmili, J. L. Miane, H. Zangar, T. Olinga, Design of microstrip-fed proximity-coupled conducting polymer patch antenna, *Micro. Optic. Tech. Lett.*, 4 (2006) 655–660. DOI:10.1002/mop.

[34] T. Sekitani, H. Nakajima, H. Maeda, T. Fukushima, T. Aida, K. Hata, T. Someya, Stretchable active-matrix organic light-emitting diode display using printable elastic conductors, *Nat. Mater*. 8 (2009) 494–499. DOI:10.1038/nmat2459.

[35] T. Saito, T. Furuta, J.-H. Hwang, S. Kuramoto, K. Nishino, N. Suzuki, R. Chen, A. Yamada, K. Ito, Y. Seno, others, Multifunctional alloys obtained via a dislocation-free plastic deformation mechanism, *Science* 300 (2003) 464–467.

[36] T. Sekitani, Y. Noguchi, K. Hata, T. Fukushima, T. Aida, T. Someya, A rubberlike stretchable active matrix using elastic conductor, *Science* 321 (2008) 1468-1472.

[37] L. Adam, M. Batzle, I. Brevik, Gassmann's fluid substitution and shear modulus variability in carbonates at laboratory seismic and ultrasonic frequencies, *Geophysics*. 71 (2006) 173–183. DOI:10.1190/1.2358494.

[38] C. Hua, Z. Shen and J. Lu, High-efficiency sea-water monopole antenna for maritime wireless communications, *IEEE Tran. on Antennas and Propagation*, 62 (2014) 5968-5973, DOI: 10.1109/TAP.2014.2360210

[39] J.H. So, J. Thelen, A. Qusba, G.J. Hayes, G. Lazzi, M.D. Dickey, Reversibly deformable and mechanically tunable fluidic antennas, *Adv. Funct. Mater*. 19 (2009) 3632–3637. DOI:10.1002/adfm.200900604.

[40] R.J. Whitney, The measurement of volume changes in human limbs, *J. Physiology*, 121.1 (1953) 1-27.

[41] T. Liu, P. Sen, C.J. Kim, Characterization of nontoxic liquid-metal alloy galinstan for applications in microdevices, *J. Microelectromechanical Syst*. 21 (2012) 443–450. DOI:10.1109/JMEMS.2011.2174421.

[42] R.C. Chiechi, E.A. Weiss, M.D. Dickey, G.M. Whitesides, Eutectic gallium-indium (EGaIn): A moldable liquid metal for electrical characterization of self-assembled monolayers, *Angew. Chemie*. Int. Ed. 47 (2008) 142–144. DOI:10.1002/anie.200703642.

[43] A.C. Siegel, S.S. Shevkoplyas, D.B. Weibel, D.A. Bruzewicz, A.W. Martinez, G.M. Whitesides, Cofabrication of electromagnets and microfluidic systems in poly(dimethylsiloxane), *Angew. Chemie.* Int. Ed. 45 (2006) 6877–6882. DOI:10.1002/anie.200602273.

[44] A.C. Siegel, D. a. Bruzewicz, D.B. Weibel, G.M. Whitesides, Microsolidics: Fabrication of three-dimensional metallic microstructures in poly(dimethylsiloxane), *Adv. Mater*. 19 (2007) 727–733. DOI:10.1002/adma.200601787.

[45] P. Sen, C.-J. Kim, Microscale liquid-metal switches-a review, *IEEE Trans. Ind. Electron.* 56 (2009) 1314–1330. DOI:10.1109/TIE.2008.2006954.

[46] K.E. Spells, The determination of the viscosity of liquid gallium over an extended range of temperature, *Proc. Phys. Soc.* 48 (2002) 299–311. DOI:10.1088/0959-5309/48/2/308.

[47] S.J. French, D.J. Sauxders, G.W. Ikgle, The System Gallium-Indium, *J. Phys. Chem*. (1937) 265–274.

[48] J. Wood, K. Vummidi, P. Ralston, L. Chen, N.S. Barker, S. Raman, Liquid metal vertical interconnects for RF flip-chip assembly, *IEEE MTT-S Int. Microw. Symp. Dig*est (2009) 461–464. DOI:10.1109/MWSYM.2009.5165733.

[49] B.L. Cumby, G.J. Hayes, M.D. Dickey, R.S. Justice, C.E. Tabor, J.C. Heikenfeld, Reconfigurable liquid metal circuits by Laplace pressure shaping, *Appl. Phys. Lett.* 101 (2012) 174102. DOI:10.1063/1.4764020.

[50] R.J. Larsen, M.D. Dickey, G.M. Whitesides, D. a. Weitz, Viscoelastic properties of oxide-coated liquid metals, *J. Rheology*. 53 (2009) 1305. DOI:10.1122/1.3236517.

[51] R.K. Kramer, J.W. Boley, H.A. Stone, J.C. Weaver, R.J. Wood, Effect of microtextured surface topography on the wetting behavior of eutectic gallium − indium alloys, *Langmuir* 30 (2014): 533-539.

[52] F. Aqra, A. Ayyad, Theoretical calculations of the surface tension of liquid transition metals, *Metall. Mater. Trans. B*., 42 (2011) 5–8. DOI:10.1007/s11663-010-9456-3.

[53] J.N. Koster, Directional solidification and melting of eutectic GaIn, *Cryst. Res. Technol*. 34 (1999) 1129–1140. DOI:10.1002/(SICI)

[54] P. Surmann, H. Zeyat, Voltammetric analysis using a self-renewable non-mercury electrode, *Anal. Bioanal. Chem*. 383 (2005) 1009–1013. DOI:10.1007/s00216-005-0069-7.

[55] T. D. Truong, "Selective deposition of micro scale liquid gallium alloy droplets," M.S. thesis*, Univ. California, (UCLA)*, Los Angeles, CA, 2000.

[56] D. Zrnic, D. Swatik, On the resistivity and surface tension of the eutectic alloy of gallium and indium, *J. Less Common Met.* 18 (1969) 67–68. DOI 10.1016/0022-5088(69)90121-0.

[57] Material Safety Data Sheet for Galinstan, Geratherm Medical, Geschwenda, Germany, 2004.

[58] W.R. Hunter, R.T. Williams, Grain boundary diffusion of liquid metal coolants in optical materials for use with high power synchrotron radiation, *Nucl. Instruments Methods Phys. Res.* 222 (1984) 359–363. DOI:10.1016/0167-5087(84)90559-3.

[59] T. Ishikawa, H. Ikoma, X-Ray Photoelectron Spectroscopic Analysis of the Oxide of GaAs, *Japanese J. Appl. Phys.* 31 (1992) 3981.

[60] M.J. Regan, H. Tostmann, P.S. Pershan, O.M. Magnussen, E. DiMasi, B.M. Ocko, M. Deutsch, X-ray study of the oxidation of liquid-gallium surfaces, *Phys. Rev. B.* 55 (1997) 10786–10790. DOI:10.1103/PhysRevB.55.10786.

[61] L. Cademartiri, M.M. Thuo, C.A. Nijhuis, W.F. Reus, S. Tricard, J.R. Barber, R.N.S. Sodhi, P. Brodersen, C. Kim, R.C. Chiechi, G.M. Whitesides, Electrical

Resistance of Ag TS–S (CH2) n− 1CH3//Ga2O3/EGaIn tunneling junctions, *J. Physical Chem. C,* 116 (2012) 10848-10860.

[62] J.M. Chabala, Oxide-growth kinetics and fractal-like patterning across liquid gallium surfaces, *Phys. Rev. B.* 46 (1992) 11346–11357. DOI:10.1103/PhysRevB.46.11346.

[63] F. Scharmann, G. Cherkashinin, V. Breternitz, C. Knedlik, G. Hartung, T. Weber, J. A. Schaefer, Viscosity effect on GaInSn studied by XPS, *Surf. Interface Anal*. 36 (2004) 981–985. DOI:10.1002/sia.1817.

[64] S. Liu, X. Sun, N. Kemme, V.G. Damle, C. Schott, M. Herrmann, K. Rykaczewski, Can liquid metal flow in microchannels made of its own oxide skin?, *Microfluid. Nanofluidics*. 20 (2016) 1–6. DOI:10.1007/s10404-015-1665-2.

[65] M.R. Khan, C. Trlica, M.D. Dickey, Recapillarity: Electrochemically Controlled Capillary Withdrawal of a Liquid Metal Alloy from Microchannels, *Adv. Funct. Mater.* 25 (2015) 671–678. DOI:10.1002/adfm.201403042.

[66] M.D. Dickey, R.C. Chiechi, R.J. Larsen, E. a. Weiss, D. a. Weitz, G.M. Whitesides, Eutectic Gallium-Indium (EGaIn): A Liquid Metal Alloy for the Formation of Stable Structures in Microchannels at Room Temperature*, Adv. Funct. Mater*. 18 (2008) 1097–1104. DOI:10.1002/adfm.200701216.

[67] Q. Xu, N. Oudalov, Q. Guo, H.M. Jaeger, E. Brown, Effect of oxidation on the mechanical properties of liquid gallium and eutectic gallium-indium*, Phys. Fluids.* 24 (2012). DOI:10.1063/1.4724313.

[68] J.W. Boley, E.L. White, R.K. Kramer, Mechanically sintered gallium-indium nanoparticles, *Adv. Mater.* 27 (2015) 2355–2360. DOI:10.1002/adma.201404790.

[69] J.H. So, H.J. Koo, M.D. Dickey, O.D. Velev, Ionic current rectification in soft-matter diodes with liquid-metal electrodes, *Adv. Funct. Mater*. 22 (2012) 625–631. DOI:10.1002/adfm.201101967.

[70] H.J. Koo, J.H. So, M.D. Dickey, O.D. Velev, Towards all-soft matter circuits: Prototypes of quasi-liquid devices with memristor characteristics, *Adv. Mater*. 23 (2011) 3559–3564. DOI:10.1002/adma.201101257.

[71] M.D. Dickey, Emerging Applications of Liquid Metals Featuring Surface Oxides, *ACS applied materials & interfaces* 6.21 (2014): 18369-18379. DOI:10.1021/am5043017.

[72] D. Kim, P. Thissen, G. Viner, D.W. Lee, W. Choi, Y.J. Chabal, J.B. Lee, Recovery of nonwetting characteristics by surface modification of gallium-based liquid metal droplets using hydrochloric acid vapor, *ACS Appl. Mater. Interfaces*. 5 (2013) 179–185. DOI:10.1021/am302357t.

[73] T. Liu, P. Sen, C.J. Kim, Characterization of nontoxic liquid-metal alloy galinstan for applications in microdevices*, J. Microelectromechanical Syst*. 21 (2012) 443–450. DOI:10.1109/JMEMS.2011.2174421.

[74] J. Kim, W. Shen, L. Latorre, C.J. Kim, A micromechanical switch with electrostatically driven liquid-metal droplet, *Sensors Actuators, A Phys.* 97–98 (2002) 672–679. DOI:10.1016/S0924-4247(02)00022-5.

[75] C.G.L. Furmidge, Studies at phase interfaces. I. The sliding of liquid drops on solid surfaces and a theory for spray retention*, J. Colloid Sci.* 17 (1962) 309–324. DOI:10.1016/0095-8522(62)90011-9.

[76] D. Quéré, Rough ideas on wetting, Phys. A: Stat. Mech. Appl. 313 (2002) 32–46. DOI:10.1016/S0378-4371(02)01033-6.

[77] R.N. Wenzel, Surface Roughness and Contact Angle., *J. Psychosom. Res.* 30 (1986) 387. DOI:10.1016/0022-3999(86)90018-8.

[78] G. Li, P. Mitesh, D. W. Lee, An oxidized liquid metal-based microfluidic platform for tunable electronic device application*s." Lab on a Chip* 15 (2015): 766-775. DOI:10.1039/c4lc00193a.

[79] A.B.D. Cassie, S. Baxter, wettability of porous surfaces, *Transactions of the Faraday society* 40 (1944) 546-551.

[80] R.K. Kramer, J.W. Boley, H.A. Stone, J.C. Weaver, R.J. Wood, Effect of microtextured surface topography on the wetting behavior of eutectic gallium-indium alloys, *Langmuir.* 30 (2014) 533–539. DOI:10.1021/la404356r.

[81] D.M. Spori, T. Drobek, S. Zürcher, M. Ochsner, C. Sprecher, A. Mühlebach, N.D. Spencer, Beyond the lotus effect: Roughness influences on wetting over a wide surface-energy range, *Langmuir*. 24 (2008) 5411–5417. DOI:10.1021/la800215r.

[82] C.H. Chen, J. Whalen, D. Peroulis, Non-toxic liquid-metal 2-100 GHz MEMS switch, *IEEE MTT-S Int. Microw. Symp. Digest* (2007) 363–366. DOI:10.1109/MWSYM.2007.380446.

[83] K. Doudrick, S. Liu, E.M. Mutunga, K.L. Klein, V. Damle, K.K. Varanasi, K. Rykaczewski, Different Shades of Oxide: From Nanoscale Wetting Mechanisms to Contact Printing of Gallium-Based Liquid Metals, *Langmuir* 23 (2014) 6867-6877. DOI:10.1021/la5012023.

[84] J. Thelen, M.D. Dickey, T. Ward, A study of the production and reversible stability of EGaIn liquid metal microspheres using flow focusing*, Lab Chip*. 12 (2012) 3961–3967. DOI:10.1039/c2lc40492c.

[85] T. Hutter, W.A.C. Bauer, S.R. Elliott, W.T.S. Huck, Formation of spherical and non-spherical eutectic Gallium-Indium liquid-metal microdroplets in microfluidic channels at room temperature, *Adv. Funct. Mater*. 22 (2012) 2624–2631. DOI:10.1002/adfm.201200324.

[86] M.R. Khan, C. Trlica, J. So, M. Valeri, M.D. Dickey, Influence of water on the interfacial behavior of gallium liquid metal alloys., *ACS Appl. Mater. Interfaces*. 6 (2014) 22467–73. DOI:10.1021/am506496u.

[87] S. Liu, X. Sun, O.J. Hildreth, K. Rykaczewski, Design and characterization of a single channel two-liquid capacitor and its application to hyperelastic strain sensing, *Lab Chip*. 15 (2015) 1376–1384. DOI:10.1039/C4LC01341G.

[88] V. Kocourek, C. Karcher, M. Conrath, D. Schulze, Stability of liquid metal drops affected by a high-frequency magnetic field, *Physical Review E* 74 (2006) *Physical Review E* 74.
DOI:10.1103/PhysRevE.74.026303.

[89] D. Kim, Y. Lee, D.W. Lee, W. Choi, J.B. Lee, Hydrochloric acid-impregnated paper for liquid metal microfluidics, *(TRANSDUCERS & EUROSENSORS XXVII), 2013*

Transducers & Eurosensors XXVII: The 17th International Conference on. IEEE, (2013). 2620–2623. DOI:10.1109/Transducers.2013.6627343.

[90] G. Li, M. Parmar, D. Kim, J.B. Lee, D.W. Lee, PDMS based coplanar microfluidic channels for the surface reduction of oxidized Galinstan., *Lab Chip*. 14 (2014). DOI:10.1039/c3lc50952d.

[91] M. Zandvakili, M.M. Honari, D. Sameoto, P. Mousavi, Microfluidic Liquid Metal Based Mechanically Reconfigurable Antenna Using Reversible Gecko Adhesive Based Bonding, *Microwave Symposium (IMS), 2016 IEEE MTT-S International*. IEEE, (2016) 1-4.

[92] V. Sivan, S.Y. Tang, A.P. O'Mullane, P. Petersen, N. Eshtiaghi, K. Kalantar-Zadeh, A. Mitchell, Liquid metal marbles, *Adv. Funct. Mater.* 23 (2013) 144–152. DOI:10.1002/adfm.201200837.

[93] D. Kim, D. Jung, J.H. Yoo, Y. Lee, W. Choi, G.S. Lee, K. Yoo, J.-B. Lee, Stretchable and bendable carbon nanotube on PDMS super-lyophobic sheet for liquid metal manipulation, *J. Micromechanics Microengineering.* 24 (2014) 55018. DOI:10.1088/0960-1317/24/5/055018.

[94] D. Kim, D.W. Lee, W. Choi, J.B. Lee, A super-lyophobic PDMS micro-tunnel as a novel microfluidic platform for oxidized Galinstan, *Proc. IEEE Int. Conf. Micro Electro Mech. Syst.* (2012) 1005–1008. DOI:10.1109/MEMSYS.2012.6170184.

[95] D. Kim, D.W. Lee, W. Choi, J.B. Lee, A super-lyophobic 3-D PDMS channel as a novel microfluidic platform to manipulate oxidized galinstan, *J. Microelectromechanical Syst.* 22 (2013) 1267–1275. DOI:10.1109/JMEMS.2013.2278625.

[96] S.H. Jeong, A. Hagman, K. Hjort, M. Jobs, J. Sundqvist, Z. Wu, Liquid alloy printing of microfluidic stretchable electronics, *Lab Chip*. 12 (2012) 4657. DOI:10.1039/c2lc40628d.

[97] P. Roberts, D.D. Damian, W. Shan, T. Lu, C. Majidi, Soft-matter capacitive sensor for measuring shear and pressure deformation, *Proc. - IEEE Int. Conf. Robot. Autom*. (2013) 3529–3534. DOI:10.1109/ICRA.2013.6631071.

[98] W. Shan, T. Lu, C. Majidi, Soft-matter composites with electrically tunable elastic rigidity, *Smart Mater. Struct*. 22 (2013) 85005. DOI:10.1088/0964-1726/22/8/085005.

[99] R.K. Kramer, C. Majidi, R.J. Wood, Masked deposition of gallium-indium alloys for liquid-embedded elastomer conductors, *Adv. Funct. Mater*. 23 (2013) 5292–5296. DOI:10.1002/adfm.201203589.

[100] Y. Xia, G.M. Whitesides, Soft lithography, *Annu. Rev. Mater. Sci.* 28 (1998) 153–184. DOI:10.1146/annurev.matsci.28.1.153.

[101] A. Tabatabai, A. Fassler, C. Usiak, C. Majidi, Liquid-phase gallium-indium alloy electronics with microcontact printing, *Langmuir*. 29 (2013) 6194–6200. DOI:10.1021/la401245d.

[102] I.D. Joshipura, H.R. Ayers, C. Majidi, M.D. Dickey, Methods to pattern liquid metals, *J. Mater. Chem. C.* 3 (2015) 3834–3841. DOI:10.1039/C5TC00330J.

[103] M. Kim, H. Alrowais, S. Pavlidis, O. Brand, C. Engineering, Scalable liquid metal thin line patterning for passive electronic components using soft lithography, *Solid-state Sensors, Actuat. Microsystem. Workshop* (2016) 62–63.

[104] G. Li, X. Wu, D.W. Lee, Selectively Plated Stretchable Liquid Metal Wires for Transparent Electronics, *Sensors Actuators B Chem*. 221 (2015) 1114–1119. DOI:10.1016/j.snb.2015.07.062.

[105] B.A. Gozen, A. Tabatabai, O.B. Ozdoganlar, C. Majidi, High-density soft-matter electronics with micron-scale line width, *Adv. Mater*. 26 (2014) 5211–5216. DOI:10.1002/adma.201400502.

[106] C. Ladd, J.H. So, J. Muth, M.D. Dickey, 3D printing of free standing liquid metal microstructures, *Adv. Mater.* 25 (2013) 5081–5085. DOI:10.1002/adma.201301400.

[107] Y. Zheng, Z. He, Y. Gao, J. Liu, Direct desktop Printed-Circuits-on-Paper flexible electronics, *Scientific Reports* 3 (2013) 1786. DOI:10.1038/srep01786.

[108] L. Sheng, S. Teo, J. Liu, Liquid-Metal-Painted Stretchable Capacitor Sensors for Wearable Healthcare Electronics, *J. Med. Biol. Eng.* 36 (2016) 265–272. DOI:10.1007/s40846-016-0129-9.

[109] Y. Zheng, Q. Zhang, J. Liu, Pervasive liquid metal based direct writing electronics with roller-ball pen, *AIP Adv.* 3 (2013) 1–7. DOI:10.1063/1.4832220.

[110] J.W. Boley, E.L. White, G.T.C. Chiu, R.K. Kramer, Direct writing of gallium-indium alloy for stretchable electronics, *Adv. Funct. Mater*. 24 (2014) 3501–3507. DOI:10.1002/adfm.201303220.

[111] H. Yan, Y. Chen, Y. Deng, L. Zhang, X. Hong, W. Lau, J. Mei, D. Hui, H. Yan, Y. Liu, Coaxial printing method for directly writing stretchable cable as strain sensor, *Appl. Phys. Lett.* 109 (2016) 83502. DOI:10.1063/1.4961493.

[112] Y.L. Kong, I.A. Tamargo, H. Kim, B.N. Johnson, M.K. Gupta, T. Koh, H. Chin, D.A. Steingart, B.P. Rand, M.C. Mcalpine, 3D Printed Quantum Dot Light-Emitting Diodes, *Nano Lett.* 14 (2014) 7017-7023. DOI: 10.1021/nl5033292.

[113] A. Gannarapu, B.A. Gozen, Freeze-Printing of Liquid Metal Alloys for Manufacturing of 3D, Conductive, and Flexible Networks, *Adv. Mater. Technol.* 1 (2016). DOI:10.1002/admt.201600047.

[114] J.P. Swensen, L.U. Odhner, B. Araki, A.M. Dollar, Printing Three-Dimensional Electrical Traces in Additive Manufactured Parts for Injection of Low Melting Temperature Metals, *J. Mech. Robot.* 7 (2015) 21004. DOI:10.1115/1.4029435.

[115] T. Liu, P. Sen, C.J. Kim, Characterization of liquid-metal Galinstan® for droplet applications, *Proc. IEEE Int. Conf. Micro Electro Mech. Syst.* (2010) 560–563. DOI:10.1109/MEMSYS.2010.5442440.

[116] D. Kim, J.H. Yoo, Y. Lee, W. Choi, K. Yoo, J.B.J. Lee, Gallium-based liquid metal inkjet printing, *Proc. IEEE Int. Conf. Micro Electro Mech. Syst.* (2014) 967–970. DOI:10.1109/MEMSYS.2014.6765804.

[117] S.H. Jeong, K. Hjort, Z. Wu, Tape transfer atomization patterning of liquid alloys for microfluidic stretchable wireless power transfer, *Sci. Rep.* 5 (2015) 8419. DOI:10.1038/srep08419.

[118] S.H. Jeong, K. Hjort, Z. Wu, Tape transfer printing of a liquid metal alloy for stretchable RF electronics., *Sensors (Basel).* 14 (2014) 16311–21. DOI:10.3390/s140916311.

[119] T. Lu, L. Finkenauer, J. Wissman, C. Majidi, Rapid prototyping for soft-matter electronics*, Adv. Funct. Mater.* 24 (2014) 3351–3356. DOI:10.1002/adfm.201303732.

[120] J. Wang, S. Liu, S. Guruswamy, A. Nahata, Reconfigurable liquid metal based terahertz metamaterials via selective erasure and refilling to the unit cell level, *Appl. Phys. Lett.* 103 (2013) 0–5. DOI:10.1063/1.4837675.

[121] D. Corning, Electronics Sylgard ® 184 Silicone Elastomer, Prod. Datasheet. (2013) 1–3.

[122] J.C. McDonald, G.M. Whitesides, Poly(dimethylsiloxane) as a material for fabricating microfluidic devices, *Acc. Chem. Res.* 35 (2002) 491–499. DOI:10.1021/ar010110q.

[123] D. Sameoto, A. Wasay, Materials selection and manufacturing of thermoplastic elastomer microfluidics, *SPIE BiOS*. International Society for Optics and Photonics 9320 (2015) 932001. DOI:10.1117/12.2081291.

[124] B. Balakrisnan, S. Patil, E. Smela, Patterning PDMS using a combination of wet and dry etching, *J. Micromechanics Microengineering.* 19 (2009) 47002. DOI:10.1088/0960-1317/19/4/047002.

[125] J.C. Lötters, W. Olthuis, P.H. Veltink, P. Bergveld, The mechanical properties of the rubber elastic polymer polydimethylsiloxane for sensor applications, *J. Micromechanics Microengineering*. 7 (1999) 145–147. DOI:10.1088/0960-1317/7/3/017.

[126] I.D. Johnston, D.K. McCluskey, C.K.L. Tan, M.C. Tracey, Mechanical characterization of bulk Sylgard 184 for microfluidics and microengineering, *J. Micromechanics Microengineering.* 24 (2014) 35017. DOI:10.1088/0960-1317/24/3/035017.

[127] K.P. Mineart, Y. Lin, S.C. Desai, A.S. Krishnan, R.J. Spontak, M.D. Dickey, Ultrastretchable, cyclable and recyclable 1- and 2-dimensional conductors based on physically cross-linked thermoplastic elastomer gels, *Soft Matter.* 9 (2013) 7695-7700. DOI:10.1039/c3sm51136g.

[128] J. Park, S. Wang, M. Li, C. Ahn, J.K. Hyun, D.S. Kim, D.K. Kim, J. a Rogers, Y. Huang, S. Jeon, Three-dimensional nanonetworks for giant stretchability in dielectrics and conductors., *Nat. Commun*. 3 (2012) 916. DOI:10.1038/ncomms1929.

[129] G.J. Hayes, J.-H. So, A. Qusba, M.D. Dickey, G. Lazzi, Flexible Liquid Metal Alloy (EGaIn) Microstrip Patch Antenna, *IEEE Trans. Antennas Propag.* 60 (2012) 2151–2156. DOI:10.1109/TAP.2012.2189698.

[130] S. Cheng, Z. Wu, P. Hallbjörner, K. Hjort, A. Rydberg, Foldable and stretchable liquid metal planar inverted cone antenna, *IEEE Trans. Antennas Propag.* 57 (2009) 3765–3771. DOI:10.1109/TAP.2009.2024560.

[131] K.O. Siegenthaler, A. Künkel, G. Skupin, M. Yamamoto, Ecoflex® and Ecovio®: biodegradable performance-enabling plastics, *Adv. Polym. Sci*. 245 (2012) 91-136. DOI: 10.1007/12_2010_106

[132] A.S. Kurian, T. Giffney, J. Lee, J. Travas-Sejdic, K.C. Aw, Printing of CNT/silicone rubber for a wearable flexible stretch sensor, *SPIE Smart Structures and Materials+ Nondestructive Evaluation and Health monitoring, International Society for Optics and Photonics* 9798 (2016) 97980K. DOI:10.1117/12.2218224.

[133] N. Lazarus, S.S. Bedair, Improved power transfer to wearable systems through stretchable magnetic composites*, Appl. Phys. A.* 122 (2016) 543. DOI:10.1007/s00339-016-0067-y.

[134] S.H. Jeong, S. Zhang, K. Hjort, J. Hilborn, Z. Wu, PDMS-Based Elastomer Tuned Soft, Stretchable, and Sticky for Epidermal Electronics*., Adv. Mater.* 28 (2016) 5830-5836. DOI:10.1002/adma.201505372.

[135] M. Kubo, X. Li, C. Kim, M. Hashimoto, B.J. Wiley, D. Ham, G.M. Whitesides, Stretchable microfluidic radiofrequency antennas, *Adv. Mater.* 22 (2010) 2749–2752. DOI:10.1002/adma.200904201.

[136] Y.-L. Park, B. Chen, R.J. Wood, Design and Fabrication of Soft Artificial Skin using Embedded Microchannels and Liquid Conductors, *IEEE Sens J.* 12 (2012) 2711–2718.

[137] A. Fassler, C. Majidi, Soft-matter capacitors and inductors for hyperelastic strain sensing and stretchable electronics, *Smart Mater. Struc*t. 22 (2013) 55023. DOI:10.1088/0964-1726/22/5/055023.

[138] Kraton, Kraton ® G1657 M Polymer, Prod. Data sheet, (2009) 29–31.

[139] S. Zhu, J.H. So, R. Mays, S. Desai, W.R. Barnes, B. Pourdeyhimi, M.D. Dickey, Ultrastretchable fibers with metallic conductivity using a liquid metal alloy core, *Adv. Funct. Mater.* 23 (2013) 2308–2314. DOI:10.1002/adfm.201202405.

[140] A. Lakhtakia, Scattering by a nihility sphere, 56 (2006) 895–896. DOI:10.1002/mop.

[141] C.W. Tsao, D.L. DeVoe, Bonding of thermoplastic polymer microfluidics, *Microfluid. Nanofluidics.* 6 (2009) 1–16. DOI:10.1007/s10404-008-0361-x.

[142] T.H.N. Dinh, H.H. Cao, F.S. Hamdi, M. Couty, E. Martincic, M. Woytasik, E. Dufour-Gergam, Development of reversible bonding for microfluidic applications, *Microfluid. Nanofluidics*. 19 (2015) 751–756. DOI:10.1007/s10404-015-1599-8.

[143] H. Becker, C. Gärtner, Polymer microfabrication technologies for microfluidic systems, Anal. Bioanal. *Chem.* 390 (2008) 89–111. DOI:10.1007/s00216-007-1692-2.

[144] R.T. Kelly, A.T. Woolley, Thermal bonding of polymeric capillary electrophoresis microdevices in water, *Anal. Chem.* 75 (2003) 1941–1945. DOI:10.1021/ac0262964.

[145] K. Kistrup, C.E. Poulsen, M. Hansen, A. Wolff, Ultrasonic welding for fast bonding of self-aligned structures in lab-on-a-chip systems*, Lab Chip*. 15 (2015) 1998–2001. DOI:10.1039/C5LC00174A.

[146] H. Klank, J.P. Kutter, O. Geschke, CO(2)-laser micromachining and back-end processing for rapid production of PMMA-based microfluidic systems., *Lab Chip*. 2 (2002) 242–246. DOI:10.1039/b206409j.

[147] M.A. Eddings, M.A. Johnson, B.K. Gale, Determining the optimal PDMS–PDMS bonding technique for microfluidic devices, J. *Micromechanics Microengineering*. 18 (2008) 67001. DOI:10.1088/0960-1317/18/6/067001.

[148] M.J. Shenton, M.C. Lovell-Hoare, G.C. Stevents, M. Iopscience, Adhesion enhancement of polymer surfaces by atmospheric plasma treatment, J*ournal of Physics D: Applied Physics,* 34 (2001) 2754.

[149] Y. Kusano, Atmospheric Pressure Plasma Processing for Polymer Adhesion: A Review, *J. Adhes*. 90 (2014) 755–777. DOI:10.1080/00218464.2013.804407.

[150] S. Bhattacharya, A. Datta, J.M. Berg, S. Gangopadhyay, Studies on surface wettability of poly(dimethyl) siloxane (PDMS) and glass under oxygen-plasma, *J.MicroElecMechSys*. 14 (2005) 590–597. DOI:10.1109/JMEMS.2005.844746.

[151] A. Khademhosseini, J. Yeh, G. Eng, J. Karp, H. Kaji, J. Borenstein, O.C. Farokhzad, R. Langer, Cell docking inside microwells within reversibly sealed microfluidic channels for fabricating multiphenotype cell arrays*, Lab Chip*. 5 (2005) 1380. DOI:10.1039/b508096g.

[152] M. Varenberg, A. Peressadko, S. Gorb, E. Arzt, Effect of real contact geometry on adhesion, *Appl. Phys. Lett*. 89 (2006) 23–26. DOI:10.1063/1.2356099.

[153] K.L. Johnson, K. Kendall, and A. D. Roberts. Surface energy and the contact of elastic solids, *Proceedings of the Royal Society of London A: Mathematical, Physical and Engineering Sciences, The Royal Society*. 324 (1971) 301-313.

[154] M. Kamperman, E. Kroner, A. Del Campo, R.M. McMeeking, E. Arzt, Functional adhesive surfaces with “Gecko” effect: The concept of contact splitting, *Adv. Eng. Mater.* 12 (2010) 335–348. DOI:10.1002/adem.201000104.

[155] K. Autumn, M. Sitti, Y. a Liang, A.M. Peattie, W.R. Hansen, S. Sponberg, T.W. Kenny, R. Fearing, J.N. Israelachvili, R.J. Full, Evidence for van der Waals adhesion in gecko setae., *Proc. Natl. Acad. Sci. USA*. 99 (2002) 12252–12256. DOI:10.1073/pnas.192252799.

[156] W. Bin Khaled, D. Sameoto, Fabrication and characterization of thermoplastic elastomer dry adhesives with high strength and low contamination, *ACS Appl. Mater. Interfaces*. 6 (2014) 6806–6815. DOI:10.1021/am500616a.

[157] M. Henrey, J.P. Díaz Téllez, K. Wormnes, L. Pambaguian, C. Menon, Towards the use of mushroom-capped dry adhesives in outer space: Effects of low pressure and

temperature on adhesion strength, *Aerosp. Sci. Technol.* 29 (2013) 185–190. DOI:10.1016/j.ast.2013.03.003.

[158] D. Sameoto, C. Menon, Recent advances in the fabrication and adhesion testing of biomimetic dry adhesives, *Smart Mater. Struct*. 19 (2010) 103001–18. DOI:10.1088/0964-1726/19/10/103001.

[159] A. Del Campo, C. Greiner, E. Arzt, Contact shape controls adhesion of bioinspired fibrillar surfaces, *Langmuir.* 23 (2007) 10235–10243. DOI:10.1021/la7010502.

[160] G. Carbone, E. Pierro, S.N. Gorb, Origin of the superior adhesive performance of mushroom-shaped microstructured surfaces, *Soft Matter*. 7 (2011) 5545–52. DOI:10.1039/c0sm01482f.

[161] a Wasay, D. Sameoto, Gecko gaskets for self-sealing and high-strength reversible bonding of microfluidics, *Lab Chip*. 15 (2015) 2749–2753. DOI:10.1039/c5lc00342c.

[162] S.J. Mazlouman, X.J. Jiang, A.N. Mahanfar, C. Menon, R.G. Vaughan, A Reconfigurable Patch Antenna Using Liquid Metal Embedded in a Silicone Substrate, *IEEE Transactions on Antennas and Propagation* 59 (2011) 4406–4412.

[163] M. Le Berre, C. Crozatier, G. Velve Casquillas, Y. Chen, Reversible assembling of microfluidic devices by aspiration, *Microelectron. Eng*. 83 (2006) 1284–1287. DOI:10.1016/j.mee.2006.01.257.

[164] E. Tkachenko, E. Gutierrez, M.H. Ginsberg, A. Groisman, An easy to assemble microfluidic perfusion device with a magnetic clamp*., Lab Chip.* 9 (2009) 1085–1095. DOI:10.1039/b812184b.

[165] H.J. Kim, C. Son, B. Ziaie, A multiaxial stretchable interconnect using liquid-alloy-filled elastomeric microchannels, *Appl. Phys. Lett*. 92 (2008) 1–4. DOI:10.1063/1.2829595.

[166] J.-H. So, M.D. Dickey, Inherently aligned microfluidic electrodes composed of liquid metal., *Lab Chip*. 11 (2011) 905–911. DOI:10.1039/c0lc00501k.

[167] Y. Gao, R. Liu, X. Wang, J. Liu, Q. Fang, Flexible RFID tag inductor printed by liquid metal ink printer and its characterization, *J. Electron. Packag*. 138 (2016) 31007. DOI:10.1115/1.4034062.

[168] N. Behdad, Liquid-Tunable Frequency Selective Surfaces*, IEEE Microw. Wirel. Components Lett.* 20 (2010) 423–425. DOI:10.1109/LMWC.2010.2049257.

[169] S. Yang, P. Liu, M. Yang, Q. Wang, J. Song, L. Dong, From Flexible and Stretchable Meta-Atom to Metamaterial: A Wearable Microwave Meta-Skin with Tunable Frequency Selective and Cloaking Effects., *Sci. Rep.* 6 (2016) 21921. DOI:10.1038/srep21921.

[170] M. Jobs, K. Hjort, A. Rydberg, Z. Wu, A tunable spherical cap microfluidic electrically small antenna, *Small.* 9 (2013) 3230–3234. DOI:10.1002/smll.201300070.

[171] D.H. Kim, N. Lu, R. Ma, Y.S. Kim, R.H. Kim, S. Wang, J. Wu, S.M. Won, H. Tao, A. Islam, K.J. Yu, T. Kim, R. Chowdhury, M. Ying, L. Xu, M. Li, H.J. Chung, H. Keum, M. McCormick, P. Liu, Y.-W. Zhang, F.G. Omenetto, Y. Huang, T. Coleman, J.A. Rogers, Epidermal Electronics, *Science*. 333 (2011) 838–843. DOI:10.1126/science.1206157.

[172] J.Y. Lee, S.N. Hwang, A high-gain boost converter using voltage-stacking cell, *Trans. Korean Inst. Electr. Eng*. 57 (2008) 982–984. DOI:10.1049/el.

[173] S. Jalali Mazlouman, A. Mahanfar, C. Menon, R.G. Vaughan, Mechanically reconfigurable antennas using electro-active polymers (EAPs), *IEEE Antennas Propag. Soc. AP-S Int. Symp.* (2011) 742–745. DOI:10.1109/APS.2011.5996819.

[174] M. Rashed Khan, G.J. Hayes, J.H. So, G. Lazzi, M.D. Dickey, A frequency shifting liquid metal antenna with pressure responsiveness, *Appl. Phys. Lett*. 99 (2011) 2009–2012. DOI:10.1063/1.3603961.

[175] A. Dey, G. Mumcu, R. Guldiken, Microfluidically Reconfigured Wideband Frequency Tunable Liquid Metal Monopole Antenna, *IEEE Trans. Antennas Propag*. (2016) 1–1. DOI:10.1109/TAP.2016.2551358.

[176] M. Wang, C. Trlica, M.R. Khan, M.D. Dickey, J.J. Adams, A reconfigurable liquid metal antenna driven by electrochemically controlled capillarity*, J. Appl. Phys*. 117 (2015). DOI:10.1063/1.4919605.

[177] D. Kim, R.G. Pierce, R. Henderson, S.J. Doo, K. Yoo, J.-B. Lee, Liquid metal actuation-based reversible frequency tunable monopole antenna, *Appl. Phys. Lett*. 105 (2014) 234104. DOI:10.1063/1.4903882.

[178] S. Cheng, Z. Wu, A microfluidic, reversibly stretchable, large-area wireless strain sensor, *Adv. Funct. Mater.* 21 (2011) 2282–2290. DOI:10.1002/adfm.201002508.

[179] S. Cheng, A. Rydberg, K. Hjort, Z. Wu, Liquid metal stretchable unbalanced loop antenna, *Appl. Phys. Lett.* 94 (2009) 15–18. DOI:10.1063/1.3114381.

[180] S. Cheng, Z. Wu, Microfluidic stretchable RF electronics., *Lab Chip*. 10 (2010) 3227–3234. DOI:10.1039/c005159d.

[181] D. Kim, D. Kim, H. Lee, Y.R. Jeong, S.-J. Lee, G. Yang, H. Kim, G. Lee, S. Jeon, G. Zi, J. Kim, J.S. Ha, Body-Attachable and Stretchable Multisensors Integrated with Wirelessly Rechargeable Energy Storage Devices, *Adv. Mater.* (2015) 748-756. DOI:10.1002/adma.201504335.

[182] C. Majidi, R. Kramer, R.J. Wood, A non-differential elastomer curvature sensor for softer-than-skin electronics, *Smart Mater. Struct*. 20 (2011) 105017. DOI:10.1088/0964-1726/20/10/105017.

[183] R.D. Ponce Wong, J.D. Posner, V.J. Santos, Flexible microfluidic normal force sensor skin for tactile feedback, *Sensors Actuators*, *A Phys.* 179 (2012) 62–69. DOI:10.1016/j.sna.2012.03.023.

[184] X. Shi, C.-H. Cheng, Y. Zheng, P.K.A. Wai, An EGaIn-based flexible piezoresistive shear and normal force sensor with hysteresis analysis in normal force direction*, J. Micromechanics Microengineering.* 26 (2016) 105020. DOI:10.1088/0960-1317/26/10/105020.

[185] Y.-L. Park, C. Majidi, R. Kramer, P. Bérard, R.J. Wood, Hyperelastic pressure sensing with a liquid-embedded elastomer*, J. Micromechanics Microengineering*. 20 (2010) 125029. DOI:10.1088/0960-1317/20/12/125029.

[186] H.J. Kim, T. Maleki, P. Wei, B. Ziaie, A biaxial stretchable interconnect with liquid-alloy-covered joints on elastomeric substrate, *J. Microelectromechanical Syst*. 18 (2009) 138–146. DOI:10.1109/JMEMS.2008.2011118.

[187] E. Palleau, S. Reece, S.C. Desai, M.E. Smith, M.D. Dickey, Self-healing stretchable wires for reconfigurable circuit wiring and 3D microfluidics, *Adv. Mater.* 25 (2013) 1589–1592. DOI:10.1002/adma.201203921.

[188] A.L. Richards, M.D. Dickey, A.S. Kennedy, G.D. Buckner, Design and demonstration of a novel (micro-Coulter) counter utilizing liquid metal electrodes*, J. Micromechanics Microengineering.* 22 (2012) 115012. DOI:10.1088/0960-1317/22/11/115012.

[189] M. Gao, L. Gui, Development of a fast thermal response microfluidic system using liquid metal, *J. Micromechanics Microengineering*. 26 (2016) 75005. DOI:10.1088/0960-1317/26/7/075005.

[190] J. Valentine, S. Zhang, T. Zentgraf, E. Ulin-Avila, D.A. Genov, G. Bartal, X.B. Zhang, Three-dimensional optical metamaterial with a negative refractive index*, Nature*. 455 (2008) 376–379. DOI:10.1038/nature07247.

[191] H.K. Kim, D. Lee, S. Lim, Wideband-Switchable Metamaterial Absorber Using Injected Liquid Metal, *Sci. Rep*. 6 (2016) 31823. DOI:10.1038/srep31823.

[192] S.W. Jin, J. Park, S.Y. Hong, H. Park, Y.R. Jeong, Stretchable Loudspeaker using Liquid Metal Microchannel*, Nat. Publ. Gr.* (2000) 1–13. DOI:10.1038/srep11695.

[193] D. Kim, J.H. Yoo, J.-B. Lee, Liquid metal-based reconfigurable and stretchable photolithography, *J. Micromechanics Microengineering*. 26 (2016) 45004. DOI:10.1088/0960-1317/26/4/045004.

[194] Y.G. Deng, J. Liu, Corrosion development between liquid gallium and four typical metal substrates used in chip cooling device, *Appl. Phys. A Mater. Sci. Process*. 95 (2009) 907–915. DOI:10.1007/s00339-009-5098-1.

[195] M.A.H. Khondoker, D. Sameoto, Fabrication methods and applications of microstructured gallium based liquid metal alloys*, Smart Mater. Struct*. 25 (2016) 93001. DOI:10.1088/0964-1726/25/9/093001.

[196] N.B. Morley, J. Burris, L.C. Cadwallader, M.D. Nornberg, GaInSn usage in the research laboratory, *Rev. Sci. Instrum*. 79 (2008) 2014–2017. DOI:10.1063/1.2930813.

[197] P. Ahlberg, S.H. Jeong, M. Jiao, Z. Wu, U. Jansson, S.L. Zhang, Z. Bin Zhang, Graphene as a diffusion barrier in galinstan-solid metal contacts, *IEEE Trans. Electron Devices*. 61 (2014) 2996–3000. DOI:10.1109/TED.2014.2331893.

[198] A.C. Siegel, S.K.Y. Tang, C.A. Nijhuis, M. Hashimoto, T. Phillips, M.D. Dickey, G.M. Whitesides, *NIH Public Access*, 43 (2011) 518–528. DOI:10.1021/ar900178k.Co-Fabrication.

[199] M.R. Khan, C.B. Eaker, E.F. Bowden, M.D. Dickey, Giant and switchable surface activity of liquid metal via surface oxidation, *Proc. Natl. Acad. Sci.* 111 (2014) 14047–14051. DOI:10.1073/pnas.1412227111.

[200] S.-Y. Tang, Y. Lin, I. Joshipura, K. Khoshmanesh, M. Dickey, Steering liquid metal flow in microchannels using low voltages, *Lab Chip*. (2015). DOI:10.1039/C5LC00742A.

[201] M.R. Khan, G.J. Hayes, S. Zhang, M.D. Dickey, G. Lazzi, A pressure responsive fluidic microstrip open stub resonator using a liquid metal alloy, *IEEE Microw. Wirel. Components Lett.* 22 (2012) 577–579. DOI:10.1109/LMWC.2012.2223754.

[202] R. Morent, N. De Geyter, F. Axisa, N. De Smet, L. Gengembre, E. De Leersnyder, C. Leys, J. Vanfleteren, M. Rymarczyk-Machal, E. Schacht, E. Payen, Adhesion enhancement by a dielectric barrier discharge of PDMS used for flexible and stretchable electronics, *J. Phys. D. Appl. Phys.* 40 (2007) 7392–7401. DOI:10.1088/0022-3727/40/23/021.

[203] J. Sarrazin, Y. Mahé, S. Avrillon, S. Toutain, Pattern reconfigurable cubic antenna, IEEE *Trans. Antennas Propag*. 57 (2009) 310–317. DOI:10.1109/TAP.2008.2011221.

[204] N. Tiercelin, P. Coquet, R. Sauleau, V. Senez, H. Fujita, Polydimethylsiloxane membranes for millimeter-wave planar ultraflexible antennas, *J. Micromechanics Microengineering.* 16 (2006) 2389–2395. DOI:10.1088/0960-1317/16/11/020.

[205] B.P. Pashaey, V.V. Seleznev, Magnetic susceptibility of gallium-indium alloys in liquid state, *Russian Physics Journal* 16 (1973) 565-566.

[206] R. Schmitt. Electromagnetics explained: a handbook for wireless/RF, EMC, and high-speed electronics. *Newnes*, 2002.

[207] http://www.emscan.com/.

[208] H. Moghadas, M. Daneshmand, P. Mousavi, MEMS-tunable half phase gradient partially reflective surface for beam-shaping, *IEEE Trans. Antennas Propag*. 63 (2015) 369–373. DOI:10.1109/TAP.2014.2364303.

[209] S. V. Hum, J. Perruisseau-Carrier, "Reconfigurable reflectarrays and array lenses for dynamic antenna beam control: A review", *IEEE Trans. Antenna Propagat*, 62 (2014) 183-198.

[210] T. Debogović, J. Bartolić, J. Perruisseau-Carrier, Dual-polarized partially reflective surface antenna with MEMS-based beamwidth reconfiguration, *IEEE Trans. Antennas Propag.* 62 (2014) 228–236. DOI:10.1109/TAP.2013.2287013.

[211] S.V. Hum, J. Perruisseau-Carrier, Reconfigurable reflectarrays and array lenses for dynamic antenna beam control: A review, *IEEE Trans. Antennas Propag*. 62 (2014) 183–198. DOI:10.1109/TAP.2013.2287296.

[212] W. Pan, C. Huang, P. Chen, M. Pu, X. Ma, X. Luo, A beam steering horn antenna using active frequency selective surface*, IEEE Trans. Antennas Propag*. 61 (2013) 6218–6223. DOI:10.1109/TAP.2013.2280592.

[213] A.R. Weily, T.S. Bird, Y.J. Guo, A reconfigurable high-gain partially reflecting surface antenna, *IEEE Trans. Antennas Propag.* 56 (2008) 3382–3390. DOI:10.1109/TAP.2008.2005538.

[214] S.V. Hum, G. McFeetors, M. Okoniewski, Integrated MEMS reflectarray elements, *Proc. 1st Eur. Conf. on Antennas and Propagation* (2006) 1-6. DOI:10.1109/EUCAP.2006.4584619.

[215] S.M.A. Momeni Hasan Abadi, J.H. Booske, N. Behdad, Exploiting mechanical flexure to design tunable periodic structures*, IEEE Antennas Propag. Soc. AP-S Int. Symp.* (2015) 888-889. DOI:10.1109/APS.2015.7304831.

[216] M. Zandvakili, H. Moghadas, D. Sameoto, P. Mousavi, Mechanically tunable periodic electromagnetic surface using stretchable polymer, *Antenna Technology and Applied Electromagnetics (ANTEM), 2016 17th International Symposium on*. IEEE, (2016) 1-2.

[217] P. Gutruf, C. Zou, W. Withayachumnankul, M. Bhaskaran, S. Sriram, C. Fumeaux, Mechanically tunable dielectric resonator metasurfaces at visible frequencies, *ACS Nano*. 10 (2016) 133–141. DOI:10.1021/acsnano.5b05954.

APPENDICES

Appendix A: Mask Designs

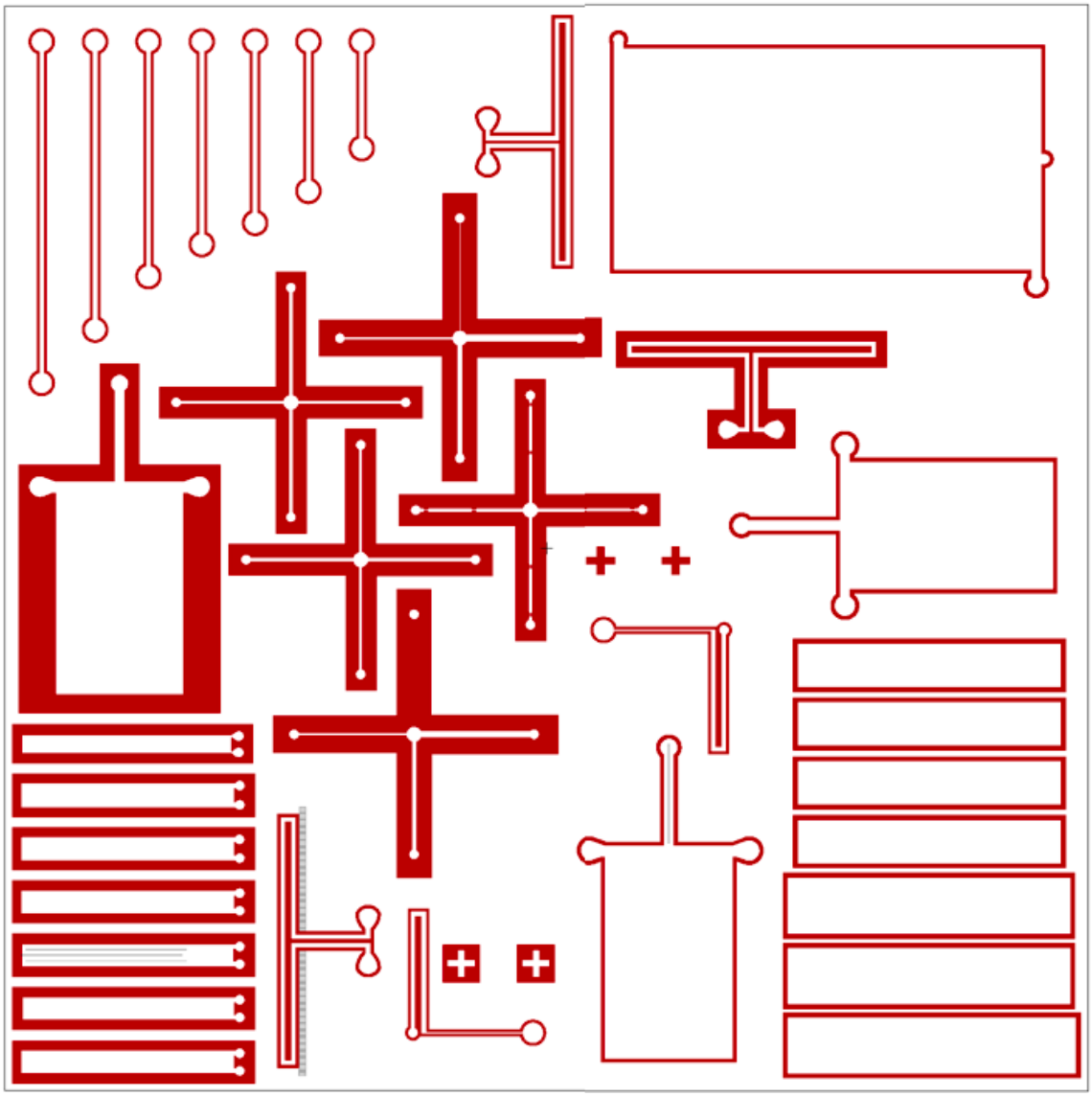

Fig. 80. L-edit design of the first mask for photolithography process.

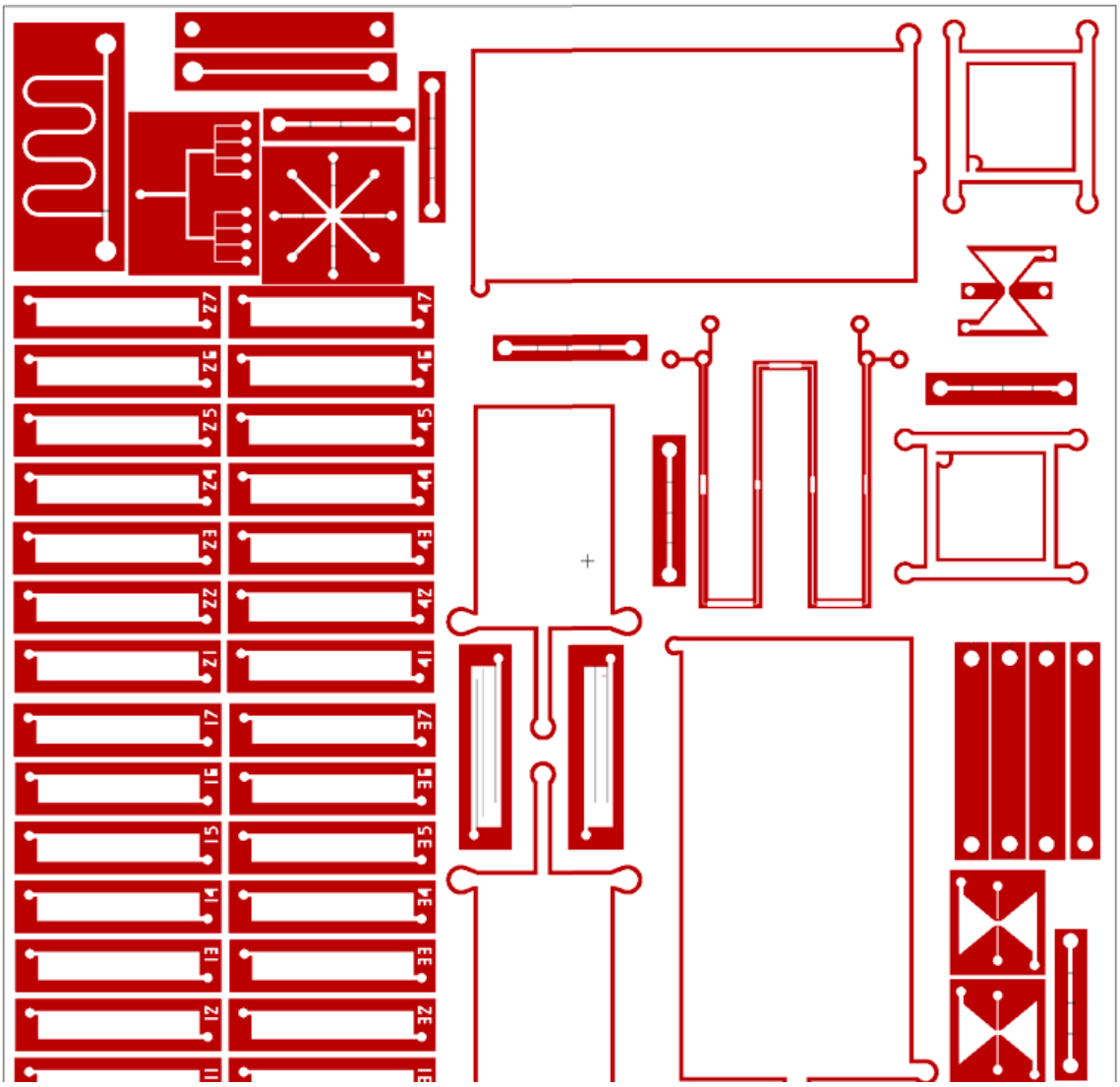

Fig. 81. L-edit design of the second mask for photolithography process.

Appendix B: Filling Pressure Measurements

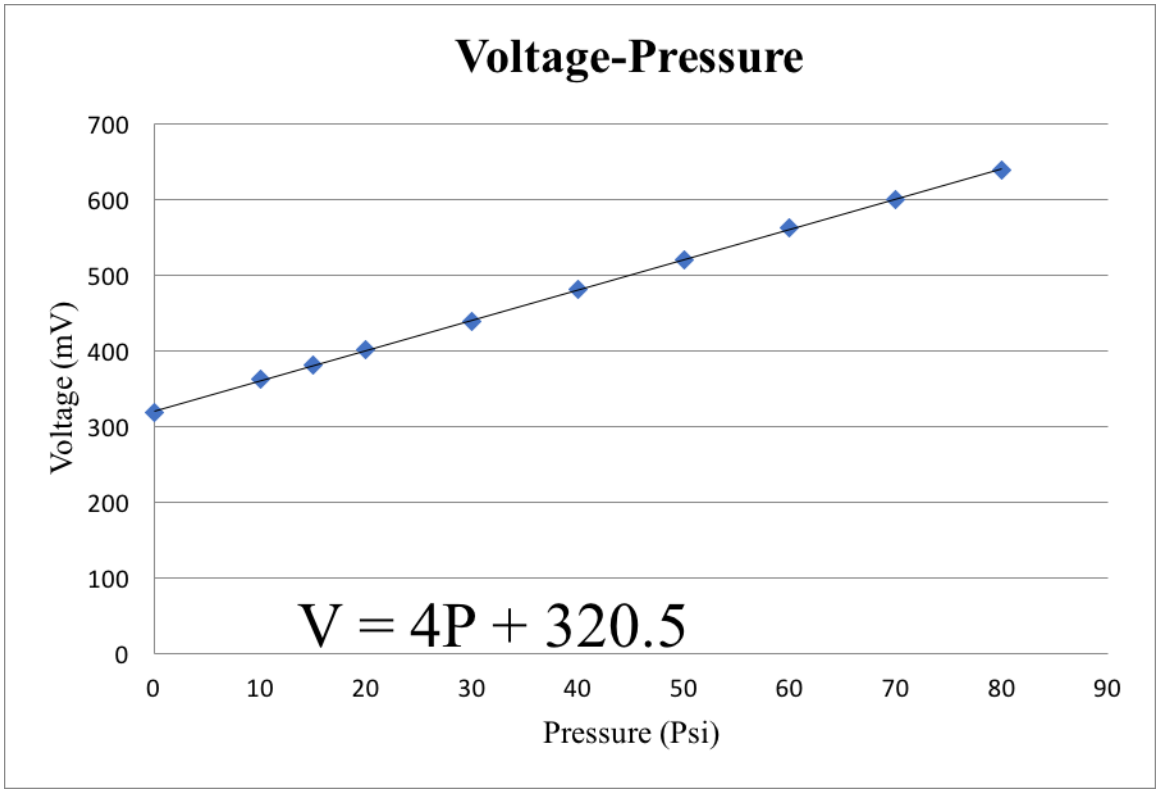

Fig. 82. The voltage-pressure relationship in calibration of the pressure gauge.

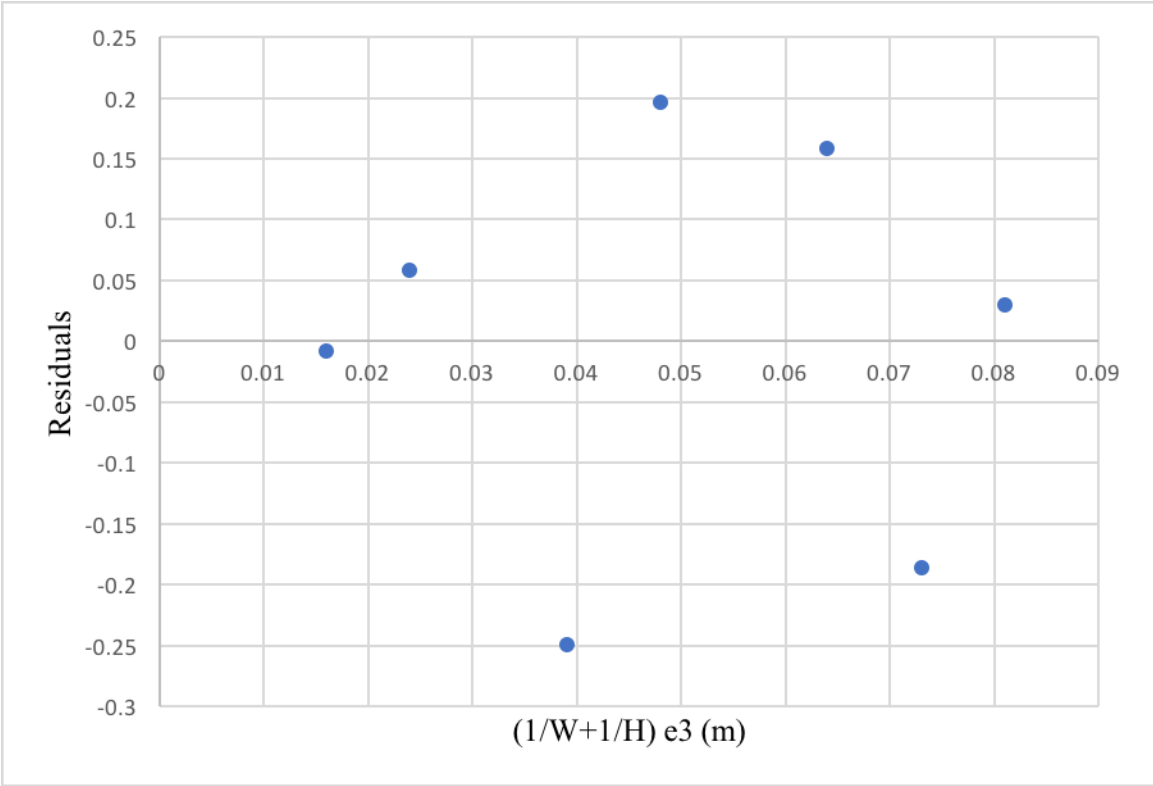

Fig. 83. Randomly distributed residual Plot of the linear fit for ciritial pressure versus (1/W+1/H).